AN ELECTRON PARAMAGNETIC RESONANCE STUDY OF FERRIC IRON IN STRONG CRYSTAL FIELDS

by

R.G. Pontin M.Sc.

A thesis

submitted to the University of Keele

for the Degree of Doctor of Philosophy

Department of Physics,
University of Keele,
Staffordshire.

September, 1968.

ACKNOWLEDGEMENTS

The author would like to express his thanks to the following:

Professor D.J.E. Ingram for the provision of laboratory facilities and for his supervision of this work.

Dr. E.F. Slade for permission to reproduce fig. 5.2 from his thesis and to Dr. E.F. Slade and to all other members of the resonance group for helpful discussions.

Dr. B. Henderson for the use of his X- and Q-band spectrometers.

Dr. K.A. Müller of I.B.M., Zurich; Mrs. Barbara Wanklyn of the Clarendon Laboratory; Mr. H. Maguire of Imperial College; and Mr. F.C. Thorpe of A.E.I. Rugby, for the provision of iron-doped single crystals.

Mr. P.G. Collis and Mr. D. Cresswell of the Chemistry and Geology Departments for assistance with X-ray and optical studies of samples.

The Technical Staff of the Physics Department for their cooperation.

Mrs. M. Furnival for her care and patience in typing this thesis.

The S.R.C. for a maintenance grant.

ABSTRACT

The work described in this thesis is concerned with the measurement of the large zero-field splittings of ferric iron substituted into a number of mixed metal oxide host lattices.

The first chapters give an outline of the crystal field approach to the interpretation of E.P.R. spectra with particular emphasis on the zero-field splitting of S-state ions and the approximations underlying the conventional spin Hamiltonian. There follows a survey of previous measurements on S-state ions in various host lattices and a discussion of the previously reported E.P.R. spectra in the crystals chosen for study in the present work

Chapter V contains a description of the 4mm. spectrometer on which the bulk of the measurements were made and a summary of the experimental techniques.

The final chapter is devoted mainly to a discussion of the results obtained from a series of measurements on strontium titanate and lead titanate. The zero-field splitting experienced by ferric iron substituted at the titanium site in both these lattices has been measured and in addition small cubic variations of the E.P.R. spectra have been found. The significance of the results has been discussed from the viewpoint of a simple point-charge model.

CONTENTS

CHAPTER I

INTRODUCTION

This thesis is concerned with an evaluation of the energy level structure of ferric iron, Fe^{3+}, in host lattices where the electro-static crystal field is sufficiently strong to split the lowest lying energy levels by several wavenumbers instead of a few hundredths of a wavenumber as is usually the case. This "zero - field splitting" is not measured directly but is inferred from E.P.R. measurements carried out in external magnetic fields of several kilogauss which also split these energy levels.

Electron paramagnetic resonance spectroscopy is concerned with the observation of transitions between the lowest lying energy levels of paramagnetic systems - commonly transition metal ions substituted into diamagnetic host lattices. If the individual ionic - or for that matter atomic or molecular - paramagnets of the system may be considered as non-interacting then each has an energy in an external magnetic field of $-\mu.H$ where the magnetic moment μ is proportional to the angular momentum J of the ion. Each ion then has a series of $2J + 1$ accessible energy levels between which transitions may be induced. When substituted

into a crystal lattice the $2J + 1$ evenly spaced levels of the free ion are greatly modified and from a study of the modified energy levels one may gain considerable information on the immediate surroundings of the paramagnetic ion.

The observation of electron resonance is not limited to transition metal ions however but is possible whenever there are unpaired electrons giving rise to a nonzero resultant total angular momentum J. Other important categories of paramagnets are stable free radicals, triplet state molecules, conduction electrons in metals, donors and acceptors in semiconductors and damage centres and other impurities in solids.

The energy level separations encountered in solids are normally of the order of a few tenths of a wavenumber or less and hence transitions can be induced between them with readily-available radiation sources in the wavelength range $1 - 3$ cm^{-1}. In certain systems however the energy level spacings may be considerably greater than this and it becomes necessary to use short millimetre wavelength radiation and/or large magnetic fields in order to excite the transitions. One instance of such a case is the splitting of the lowest levels of the ferric ion in strong crystal fields of low symmetry. Such a situation was first encountered

in certain haemoglobin derivatives and in silica glass and has since been observed in numerous other lattices among them the groups of mixed metal oxides having the perovskite and scheelite structures. It is with these latter systems that the present work is concerned.

The interpretation of the E.P.R. spectra of S-state ions i.e. those in which the expectation value of the orbital angular momentum is zero, and of which Fe^{3+} is an example is somewhat different from the majority of non-S-state ions and has recently been the object of considerable theoretical attention. Measurements of large zero field splittings provide a useful check of the various theories and are also of interest in discussing the range of applicability of the conventional spin Hamiltonian in terms of which E.P.R. results are generally quoted, and which may be expected to become invalid at very short wavelengths and/or very high magnetic fields.

CHAPTER II

BASIC THEORY OF ELECTRON PARAMAGNETIC RESONANCE SPECTROSCOPY

Introduction

This chapter begins with a qualitative discussion of the phenomenon of electron paramagnetic resonance followed by an exposition of the fundamentals of crystal field theory which provides the link between the laboratory measurements and the inferences regarding crystal structure and symmetry which can be drawn from them. The final sections introduce some of the problems peculiar to S-state ions.

2.1 The Resonance Condition for a Free Ion.

The resonance problem may be considered from a classical viewpoint and while it is not generally profitable to pursue such an approach very far it nevertheless gives valuable physical insight into the resonance phenomenon and warrants a brief discussion.

Any rotating electric charge will have an associated angular momentum $J\hbar$ and an associated magnetic moment μ. It may thus be considered as a "gyromagnetic top" and when placed in a magnetic field H will precess about it with the Larmor frequency

$$\omega_0 = -\mu H / J\hbar \qquad 2.1$$

The phenomenon of magnetic resonance occurs when an additional magnetic field rotating in the same sense and at the same frequency as the Larmor precession of μ about H is applied; the rotating field exerts a constant couple on μ causing it to turn over and reverse its projection on H, and in this way energy is exchanged between the magnetic moment and the rotating field. This is the resonance phenomenon. The resonance condition is just that the frequency ω of the applied field be equal to ω_0.

On the semiclassical vector model of the atom we assume J is an integer and that there are only 2J + 1 allowed projections of J (or μ) on H. Since the energy of a magnetic dipole in a field H is $-\underline{\mu}.\underline{H}$ we thus have a series of discrete energy levels and in order to induce transitions between these levels i.e. to make $\underline{\mu}$ change its orientation with respect to the static field we must supply radiation at the resonance frequency. Assuming Russel-Saunders coupling the relationship between $\underline{\mu}$ and J can be shown to be

$$\underline{\mu} = -g\beta\underline{J} \qquad 2.2.$$

where g is the Landé g-factor, a function of J, L and S where L and S are respectively the total orbital and spin

angular momentum quantum numbers of the atom, and β is the Bohr-magneton. The resonance condition thus becomes

$$\hbar\omega = g\beta H \qquad 2.3$$

The more formal wave-mechanical approach consists of setting up the Hamiltonian of an ion of total angular momentum $J\hbar$ in a static magnetic field and solving it to find the eigenvalues. The Hamiltonian is simply

$$\mathcal{H} = -\underline{\mu}.\underline{H} \qquad 2.4$$

and the eigenvalues (for H parallel to z)

$$E = g\beta H M_J \qquad 2.5$$

where $M_J \leq |J|$. These correspond to a series of $2J + 1$ equally spaced levels between which we wish to induce transitions. To do this we must introduce a perturbation which couples the levels, usually an alternating magnetic field applied at right angles to the static field. An operator representing such a perturbation is

$$\mathcal{H}_{pert} = - g\beta H_x J_x \cos\omega t \qquad 2.6$$

and since J_x connects states with M_J differing by one, transitions may be induced between adjacent levels only. The resonance condition is that the energy separation between adjacent levels be equal to the energy quantum $\hbar\omega$ i.e.

$$\hbar\omega = M_J\, g\beta H - (M_J - 1)\, g\beta H = g\beta H \qquad 2.7$$

as before. Thus both viewpoints give the same description of the resonance phenomenon and after the next section we drop the classical approach.

2.2. Magnetic Resonance in a Coupled System.

Magnetic resonance experiments are of course not carried out on isolated free ions but on ions coupled together in gaseous, liquid or solid form. Imagine then an assembly of ions with, for simplicity, two accessible energy levels 1 (upper) and 2 (lower) and that N_1 atoms are in level 1 and N_2 in level 2. Now a wellknown result of time-dependent perturbation theory is that the probability of an interaction $V(t)$ inducing a transition from level 1 to level 2 is equal to the probability of its inducing the reverse process from level 2 to level 1. Thus on application of the perturbation there will be a nett loss of energy from the field if $N_2 > N_1$ (resonance absorption) and a nett gain if $N_1 > N_2$ (the basis of maser action). Furthermore whatever the initial distribution of the ions between 1 and 2 the populations will eventually equalize. This last fact is quite contrary to what is observed and appears because of our neglect of the coupling of the elementary paramagnets one with another and with the lattice which they form:

The resonance as we have described it so far is an oscillatory one, the magnetic moments alternating between parallel and antiparallel to the magnetic field.

The coupling with the lattice means that the transition probabilities in the spin system depend not only on the matrix elements of the perturbation operator but also on the probability that the lattice is in a state that permits a transition. In other words in order to conserve energy an upward transition in the spin system must be accompanied by a downward transition in the lattice system and vice versa. Thus the spin system is in thermal equilibrium with the lattice and will be populated according to the Boltzmann distribution

$$N_2/N_1 = e^{-\hbar\omega/KT} \qquad 2.8$$

- in the absence of a perturbing field there will be an excess of spins in level 2 and the conditions will be right for resonance absorption. In order that continuous resonance absorption shall occur it is clear that the spins must be able to "relax" to level 2 faster than they are "pumped up" to level 1 by the perturbing field.

The detailed analysis of this situation was first given by Bloch (1946). He was led to define two relaxation times T_1 and T_2 whereby the spin system,

or more precisely the macroscopic magnetic moment $\underline{M}$ could relax to its thermal equilibrium value. Suppose that somehow we have produced a non-equilibrium distribution of spins. In the absence of the static magnetic field all directions are equivalent and any magnetic moment decays exponentially to zero with characteristic time T_1, the so-called "spin lattice" or "longitudinal" relaxation time. On introduction of H along the z-direction M_z does not decay to zero but approaches an equilibrium value M_o corresponding to the static magnetic susceptibility χ_o - again with characteristic time T_1, M_x and My however still decay exponentially to zero but this time with a different relaxation time T2 - the so-called "transverse" or "spin-spin" relaxation time. T_2 differs from T_1 because it involves a different mechanism - direct coupling between the spins involving no change in the Zeeman energy - whereas T_1 relaxation involves a transfer of energy between the spins and the lattice. Both T_1 and T_2 relaxation are caused by time dependent electric and magnetic fields at the site of the electron and both confer a "width" on the electron magnetic resonance absorption line in addition to the "spontaneous" width. The Lorentzian shape of the normal E.P.R. absorption line comes directly out of Bloch's equations. These may be manipulated to yield an expression for the complex susceptibility

$$\chi = \chi' + i\chi'' \qquad 2.9$$

as a function of ω, and the imaginary part, χ'', which can be shown to be directly proportional to the power absorbed from the perturbing field, is seen to be a Lorentzian function centred on $\omega = \omega_0$. The real part χ' is directly related to χ'' and corresponds to a change in phase of ω on sweeping through ω_0.

The approach outlined above may be pursued further (Slichter 1963, Pake 1962) and is instructive in discussing dynamic effects in electron and nuclear resonance and in the theory of linewidths. However, these will not concern us directly in the rest of this thesis and having developed them sufficiently far to gain an understanding of the resonance phenomenon we now turn to a more specific consideration of the paramagnetic ion in a regular crystal lattice.

2.3. The Paramagnetic Ion in a Crystal Lattice.

2.3. 1. Introduction.

A complete analysis of the paramagnetic ion in a crystal lattice would involve solving the Schrödinger equation for the electrons of the entire lattice, which is of course impracticable. A first simplification would be just to treat a cluster of atoms, molecules or

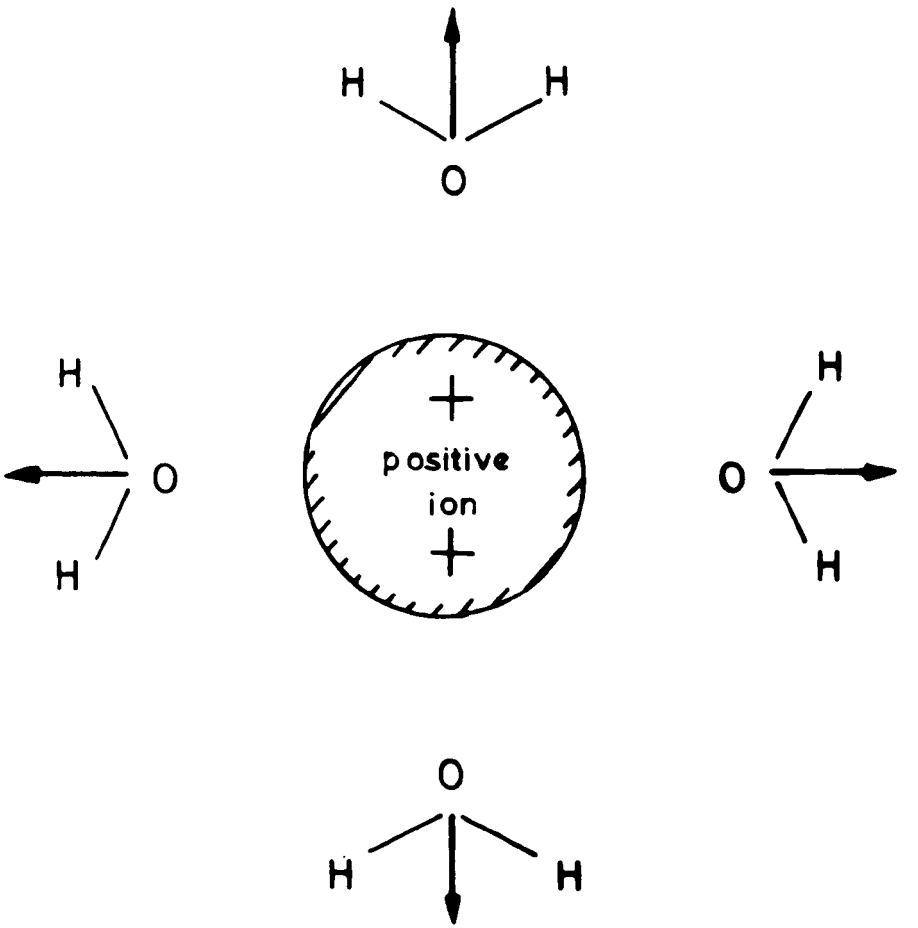

Fig. 2.1. Illustrating the concept of a ligand field (after Pake)

ions with the paramagnetic ion as centre. This, the "Molecular-Orbital" approach is primarily useful in discussing the situation in which the unpaired electrons are largely delocalized from the parent ion. Even more drastic approximations are involved in "Crystal Field Theory" which assumes the unpaired electrons to be localized on the paramagnetic ion which is itself assumed to be surrounded by an array of point charges or point dipoles the only effect of which is to produce a static electric field. Such an approach is justified since it leads to a situation which can be fairly rigorously analyzed - and the results of the analyses are in substantial agreement with experiment.

Crystal field theory concerns itself with an ion in a regular crystal lattice. However few of its results depend on the existence of the lattice and most of them can be carried over to the "coordination cluster". By a coordination cluster is just meant a central metal ion associated with a number of attached ligands the whole forming a distinguishable entity. (Fig. 2.1) The coordination clusters may themselves pack into a lattice though this is not of primary importance - the principal contribution to the electrostatic field comes from the atoms closest to the metal ion, the attached ligands. The presence of the ligands may set up additional

potentials, not necessarily of simple electrostatic origin, at the central metal ion. The term "Ligand Field Theory" is employed to cover all aspects of the manner in which an ion or atom is influenced by its nearest neighbours. It contains crystal field theory as a special case. Henceforth only the restricted crystal field theory will be used since it is quite adequate in dealing with the magnetic properties of crystal lattices.

2.3. 2. The Free Ion Hamiltonian.

Since the starting point of all Crystal Field Theory calculations is the free ion Hamiltonian a brief résumé of its principal features will now be given. The leading terms in the free ion Hamiltonian are

$$\mathcal{H} = \Sigma_i \left[\nabla_i^2 / 2m - Ze^2/r_i\right] + \sum_{i>j} e^2/r_{ij} + \zeta(r_i) l_i . S_i \quad 2.10$$

They represent respectively the kinetic energy of the electrons, the Coulomb attraction between electron and nucleus and repulsion between pairs of electrons, and the spin-orbit coupling. In practise this equation cannot be solved directly because of the non-spherically symmetric interelectronic repulsion and spin-orbit coupling terms. To simplify the problem $\mathcal{H}$ is decomposed into two parts one of which, by far the larger is spherically symmetric, and a perturbation term which is

not. We write

$$\mathcal{H} = \mathcal{H}_0 + \mathcal{H}^1 \qquad 2.11$$

where $\mathcal{H}_0 = \sum_i [\nabla_i^2 / 2m + U(r_i)]$ is spherically symmetric and $\mathcal{H}^1$ is the remaining non-spherically-symmetric part of the interelectronic term plus the spin-orbit coupling. The physical assumption behind this idea is that each electron may be considered to move independently of all the others which just provide a constant "screening" charge in addition to the main central force field of the nucleus.

The eigenfunctions of $\mathcal{H}_0$ are first found by the "Self-Consistent Field" method. Briefly, following Hartree (Hartree 1946, Tinkham 1964) we assume these eigenfunctions to be simple products of one-electron wavefunctions u_i. We wish to find the radial parts of these functions $u_i(r_i)$ which minimize the total energy. First we guess at a set of $u_i(r_i)$ and calculate the potential U_i seen by each electron, by averaging the potential produced by all the other electrons ($j \neq i$) and the nucleus. The one-electron Schrödinger equations involving these potentials

$$[\nabla_i^2 / 2m + U_i] u_i = E_i u_i \qquad 2.12$$

are solved by numerical integration. The resulting set of u_i will not in general be the same as the original set. On this basis a new guess is made and the calculation repeated over and over until self-consistency is obtained.

These self-consistent solutions can be shown to give a minimum total energy $E = \sum_i E_i$.

We thus arrive at the eigenstates of $\mathcal{H}_o$ characterized by one-electron quantum numbers - a consequence of our separating the variables of each electron. We define a "configuration" by saying which of these one-electron central-field eigenstates are occupied.

In the case of Russel-Saunders coupling applicable to the lighter atoms we now assume the remaining non-spherically-symmetric part of the interelectronic repulsion term to be much greater than the spin-orbit coupling, and apply it first as a perturbation to each configuration. Since each configuration is highly degenerate perturbation theory cannot be used to calculate the new eigenstates and the matrix of $\sum' e^2/r_{ij}$ must be diagonalized directly. This would be extremely tedious were a large amount of initial factorization not possible. Such factorization comes about because of the group-theoretical properties of angular momentum.

Now while the central-force field Hamiltonian is invariant under a rotation of the coordinates of each electron, the new Hamiltonian

$$\mathcal{H}^{11} = \sum_i \left[\nabla_i^2/2m - Ze^2/r_i\right] + \sum_{i>j} e^2/r_{ij} \qquad 2.13$$

is not, but it is invariant under a rotation of the

coordinates of the whole atom, and also under separate rotation of spatial and spin coordinates. In other words $\mathcal{H}$ commutes not only with $\underline{J}$ but also with $\underline{L}$ and $\underline{S}$ and it must therefore be possible to define precise and simultaneous eigenvalues of $\mathcal{H}$ and $\underline{L}$, $\underline{S}$ or $\underline{J}$. Thus there can be no matrix elements of $\mathcal{H}$ between states of different L, S, or J or different M_L, M_S or M_J and a large amount of factorization of the initial secular determinant will occur if combinations of one electron wavefunctions which are already angular momentum eigenfunctions are chosen as basis functions. There is a limit to the extent to which this can be taken since all momenta that commute with $\mathcal{H}$ do not necessarily commute with one another. In fact it is possible to diagonalize only four angular-momentum operators simultaneously.

We thus arrive at a series of "terms" into which each configuration is split and for which L, S, M_L and M_S are usually chosen as good quantum numbers. These terms degenerate in M_L and M_S are specified by their L and S values.

Similar considerations apply when we consider the remaining perturbation $\xi(r_i) l_i \cdot s_i$, the spin orbit coupling. The full Hamiltonian, including spin-orbit coupling, still commutes with $\underline{J}$ and J and M_J provide good quantum numbers. It is at this stage, however,

that we wish to consider the application of the crystal field potential since it may be comparable in magnitude with the spin-orbit coupling.

We thus have as our starting point the free ion terms which are linear combinations of one electron wavefunctions of definite L and S, or, more correctly, linear combinations of antisymmetrized Slater determinants which take account of the indistinguishability of electrons and the Pauli principle, whereas the simple Hartree functions do not.

2.3. 3. The Crystal Field Potential.

It is customary to divide the problem of calculating crystal field splittings into a number of cases depending upon the relative magnitudes of the interelectronic repulsion term, the crystal field potential, and the spin-orbit coupling. Various definitions are possible and following the usual convention (Figgis 1966, Ballhausen 1962) we take

$\sum e^2/r_{ij} \gg V_c \gg \mathcal{H}_{so}$ as "weak field"

$V_c \gg \sum e^2/r_{ij} \gg \mathcal{H}_{so}$ as "strong field"

There is also the situation in which

$\mathcal{H}_{so} \gg V_c$

typified by the rare-earths where the paramagnetic electrons lie deep within the atom and are well

shielded from the influences of external fields. The strong field case corresponds to the onset of covalent bonding when the electronic orbitals of the neighbouring diamagnetic atoms start to overlap those of the paramagnetic atom. This situation is found for complexes of the 4d and 5d groups and for cyanides of the 3d group. In this case even the free ion configurations are broken down and configurations are specified not by which one electron states are occupied but by which linear combinations of one electron states which transform irreducibly under the symmetry operations of the crystal field are occupied.

The weak field approximation pertains to most ions of the first transition series and hence forward we limit our discussion to this case. First, however, we consider the form of the potential V_c.

If the ligands are considered as point charges then in the region of the central ion there will be no space charge and the potential V_c must obey Laplace's equation

$$\nabla^2 V_c = 0 \qquad 2.14$$

Solutions are generalized Legendre polynomials of the form

$$V_c = \sum_i \sum_{m,n} A_n^m Y_n^m (\theta, \phi) \qquad 2.15$$

where

$$Y_n^m(\theta,\phi) = (-1)^n \left[\frac{1}{4\pi}\frac{(2n+1)(n-|m|)!}{(n+|m|!)}\right]^{\frac{1}{2}} P_n^m(\cos\theta)e^{im\phi}$$

and the summation i is over the electrons of the central ion. If attention is confined to d-orbitals it is never necessary to consider terms of higher than fourth order since all matrix elements of such terms will be zero. In addition all terms with odd n must vanish since the matrix elements are then integrals over all space of functions of odd parity. These restrictions limit n to 2 and 4 for the iron group and in addition if the potential is real $A_n^m = -(A_n^{-m})^*$.

Further restrictions are placed on the form of V_c by the symmetry of the ligands and for example for sixfold cubic coordination V_c reduces to

$$V_c = \sum_i A_4^0 \left[Y_4^0 + \sqrt{5/14}\,(Y_4^4 - Y_4^{-4})\right] \qquad 2.16$$

A fairly comprehensive table of V_c for different symmetries is given by Low (1960).

Although many of the features of the splittings produced by V_c can be obtained from quite general group-theoretical considerations in order to calculate the actual aplittings the matrix elements of V_c must be evaluated directly. This process is greatly simplified by Stevens' method of operator equivalents. The theorem of operator equivalents says that if two operators $\mathfrak{O}$ and $\mathfrak{B}$ have the same transformation properties then in a

manifold of constant J

$$\langle JM|\mathcal{H}|JM'\rangle = c_J \langle JM|\mathcal{B}|JM'\rangle \qquad 2.17$$

Thus in the expressions for V_c x, y and z may be replaced by J_x, J_y and J_z and the evaluation of the matrix elements becomes straightforward, at least in principle. Tables of operator equivalents for the common crystalline potentials are tabulated by Stevens (1952) and Low (1960).

The crystal field splits the "terms" up into a series of "levels" which are characterized by the way they transform under the symmetry operations of the field. The remaining perturbations in the crystal field treatment of the paramagnetic ion Hamiltonian, the spin-orbit coupling and Zeeman terms are usually treated together by the method of the effective spin Hamiltonian. Before going on to a discussion of the spin Hamiltonian, however, we illustrate some of the preceding ideas by an example.

2.3. 4. Qualitative Features of the Crystal Field Splitting.

Let us consider the case of V^{3+} which has the configuration $(1s)^2\ (2s)^2\ (2p)^6\ (3s)^2\ (3p)^6\ (3d)^2$. The argon core, up to $(3p)^6$, is spherically symmetric and provides the "screening" which alters the radial dependence of the 3d single-electron orbitals. The first problem is to calculate the splitting of $(3d)^2$ by the Coulomb repulsion

term. Since we know that this is going to split the configuration up into a number of terms diagonal in L, S, M_L and M_S we first construct a table of all the possible M_L, M_S states which can be derived from permutations of the two 3d electrons in the available 5 x 2 = 10 spin-orbitals. From such a table it is possible to see which terms must exist and to pick out the linear combinations of Slater determinants which are diagonal in L and S as well as in M_L and M_S, and which therefore form the term wavefunctions. Thus the terms arising from d^2 are found to be ^1S, ^1G, ^3P, ^1D, ^3F and from now on we shall only be interested in the ground term which we can find from the empirical Hund's rules which in effect summarize the tendency for electrons to share as little of space in common as possible so that the repulsions between them are minimized. Thus for the configuration d^2 the ^3F term is found to lie lowest and we now consider how this splits up, first in a field of octahedral symmetry.

We express V_c in Cartesian coordinates as

$$V_c = \sum_i D_i \, (x_i^4 + y_i^4 + z_i^4 - 3/5 \; r_i^4) \qquad 2.18$$

$$= \frac{\beta \overline{r^4}}{20} \left[35L_z^4 - 30L(L+1)L_z^2 + 25L_z^2 - L(L+1) + 3L^2(L+1)^2\right] + \frac{\beta r^4}{8}(L_+^4 + L_-^4)$$

- making use of the theorem of operator equivalents. Since V_c does not act on the spin part of the wavefunction the problem reduces to diagonalizing the orbital ($|M_L\rangle$) states of the ^3F term viz.

$|3\rangle$ $|2\rangle$ $|1\rangle$ $|0\rangle$ $|-1\rangle$ $|-2\rangle$ $|-3\rangle$

Matrix elements will be of the form

$\langle$linear combination of determinantal product of two spherical harmonics $|V_c|$1.c. of determinantal product of two spherical harmonics$\rangle$and direct evaluation is very tedious. However it yields splittings in terms of the familiar "D_q" where D depends on the crystal field strength and $q = \frac{2}{105}\overline{r^4}$ on the radial part of the wavefunction. It is much simpler to make use of group theory and look for the irreducible representations of O_h which are spanned by the representation $D^{(3)}$ of the full rotation group carried by the ^3F (L = 3) functions. The justification for this procedure is given in appendix 1, and in order to carry it out all we need to know is the character table of O_h, which is given in any standard text on group theory (e.g. Cotton 1964), and the characters of the reducible representations of the symmetry operations of O_h which have as their basis the spherical harmonics of order 3. These are given by A12 and performing the summation of A11 leads to

$$D^{(3)} = A_{2(g)} + T_{1(g)} + T_{2(g)}$$

Thus in a field of octahedral symmetry the ^3F term splits up into two triplets and a singlet, and a direct diagonalization shows that the $^3T_{1g}$ triplet lies lowest and the singlet highest. This same result could have been obtained in a more qualitative, but more easily

visualized, way by considering the real forms of the f-orbitals (which transform like the F-term): those which have lobes pointing towards the negatively charged ligands will suffer an electrostatic repulsion and hence be raised in energy, while those orbitals which avoid the ligands will be lowered in energy.

The presence of fields of lower than octahedral symmetry will cause further splittings. For example a trigonal distortion of the octahedral array of charges will further split the $^3T_{1g}$ level of the ^3F term up into a doublet ($^3E_2$) and a singlet (^3A) of which the singlet will lie lower and thus form the new ground state. In fact the ground state of most paramagnetic complexes is found to be an orbital singlet. Even if the crystal symmetry should seem to be such as to leave a degenerate ground state the Jahn-Teller theorem ensures that the crystal will distort to remove the degeneracy since by so doing the total energy of the system is lowered. This is assuming that spin-orbit coupling, which can also remove the degeneracy, does not enter at this stage to complicate matters.

When spin is introduced however, there remains one degeneracy, which can only be removed by an external magnetic field - the Kramers' degeneracy. Kramers' theorem states that all energy levels of ions with an odd number of electrons are at least doubly degenerate in

the absence of a magnetic field. This comes about because the Hamiltonian in the absence of a magnetic field is invariant under the operation, I, of time-reversal, and Ψ and $I\Psi$ must therefore be degenerate. Of course if I leaves Ψ unchanged this is not saying anything but what Kramers showed was that for an odd number of electrons Ψ and $I\Psi$ do represent distinct states, and thus in the absence of any interaction which destroys time reversal symmetry - such as the application of an external magnetic field - there must be at least a two-fold degeneracy.

The final perturbations in the treatment of the paramagnetic ion, the spin-orbit coupling and magnetic field, are usually applied together and treated by means of the effective spin Hamiltonian. This describes the final splittings among a set of states characterized by spin only and is justified because the effect of the low symmetry crystal fields considered above is to "quench" out the orbital angular momentum. Physically orbital angular momentum is associated with the ability to rotate an orbital about an axis to give an identical and degenerate orbital. Thus an orbital singlet has no angular momentum - it is "locked" into one position - and as we saw above the ground state to which we now apply the final perturbations, is just such an orbital singlet.

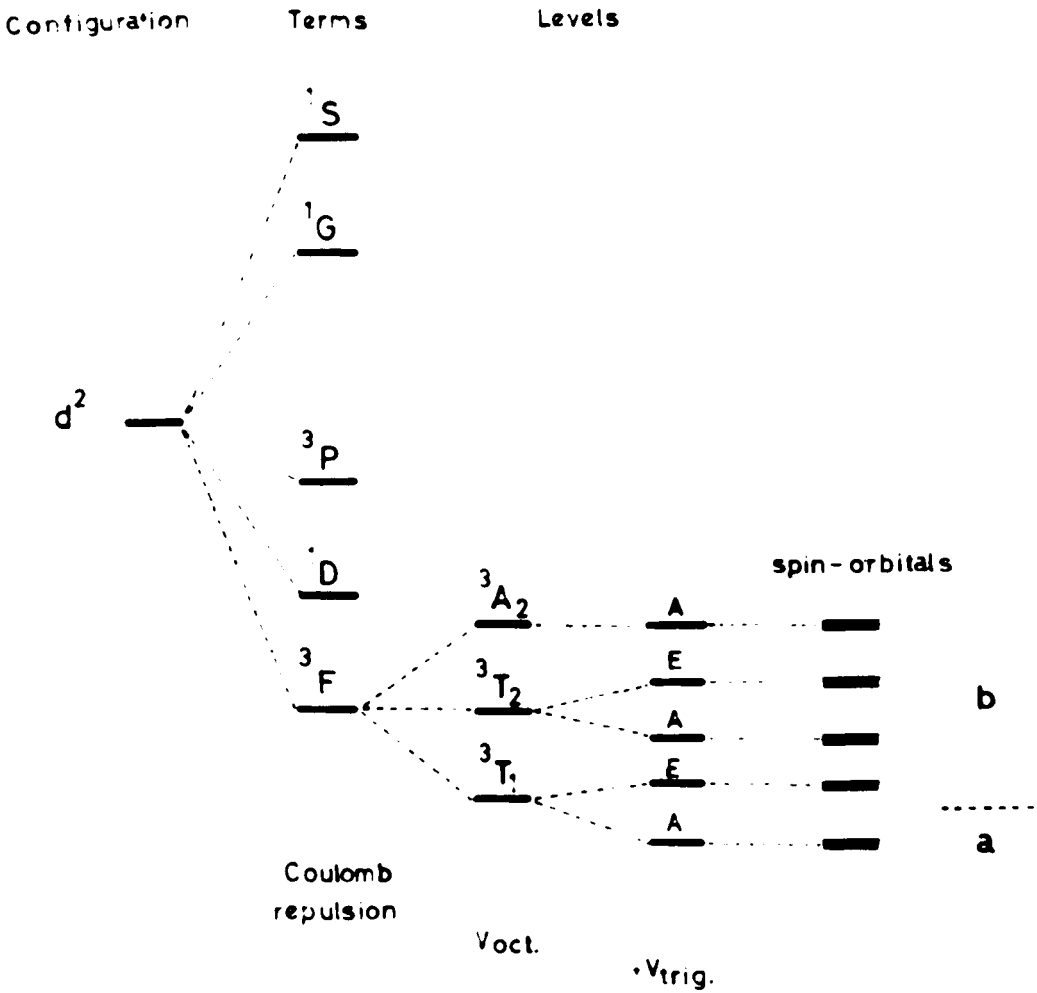

Fig. 2.2. Splitting of the d^2 configuration in a field of trigonal symmetry

2.3. 5. The Spin Hamiltonian.

The splitting of the d^2 configuration by the interactions described in the previous sections is illustrated in fig. 2.2. The remaining terms in the Hamiltonian viz. $\mathcal{H} = \lambda L.S + \beta H(L+2S)$ are now treated by perturbation theory, attention being restricted to those states arising from the free ion ground term only. The reason for treating these final two perturbations together is that the stronger spin-orbit coupling vanishes in first order for the orbital singlet ground state yet can produce splittings in second order comparable with those produced by the Zeeman term in first order.

The conventional method of treating the situation shown at the right of fig. 2.2. by perturbation theory would be first to diagonalize the spin degenerate ground state and then to apply perturbation theory to obtain the admixture of the higher orbital levels. A neater method due to Pryce (1950) more or less reverses this procedure by considering first the admixture of the higher orbital states into the ground state by perturbation theory to obtain an "effective" Hamiltonian which is then applied directly to the spin degenerate ground state. Since it is only to be evaluated between spin states the explicit dependence of the effective Hamiltonian on orbital operators can be supressed and an "effective spin Hamiltonian" left.

Consider first the orbital admixture by perturbation theory. To second order the energy shift is given by

$$\Delta E = \langle a|\lambda L.S+\beta H(L+2S)|a\rangle + \sum_{a\neq b} \frac{\langle a|\lambda L.S+\beta H(L+2S)|b\rangle^2}{Ea - Eb} \qquad 2.19$$

where $|a\rangle$ is the orbital singlet ground state and the b-orbitals are as in fig. 22. Now since orbital angular momentum is quenched for an orbital singlet and since by definition $\langle a|b\rangle = 0$ (a....b are eigenfunctions of the unperturbed Hamiltonian) this reduces to

$$\langle a|2\beta H.S|a\rangle + \sum_{a\neq b}\left[\frac{\langle a|\lambda L.S|b\rangle^2+2\langle a|\lambda L.S|b\rangle\langle b|\beta HL|a\rangle+\langle a|\beta HL|b\rangle^2}{Ea - Eb}\right]$$

This is now to be evaluated between the spin substates of $|a\rangle$. The first-order term is already between such states and just gives a contribution of $2\beta H.S$ to $\mathcal{H}_s$. The first second-order term written out more fully becomes

$$\sum_{b\neq a} \frac{\langle M_{La}\ M_{Sa}|\lambda L.S|M_{Lb}\ M_{Sb}\rangle\langle M_{Lb}\ M_{Sb}|\lambda L.S|M_{La}\ M_{Sa}'\rangle}{Ea - Eb}$$

$$= \frac{\langle M_{Sa}|\sum_{\mu,\nu}\sum_{a\neq b}\langle M_{La}|\lambda L_\mu|M_{Lb}\rangle\langle M_{Lb}|\lambda L_\nu|M_{La}\rangle\ S_\mu\ S_\nu\ |M_{Sa}'\rangle}{Ea - Eb} \qquad \mu,\nu = x,y,z$$

$$= \langle M_{Sa}|\sum_{\mu,\nu}\lambda^2\Lambda_{\mu,\nu}S_\mu\ S_\nu\ |M_{Sa}'\rangle$$

where $\Lambda_{\mu,\nu} = \sum_{b\neq a} \frac{\langle M_{La}|L_\mu|M_{Lb}\rangle\langle M_{Lb}|L_\nu|M_{La}\rangle}{Ea - Eb}$ 2.20

and thus gives a contribution to $\mathcal{H}_s$ of $\sum_{\mu,\nu}\lambda^2\ \Lambda_{\mu\nu}S_\mu S_\nu$

The remaining second order terms can be reduced in a like manner to give

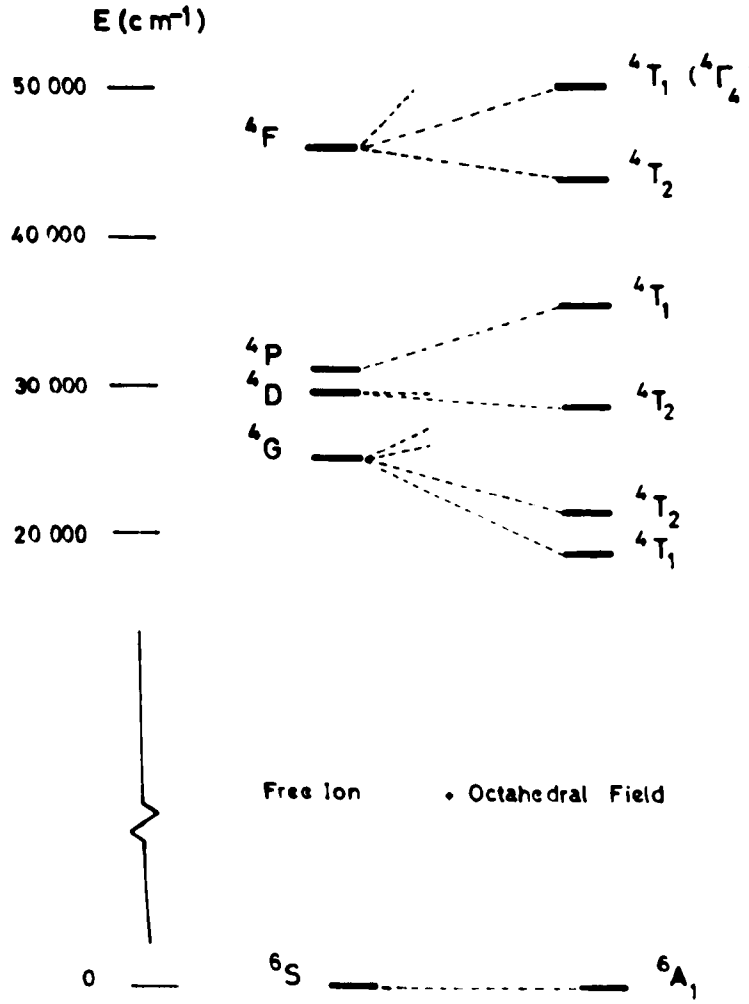

Fig.2.3. The quartet states of d^5 in an octahedral field

$$\mathcal{H}_S = \sum_{\mu,\nu} \left[\beta H_\mu (2\delta_{\mu\nu} + 2\lambda \Lambda_{\mu\nu}) S_\nu + \lambda^2 S_\mu \Lambda_{\mu\nu} S_\nu \right]$$

$$= H.g.\ S + S.D.S. \qquad 2.21$$

where $g = 2\delta_{\mu\nu} + 2\lambda \Lambda_{\mu\nu}$ and $D = \lambda^2 \Lambda_{\mu\nu}$

Several interesting conclusions can be drawn from the form of the spin Hamiltonian 2.21. In first order, or in the absence of spin-orbit coupling g=2, the free spin value - the orbital momentum remains quenched. The effect of spin-orbit coupling is to reinstate some orbital angular momentum - via admixture of higher states, and leads to departures from g = 2. In addition the spin-orbit coupling is seen to lift the 2S+1- fold degeneracy of the ground state even in the absence of a magnetic field giving rise to the so-called "zero-field Splitting". In effect the spin Hamiltonian allows us to ignore the orbital angular momentum and replace its effect by an anisotropic coupling between the electron spin and the external magnetic field.

2.4. S-State Ions.

In contrast to the configuration d^2 described above now consider the configuration d^5 for which the free ion ground term is ^6S (fig. 2.3). No crystal field whatever its symmetry can lift the degeneracy of a pure S-state and the ground term thus remains ^6S, or in group theoretical notation $^6A_1$. As we have already seen the

spin-orbit coupling cannot split an orbital singlet in first order and if, following the spin Hamiltonian formulation given above, we restrict our attention to the free ion ground term, there are no higher states which can be admixed and hence there will be no zero-field splitting. This is, of course, quite contrary to observation; the spin Hamiltonian as given above is not directly applicable to S-state ions. In order to obtain splitting of an S-state it is necessary to consider the simultaneous application of the crystal field and spin-orbit coupling and to admit admixtures of higher-lying free ion terms. Even so it is still necessary to go to higher than second order to obtain any splitting and a derivation of a spin Hamiltonian along the lines indicated above would be very complex. Since the spin Hamiltonian must reflect the symmetry of the crystal field, however, what is done instead is to construct a polynomial of order $\leqslant 2S+1$ in S, analogous to 2.21 which displays the desired symmetry. Thus the spin Hamiltonian for the iron group S-state ions (Mn^{2+}, Fe^{3+}) is usually written

$$\mathcal{H}_S = \beta\, H.g.S + D\left[S_z^2 - \tfrac{1}{3}S(S+1)\right] + E\left[S_x^2 - S_y^2\right] + \frac{F}{180}\left[35S_z^4 - 30S(S+1)S_z^2 + 25S_z^2 - 6S(S+1) + 3S^2(S+1)^2\right] + \frac{a}{6}\left[S_x^4 + S_y^4 + S_z^4 - \frac{1}{5}S(S+1)(3S^2+3S-1)\right] \quad 2.22$$

where the terms in D+F, E and a are relevant to tetragonal, rhombic and cubic fields respectively.

The problem of the zero field splitting of S-state

ions is discussed more fully in the next chapter. First, however, some other approximations involved in the spin Hamiltonian and the attempts which have been made to generalize the above treatment, are considered.

2.5 The Hamiltonian of Koster and Statz.

From the foregoing treatment it will be seen that the principal approximations involved in the spin Hamiltonian are

1) The crystal field splitting is assumed to be much greater than that produced by the spin-orbit coupling and Zeeman terms though no assumptions are made about the relative magnitudes of the latter two terms.

2) Admixtures from higher terms and higher configurations are ignored.

3) All effects of covalency and bonding are neglected.

Most of these restrictions are removed in the Hamiltonian of Koster and Statz (1959). Whereas the spin Hamiltonian starts from the crystal field eigenstates and attempts to explain both the zero-field splitting and behaviour in a magnetic field in terms of perturbation theory, the Koster and Statz approach is to start from the exact eigenstates in zero magnetic field - including interelectronic repulsion, crystal field splitting, spin-orbit coupling and bonding effects, and to consider the Zeeman term only as the perturbation. It is equally

applicable to S and non-S state ions and the only interaction which it neglects is the admixtures of higher lying levels into the ground level by the external magnetic field.

The Koster and Statz Hamiltonian may be formulated in one of two ways. First, consider an ion in a crystal at a site of symmetry G. In the absence of a magnetic field the energy levels will have degeneracies determined by the dimensions of the irreducible representations of G and the degenerate functions belonging to each energy level will provide bases for these representations. Now consider two levels $\alpha\left[E_\alpha, \psi_i^\alpha\right]$ and $\beta\left[E_\beta, \psi_j^\beta\right]$ sufficiently far removed from all others that admixtures via the external magnetic field may be neglected. The functions ψ_i^α ($i = 1 \ldots n_\alpha$, the degeneracy of E_α) and ψ_j^β which provide bases for irreducible representations $\Gamma_\alpha(R)$, $\Gamma_\beta(R)$ of G respectively need not be known explicitly - in fact in general they won't be since they are the exact eigenstates in zero magnetic field. Now on application of the magnetic field the problem becomes one of evaluating matrix elements of $\beta H.(L+2S)$ between the states ψ_i^α, ψ_j^β. If $\beta H.(L+2S)$ is decomposed into parts each of which transforms irreducibly under G then the Hamiltonian matrix will break up into blocks corresponding to the various $\Gamma_\alpha, \Gamma_\beta$ and each block will further decompose into (a small number of disposable

constants) X (matrices $U^{\alpha,\beta,\gamma}$ which will be functions of the group symmetry only). The number of independent constants in each block will just be the number of times the irreducible representation Γ_γ of G carried by the components of L+2S is contained in the direct product $\Gamma_\alpha \times \Gamma_\beta$. Thus using the $U^{\alpha,\beta,\gamma}$ matrices tabulated by Koster and Statz it is possible to write down the complete matrix describing the behaviour of the energy levels α,β in a magnetic field. This matrix will contain the minimum number of independent disposable parameters allowed by symmetry and there will in general be more of these than in the conventional spin Hamiltonian which contains physical assumptions in addition to symmetry arguments.

A more direct way of obtaining the Koster and Statz Hamiltonian is via a generalization of the spin Hamiltonian. The most general spin Hamiltonian linear in the magnetic field can be written as

$$\mathcal{H}_{KS}=H_x \sum_{n,m} A_n^m Y_n^m(S)+H_y \sum_{n,m} B_n^m Y_n^m(S)+H_z \sum_{n,m} C_n^m Y_n^m(S)+\sum_{n,m} D_n^m Y_n^m(S) \qquad 2.2\,3$$

where $A_n^m \ldots . D_n^m$ are constants and $Y_n^m(S)$ polynomials in S which transform like the spherical harmonics. In evaluating matrix elements of $\mathcal{H}_{KS}$ within a (2S+1)-fold degenerate ground manifold it will be unnecessary to consider terms with $n > 2S$ and since in the absence of a magnetic field the Hamiltonian must display time reversal

symmetry

$$D_n^m = 0 \quad \text{if } n \text{ is odd.}$$

Application of the external magnetic field destroys time reversal symmetry so that

$$A_n^m = B_n^m = C_n^m = 0 \text{ if } n \text{ is even}$$

Thus for the iron group $\mathcal{H}_{KS}$ reduces to

$$\mathcal{H}_{KS} = H_x\left[\sum_m (A_1^m Y_1^m(S) + A_3^m Y_3^m(S) + A_5^m Y_5^m(S)\right] + H_y\left[B_n^m\right] + H_z\left[C_n^m\right] + \sum_m \left[D_2^m Y_2^m(S) + D_4^m Y_4^m(S)\right] \qquad 2.24$$

and further restrictions arise from particular symmetries since $\mathcal{H}_{KS}$ must also be invariant under the symmetry operations of the group of the crystal field.

For example for cubic symmetry $\mathcal{H}_{KS}$ must carry the completely symmetric A_{1g} irreducible representation of O_h and only those terms in 2.24 which carry this representation can contribute to $\mathcal{H}_{KS}$. The last two terms in 2.24 carry the $D^{(2)}$ and $D^{(4)}$ representations of the full rotation group and as $D^{(2)}$ does not contain the A_{1g} representation of O_h and $D^{(4)}$ contains it only once, there is only one "zero-field" term viz.

$$\sum_m D_4^m Y_4^m(S)$$

in the generalized Hamiltonian. Knowing the particular combination of spherical harmonics with $n = 4$ which are invariant under the cubic group viz.

$Y_4^0 + \sqrt{5/14}\,(Y_4^4 + Y_4^{-4})$ - see e.g. Bleaney & Stevens 1953 , and the polynomials in S which transform like them

(tabulated by Koster and Statz) this term can be reduced to

$$\alpha\{(1/20)\,[35S_z^4-30S(S+1)S_z^2+25S_z^2-6S(S+1)+3S(S+1)S(S+1)] + (1/8)\,[S_+^4 + S_-^4]\}$$

The terms linear in the magnetic field may be evaluated by noticing that H_x, H_y, H_z provide a basis for the T_1 representation of O_h. In order that the direct product of T_1 and $D^{(1,3,5)}$ should contain A_1 it is necessary that $D^{(1,3,5)}$ should also contain T_1 (This may be seen directly from a simple extension of A1.1 but such direct product representations are often required and are tabulated (e.g. Figgis 1966). Now

$D^{(1)} = T_1 + ...$

$D^{(3)} = T_1 + ...$

$D^{(5)} = 2T_1 + ...$

and therefore there will be four terms linear in the magnetic field one of first order, one of third order and two of fifth order in the components of S in the generalized Hamiltonian. The precise linear combination of S must again be chosen so that each term $H.S^n$ is invariant under the symmetry operations of the cubic group.

The generalized Hamiltonian thus contains five parameters describing the behaviour of S = 5/2 in an external magnetic field as opposed to two of the

conventional spin Hamiltonian and there are even more parameters if the symmetry is lower than cubic. Of course the more fundamental problem of interpreting the additional constants in terms of the many-electron wave-functions of the paramagnetic ion in the crystal field still remains.

References.

Ballhausen C.J. 1962 "Introduction to Ligand Field Theory" (McGraw-Hill, New York)

Bleaney B. and Stevens K.W.H. 1953 Rep. Prog. Phys. 16, 108

Bloch F. 1946 Phys. Rev. 70, 460

Cotton F.A. 1964 "Chemical Applications of Group Theory" (Wiley, London)

Figgis B.N. 1966 "Introduction to Ligand Fields" (Interscience, New York)

Hartree D.R. 1946 Rep. Prog. Phys. 11, 113

Koster G.F. and Statz H. 1959 Phys. Rev. 113, 445

Low W. 1960 "Solid State Physics" Supplement 2 (Academic Press, New York)

Pake G.E. 1962 "Paramagnetic Resonance" (Benjamin, New York)

Pryce M.H.L. 1950 Proc. Phys. Soc. A63, 25

Slichter C.P. 1963 "Principles of Magnetic Resonance" Harper and Rav, New York)

Statz H. and Koster G.F. 1959 Phys. Rev. 113, 1568

Stevens K.W.H. 1952 Proc. Phys. Soc. A65, 209

Tinkham M. 1964 "Group Theory and Quantum Mechanics (McGraw-Hill, New York)

CHAPTER III

THE ZERO FIELD SPLITTING OF S-STATE IONS.

Introduction.

As was shown in the previous chapter the zero-field splitting of S-state ions must be considered as a problem set apart from other zero-field splittings. In this chapter some of the more important theories which have been put forward are reviewed with particular emphasis on the axial splitting of ferric iron. It is shown that the present theories fall somewhat short of providing a satisfactory explanation of the observed results.

3.1 Outline of Theories.

The first authors to consider the problem of the gound state splitting of ferric and manganous salts were Van Vleck and Penney (1934) who treated the combined crystal field and spin-orbit coupling as a perturbation on the free ion terms considering the ground term to be spin degenerate. Neither spin-orbit coupling nor any crystal field acting alone can remove the spin degeneracy of an S-state though simultaneous correction for the crystal field and "incipient j-j coupling" will have the desired effect - the admixture of higher terms into the S-state via $\mathcal{H}_{LS} = \sum_i (r_i)\ l_{(i)}.s_{(i)}$ will destroy its centro-symmetric charge distribution and the eigenvalues

will therefore be orientation dependent in the crystal field. As Van Vleck and Penney showed from an inspection of successive perturbation formulae it is generally necessary to go to high order in perturbation theory before any splitting is obtained, the actual order depending upon the symmetry of the crystal field.

Following the introduction of the paramagnetic resonance technique it was soon realized that Van Vleck and Penney's mechanism - which was originally applied to the calculation of susceptibilities - was insufficient to explain the observed splittings and Pryce (1950) and Abragam and Pryce (1951) proposed another mechanism involving the magnetic spin-spin coupling between pairs of electrons within the ion

$$\mathcal{H}_{ss} = \Sigma 4\beta^2 \left[\frac{S_j \cdot S_k}{r_{jk}^3} - 3 \frac{(r_{jk} \cdot S_j)(r_{jk} \cdot S_k)}{r_{jk}^5} \right]$$

based on the usual form for dipole-dipole coupling. Since this depends on position variables it also couples spins with orbits. In the crystal field even though the ion is in an S-state there will be some distortion of the orbits - suppose therefore that instead of the charge cloud being a perfect sphere it is ellipsoidal. Then the dipole-dipole energy of the spins will vary with the orientation with respect to the axes of the ellipsoid and thus the eigenvalues will depend on the spin orientation.

The first quantitative calculations of the Van Vleck and Penney (Spin-orbit) and Pryce (Spin-spin) mechanisms were carried out by Watanabe (1957). The indirect effect on the axial splitting of a large cubic field superimposed on a weaker axial one has recently been considered by Orbach et. al. (Blume and Orbach 1962, Orbach Das and Sharma 1965, Sharma, Das and Orbach 1966, 1968). Blume and Orbach showed that as a result of inter-admixture of the high lying free ion terms by the cubic field the Van Vleck and Penney mechanism could contribute to the axial zero-field splitting in relatively low order. Subsequently Orbach, Das and Sharma performed a calculation very similar to that of Blume and Orbach but using instead configurationally admixed wavefunctions, and finally Sharma, Das and Orbach repeated and extended Pryce's calculations on the spin-spin mechanism.

3.2 Quantitative Predictions.

The object of each of the theories presented above has been to derive expressions for the spin Hamiltonian parameters a and D in terms of the crystal field parameters B_2^0, B_4^0 and B_4^4. In what follows a and D have been taken as in 2.22 and the crystal field has been taken to be

$$\mathcal{H}_{\text{cubic}} + \mathcal{H}_{\text{axial}} = B_4^{\,o} \sum_i r_i^{\,4} \left\{ Y_4^{\,o}(i) + \sqrt{5/14} \left[Y_4^{\,4}(i) + Y_4^{\,-4}(i) \right] \right\}$$

$$+ B_2^{\,o} \sqrt{\frac{4\pi}{5}} \sum_i r_i^{\,2} Y_2^{\,o}(i) - B_4^{\,o\prime} \sqrt{\frac{4\pi}{9}} \sum_i r_i^{\,4} Y_4^{\,o}(i) \qquad 3.1$$

where $B_4^{\,o\prime} = B_4^{\,o} - \sqrt{14/5}\ B_4^{\,4}$ represents the so-called "unbalanced" axial component of the l=4 terms. Since each author uses a different notation the results quoted below may appear different from those in the original references.

3.2. 1. The Van Vleck and Penney Mechanism.

The free ion terms arising from the d^5 configuration are shown in fig. 2.3. In order to obtain a splitting of the ^6S ground state under the influence of an axial crystal field and the spin-orbit coupling Watanabe was led to consider a fourth order process quadratic in both $\mathcal{H}_{so}$ and $\mathcal{H}_{ax}$ which is usually represented by

$$\frac{\langle {}^6S|\mathcal{H}_{so}|{}^4P\rangle\langle {}^4P|\mathcal{H}_{ax}|{}^4D\rangle\langle {}^4D|\mathcal{H}_{ax}|{}^4P\rangle\langle {}^4P|\mathcal{H}_{so}|{}^6S\rangle}{P^2 D}$$

where P and D are the excitation energies of the P and D terms respectively. Some ^4P character is mixed into the ^6S ground state by the spin-orbit coupling and the axial potential is then able to couple the modified ground state to the excited ^4D level and so produce a splitting. By evaluating the above type of expression for the $M_S = \pm 1/2$ and $M_S = \pm 3/2$ substates of ^6S and equating

the difference to 2D, the zero-field splitting, Watanabe obtained

$$D_W = -\frac{3}{70}\frac{\zeta^2}{P^2 D}\langle r^2\rangle^2 \, (B_2^0)^2 \qquad 3.2$$

where ζ is the spin-orbit coupling parameter and $\langle r^2\rangle$ the expectation value of r^2 for the 3d orbitals.

In order to obtain splittings in a cubic field by the above procedure it is necessary to go to fifth or sixth order in perturbation theory and Watanabe has listed some dozen or so processes interior to the d^5 configuration which are expected to be important.

3.2. 2. The Pryce Mechanism.

The expression for the Pryce mechanism for an axial field is formally similar to the above except that now splittings can be obtained in low order by use of configurations external to d^5. Thus the Pryce mechanism is formulated as

$$D_P \propto \frac{\langle {}^6S(3d^5)|\mathcal{H}_{ax}|{}^6D(3d^4 4_s)\rangle\langle {}^6D(3d^4 4_s)|\mathcal{H}_{ss}|{}^6S(3d^5)\rangle}{\Delta}$$

where $\Delta = E[{}^6S(3d^5)] - E[{}^6D(3d^4 4_s)]$

which reduces to

$$D_P = \frac{48}{25}\frac{\langle r'^2\rangle}{\Delta} M \, B_2^0 \qquad 3.3$$

where $\langle r'^2\rangle = \langle 3d|r^4|4_s\rangle$ and M is an integral of the spin-spin interaction.

It is possible, following Watanabe, to consider

a combined perturbation

$$\mathcal{H}_{crystal} + \mathcal{H}_{so} + \mathcal{H}_{ss}$$

and hence obtain further splitting processes. Thus for Mn^{2+} in a cubic field Watanabe obtains

$$a = (Dq)^2 \, (8.53 - 0.10(Dq)^2.10^{-6}) \, .10^{-10} \text{ cm}^{-1}$$

and various other authors have considered similar processes for specific ions (notably Gd^{3+}) in specific crystals (Judd 1955, Elliott & Stevens 1952).

3.2. 3. The Blume-Orbach Mechanism.

The Blume-Orbach mechanism has the form

$$D_{Bo} \propto \frac{\langle {}^6S|\mathcal{H}_{so}|{}^4\Gamma_4\rangle\langle {}^4\Gamma_4|\mathcal{H}_{ax}|{}^4\Gamma_4\rangle\langle {}^4\Gamma_4|\mathcal{H}_{so}|{}^6S\rangle}{[E({}^4\Gamma_4) - E({}^6S)]^2}$$

In the absence of a cubic field the only non-zero matrix element of the spin-orbit coupling which can cause admixture of the ${}^6S$ state is $\langle {}^6S|\mathcal{H}_{so}|{}^4P\rangle$. In order to obtain any splitting the axial field must be able to admix some other state - such as ${}^4D$ in second order in the Watanabe mechanism - into the modified ground state. However if the axial field is superimposed on a stronger cubic one, as is often the case, it is first necessary to diagonalize the free ion terms in the presence of the cubic field before applying any perturbations. In a cubic field the ${}^4\Gamma_4$ component of ${}^4P$ is strongly admixed with the ${}^4\Gamma_4$ components of ${}^4G$ and ${}^4F$ and the spin-orbit coupling is

thus able to admix some $^4\Gamma_4$ ($^4P + {}^4G + {}^4F$) character into the ground state. The axial field is now able to split the ground state directly via the first order matrix element $\langle {}^4\Gamma_4 | \mathcal{H}_{ax} | {}^4\Gamma_4 \rangle$ instead of via second order admixture of ^4D as in the Watanabe process. It turns out that the matrix elements of B_2^o vanish and only the $B_4^{o'}$ part of $\mathcal{H}_{ax}$ contributes to D_{Bo}. Thus

$$D_{Bo} = - B_4^{o'} \left(\sqrt{5}/2\right) \langle r^4 \rangle \zeta^2 p_{\alpha\gamma} \left(2p_{\alpha\alpha} - p_{\alpha\beta}\right) \qquad 3.4$$

where $p_{\alpha\gamma}$, $p_{\alpha\alpha}$, $p_{\alpha\beta}$ characterize the admixture of the ^4P, ^4F and ^4G states in the cubic field ($i^4\Gamma_4 = \alpha_i |P\rangle + \beta_i |F\rangle + \gamma_i |G\rangle$)

3.2. 4. <u>The Orbach, Das, and Sharma Mechamism</u>.

This is, in effect, a recalculation of the Blume-Orbach mechanism taking account of configuration interaction. Instead of treating the admixture of higher configurations in the usual manner by second order perturbation theory Orbach, Das and Sharma go back to the S.C.F. one-electron Schrödinger equation 2.12 and add to it an axial perturbing potential. They then solve the resulting equation by numerical integration to obtain s-, d-, and g- like admixtures to the 3d wavefunctions. Using the perturbed wavefunctions the individual ^4F, ^4P and ^4G terms and the $^4\Gamma_4$ levels which arise from them in a cubic field are constructed. Spin orbit coupling is applied to find the

first-order admixture to the $|^6S M_S\rangle$ states and the matrix of $\mathcal{H}_{ax}$ within this manifold of states is evaluated directly.

The Orbach, Das and Sharma mechanism is thus represented by an expression of the form

$$D_o D_S \propto \frac{\langle {}^6S|\mathcal{H}_{so}|{}^4\Gamma_4'\rangle\langle {}^4\Gamma_4'|\mathcal{H}_{ax}|{}^4\Gamma_4'\rangle\langle {}^4\Gamma_4'|\mathcal{H}_{so}|{}^6S\rangle}{[E({}^4\Gamma_4') - E({}^6S)]^2}$$

where the prime denotes the configurationally-admixed states. This reduces to

$$D_o D_S = (B_2^o)^2 (\sqrt{5}/64\pi) \zeta^2 p_{\alpha\gamma}(2p_{\alpha\alpha} - p_{\alpha\beta})(M_2 - 4M_1 + 3M_o) \quad 3.5$$

where M_2 M_1 M_o are expectation values of r^2 averaged between the 3d and admixed g- d- and s- orbitals respectively.

3.2. 5. Other Spin-Spin Mechanisms.

In his original paper Pryce considered only admixture of the configuration $(3d^4 4s)$ into the $3d^5$ configuration by the spin-spin interaction and the axial field. Neither Pryce nor Watanabe performed the detailed atomic calculations necessary to find the magnitude of D but rather relied upon an extraction of the strength of the spin-spin interaction from free ion excited state splittings. This approach has been criticized on the grounds that other interactions which shift the free ion excited levels (e.g. spin-other orbit) may be wrongly included in an estimate of the strength of the spin-spin interaction (Blume & Watson 1965). Blume and Watson

actually calculated the 4s spin-spin admixture and found it to be much smaller than estimated by Pryce. Sharma, Das and Orbach have also recalculated the Pryce term by a somewhat more direct process. The approach closely follows that outlined in the last section: the axial field is added to the one-electron central field Schrödinger equation to obtain s-, d- and g- like admixtures to the 3d orbitals directly. The $|^6S\rangle$ ground term is then constructed out of these modified functions and the matrix of $\mathcal{H}_{ss}$ evaluated directly. In this way Orbach, Das and Sharma found d- and g- like admixtures to be more important than s-like ones and furthermore of opposite sign and so concluded that the original calculations could not have yielded results of the correct sign and magnitude for the zero-field splitting.

3.3. Comparison with Experiment.

Equations 3.2 to 3.5 can be added together to yield an overall expression for the expected dependence of the axial spin Hamiltonian parameter D on the crystal field parameters B_2^0 and $B_4^{0'}$. One final process which should be added is the Watanabe mechanism 3.2 modified by the cubic field which shifts the excited P and D terms. Denoting this by D_{wc}

$$D = D_{Bo} + D_{ss} + D_{oDs} + D_{wc} + D_{w}$$

where the contributions are listed in order of decreasing importance for Mn^{2+} in ZnF_2, the only system for which a detailed analysis exists. (Sharma, Das and Orbach 1966). The Blume Orbach process is the most important followed by the modified Pryce term. The Orbach, Das and Sharma and cubic Watanabe terms are of approximately equal magnitude and of opposite sign virtually cancelling one another, and the least important mechanism is that originally computed by Watanabe. Final agreement between experiment and theory in this case is fairly good.

When a correlation of results over a series of host lattices is attempted, however, the position is not so clear. Take for example the case of Fe^{3+} where attempts have been made to fit the experimental data to an expression of the form

$$D \sim B_2^o - K (B_2^o)^2 \qquad 3.6$$

as would be expected from the Watanabe and Pryce mechanisms.

From a series of measurements of pressure-induced axial distortions in MgO Germanier et. al. (Germanier, Gainon & Lacroix 1962) were able to show fairly conclusively that the sign of the linear term (which arises from the Pryce mechanism) is positive. Assuming the sign of the spin-spin integral M (equation 3.3) does not change on going from Mn to Fe this is in agreement with Watanabe's calculation of the Pryce mechanism and therefore in disagreement with Orbach, Das and Sharma's

more sophisticated calculation of the spin-spin mechanism since they state categorically that the Watanabe result is of the wrong sign. Germanier et. al. also performed some calculations of their own, re-evaluating the Watanabe (spin-orbit) term and adding two additional terms linear in $\mathcal{H}_{ax}$. However, it appears that there must be an error in their calculation somewhere - they give no details - since they obtain a positive sign for the quadratic (Watanabe) term and this has been independently checked by two other authors (Nicholson & Burns 1963, Friedman 1963) and found to be negative in agreement with Watanabe's original calculation. On the basis of point charge calculations of the crystal potential (which can however be rather unreliable unless considerable care is taken) for other lattices where D is known Germanier et. al. also concluded that the sign of the quadratic term in 3.6 must be negative, again in agreement with Watanabe's original calculations. It would however seem (Nicholson and Burns 1963) that the point charge calculations of Germanier et. al. are considerably in error.

From Mössbauer absorption measurements of the nuclear quadrupole splitting of Fe^{3+} substituted into a series of host lattices where D is known Nicholson and Burns (1963) have also been able to obtain a semi-empirical relationship between D and the axial field potential since the nuclear quadrupole splitting is directly proportional

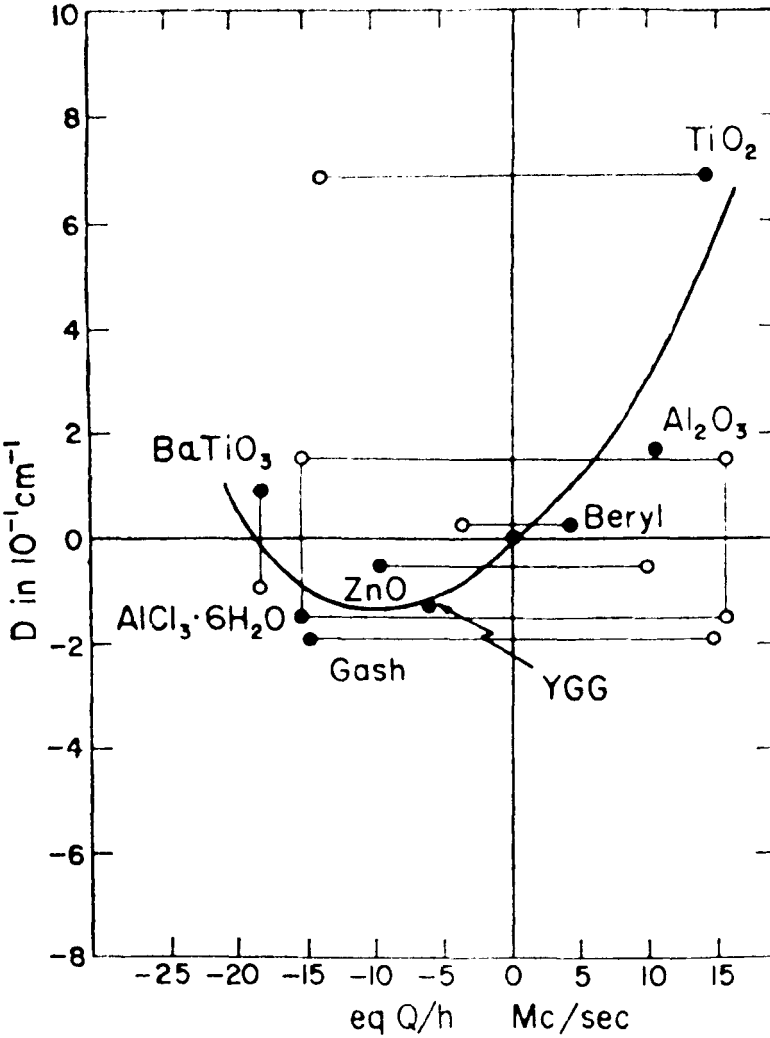

Fig.3.1. The semi-empirical relationship between D and B_2^0 (after Nicholson and Burns)

to the electric field. Nicholson & Burns' results are summarized in fig. 3.1 (reproduced from their paper). Points joined by a solid horizontal line indicate that the sign of B_2^o is uncertain (the Mössbauer measurements only give the magnitude), those joined by a solid vertical line indicate that the sign of D is uncertain. The lines join points of equal magnitude but opposite sign. In order that D be a relatively sensible function of B_2^o the choice of sign indicated by the solid circles must be taken and this leads to a relationship of the form

$$D \sim B_2^o + K(B_2^o)^2$$

albeit with a very wide scatter on the points. Nicholson & Burns' choice of the positive sign for $(B_2^o)^2$ depends on only one point, that for TiO_2 for which the sign of B_2^o is not known with certainty and Nilsen and Kurtz (1964) have more recently produced additional evidence to support the negative sign for the quadratic term: they find D for Fe^{3+} in $ZnWo_4$ to be large and negative while a point charge calculation shows B_2^o to be fairly certainly positive.

There is thus considerable doubt as to the sign of the quadratic term in 3.6 though the positive sign of the linear term would seem to be fairly well established on the basis of the nuclear quadrupole splitting and external pressure measurements. Quantitative agreement, even in cases where the signs are established, is very poor, particularly for Fe^{3+}. For example substituting

appropriate values of the constants for Fe^{3+} in 3.2 and 3.3 gives the expected dependence as

$$D = 0.12\ B_2^0 - 4.12\ (B_2^0)^2$$

where D is in cm^{-1} and B_2^0 in units of $e^2/2a_0^3$, whereas the semi-empiral expression obtained by Germanier et. al. can be rewritten as

$$D = 27\ B_2^0 - 480\ (B_2^0)^2$$

Using values of the nuclear quadrupole moment and antishielding factor for Fe^{3+} given by Chakravarty (1963), the graph drawn by Nicholson and Burns can be fitted to the approximate formula

$$D \simeq 7\ B_2^0 + 10\ (B_2^0)^2$$

Thus it is seen that the semi-empirical formulae differ radically in magnitude as well as sign and in this connexion it is perhaps worth reemphasising that the point charge calculations of Germanier et. al. which lead to the expected negative sign for the quadratic term are almost certainly considerably in error.

It is instructive to compare the results for Fe^{3+} with those obtained for Mn^{2+}. In Al_2O_3 measurements are available of both the nuclear quadrupole splitting factor eq $Q/h = 2Q\ (1 - \gamma_\infty)B_2^0/h$ (Q-nuclear quadrupole moment; γ_∞- antishielding factor) and the zero-field parameter D for both Mn^{2+} and Fe^{3+}. A comparison may be effected via the quantity

$$\Delta = \left[\frac{d\,D}{d(eqQ/h)}\right]_{q\,=\,0}$$

While the magnitude of this quantity cannot be calculated accurately from first principles its dependence on species should be reproduced by theory. Thus it is found experimentally that $\Delta(Fe) \simeq 20 \times \Delta(Mn)$ while using Slater wavefunctions to evaluate the integrals appearing in 3.2 and 3.3 and the free ion term splittings Nicholson & Burns expect $\Delta(Fe) \lesssim \Delta(Mn)$. The value for Mn is in reasonable agreement with the theoretical estimates of Watanabe. This discrepancy between the Mn^{2+} and Fe^{3+} results has been discussed by Chakravarty who suggests that the greater charge of the Fe^{3+} ion pulls in the surrounding ions to give a contribution to B_2^0 over and above that found from the point charge calculations which ignore the presence of the central ion. However, the Mössbauer measurements in Al_2O_3 and $CaCO_3$ where $D(Fe) \simeq 10 \times D(Mn)$ indicate that the crystal field is approximately the same whether Mn^{2+} or Fe^{3+} is substituted.

Summarizing, then, the major difficulties in obtaining accurate expressions for the axial zero field splitting of S-state ions are twofold. Firstly it is difficult to obtain accurate estimates of the parameters of the spin-spin interaction which involve overlap integrals between the ground state and various excited states which have large radial extents and are thus particularly

sensitive to distortions of the electron charge cloud. Secondly point charge calculations of the crystal field potential are extremely sensitive to small changes in the atomic coordinates and can easily yield results of the wrong sign let alone the wrong magnitude if great care is not taken. Finally small amounts of covalent bonding can have a very marked effect on the crystal field strength for S and non-S state ions alike. This last problem has been reviewed by Sugano (1962). Two points are worth mentioning. If the finite spread of the electron cloud at the ligands is taken into account it is found that the d_γ electrons penetrate much nearer to the ligand nuclei than the d_ε ones and the resulting attractive potential can invert the d_γ and d_ε levels with respect to the usual point charge order. Alternatively the point charge and electron penetration effects can cancel one another out and the crystal field splitting may be mainly determined by the exchange interaction between the central metal ion and the ligand electrons. This is thought to be the case in $KNiF_3$ which is traditionally regarded as an ionic crystal.

It seems clear that any successful future theory of the axial splitting of S-state ions, and particularly Fe^{3+} will have to consider at least the cubic field effect discussed by Blume and Orbach and probably

departures from a point charge model as well. It is difficult to see however, how the Blume-Orbach effect can explain the relatively larger splittings in Fe than in Mn since it depends on the admixture of the free ion quartet terms in the cubic field and these lie higher and are more widely spaced in Fe than in Mn. Measurements of large axial zero field splittings in a series of structurally similar host lattices - such as the perovskites - should provide a crucial test of any further attempts to explain the zero-field splitting of S-state ions.

References

Abragam A. and Pryce M.H.L. 1951 — Proc. Roy. Soc. (London) A205, 135

Blume M. and Orbach R. 1962 — Phys. Rev. 127, 1587

Blume M and Watson R.E. 1965 — Phys. Rev. 139A, 1209

Chakravarty A.S. 1963 — J. Chem. Phys. 39, 1004

Elliott R.J. and Stevens K.W.H. 1952 — Proc. Roy. Soc. (London) A215, 437

Friedman E.A. 1963 — unpublished: see Nicholson & Burns 1963

Germanier A.M., Gainon D. et Lacroix R. 1962 — Phys. Lett. 2, 105

Judd B.R. 1955 — Proc. Roy. Soc. (London) A232, 458

Nicholson W.J. and Burns G. 1963 — Phys. Rev. 129, 2490

Nilsen W.G. and Kurtz S.K. 1964 — Phys. Rev. 136A, 262

Orbach R., Das T.P. and Sharma R.R. 1964 — in "Proceedings of the International Conference on Magnetism, Nottingham" (I.P.P.S., London 1965)

Pryce M.H.L. 1950 — Phys. Rev. 80, 1107

Sharma R.R., Das T.P. and Orbach R. 1966 — Phys. Rev. 149, 257

Sharma R.R., Das T.P. and Orbach R. 1968 — to be published

Sugano S. 1962 — J. Appl. Phys. 33, 303

Van Vleck J.H. and Penney W.G. 1934 — Phil. Mag. 17, 961

Watanabe H. 1957 — Prog. Theoret. Phys. (Kyoto) 18, 405

CHAPTER IV

SURVEY OF HOST LATTICES

Introduction

Having considered the theoretical aspects of the zero-field splitting of S-state ions the present chapter is devoted to a description of those lattices which provide suitable hosts for Fe^{3+}. Previously reported E.P.R. spectra are described from the point of view of the information that they give on such topics as covalent binding and ferroelectric phase transitions in the perovskites: particular consideration is given to the ABO_3 perovskite structure.

4.1. Host Lattices for Ferric Iron.

The great majority of lattices give cubic (octahedral or tetrahedral) coordination for a substituted metal ion. For the S-state ions Mn^{2+} and Fe^{3+} this leads, because of the high order of the interactions involved, to small cubic splittings of the ^6S ground state. Small distortions of the regular array of charges lead to splittings of tetragonal or lower symmetry. Since the order of the interaction involved is much lower, splittings comparable with those in the cubic field are readily obtained. Indeed Pryce (1950) suggested that since the spin-orbit mechanism increases rapidly with the effective nuclear charge on the central metal ion the axial splitting should be dominant

in manganous salts while the cubic splitting should be dominant in ferric salts and the early experiments seemed to verify this picture. With low symmetry fields of increasing strength however the axial splitting begins to dominate in both cases and as was seen in the last chapter the splitting of the ferric ion becomes even greater than that of the manganous ion.

There are several classes of host lattices in which strong low symmetry crystal fields give rise to large zero-field splittings for Fe^{3+}. The spectra are usually characterized by an "effective g = 6" signal if the symmetry is tetragonal and an "effective g = 4.3" signal if it is rhombic. The first g = 4.3 signals were obtained from silica glass (Sands 1955, see also Castner et. al. 1960) and in the same year Bennett et. al. (1955) found resonances varying from g = 2 to g = 6 in their investigations of haemoglobin and its derivatives. Since then Wickman et. al. (1965) have obtained a g = 4.3 signal from polycrystalline ferrichrome and resonances due to ferric iron in strong crystal fields have been observed in many other biological systems (Ehrenberg 1966). There are also numerous inorganic crystals which provide similar environments for Fe^{3+} notably the metal oxides, tungstates and (alumino-) silicates. The simple monovalent and divalent metallic oxides tend to form cubic crystals and

give a completely cubic spin Hamiltonian. Trivalent aluminium forms the rhombohedral corundum (Al_2O_3) which gives an axial field for an ion at the Al site (Bogle and Symmons 1959). Quadrivalent titanium forms T_iO_2 and rutile, a tetragonal form, gives a large axial zero-field splitting for Fe^{3+} (Carter and Okaya 1960) and has been used to operate a maser at a frequency near 72 Gc/s. Mixed metal oxides of the form ABO_3 are the main concern of this thesis and will be discussed in the next section. Of the tungstates magnesium (Peter 1959), zinc (Nilsen and Kurtz 1964) and calcium (Kedzie et. al. 1965) all give fairly large splittings and reference will be made again to $CaWO_4$ in which the origin of the observed signals is still uncertain. The alumino-silicates, andalusite (Al_2SiO_5) which is orthorhombic and its triclinic polymorph kyanite give complex spectra and large zero-field splittings (Holuj 1966, Troup and Hutton 1964) as does amethyst, a form of α-quartz (Barry et. al. 1965). The spectrum of Fe^{3+} in topaz ($Al_2SiO_4F_2$) (Thyer et. al. 1967) shows hyperfine structure from the fluorine nuclei as well as a large zero-field splitting. This is direct evidence of covalent bonding and the existence of covalent bonding may also be inferred from the positive g-shifts obtained in several of the other crystals listed above - and also in some of the perovskites to be discussed below. In his original paper Watanabe (1957) showed that within

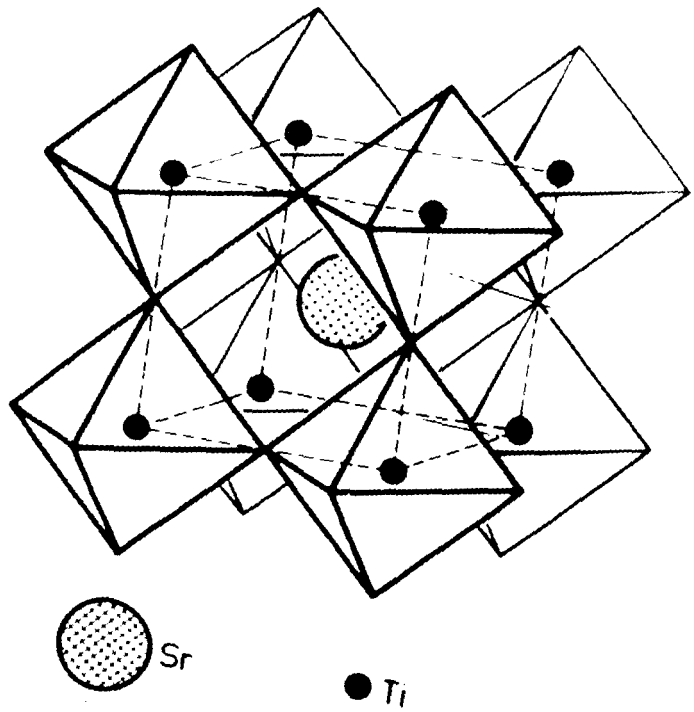

Fig. 4.1. The perovskite structure

the framework of a point charge theory the g-shift for an S-state ion should always be negative. However, in a more recent publication (1964) he shows, specifically for Fe^{3+} in cubic II-VI crystals, that small amounts of covalent admixture between the 3d orbitals and the ligand σ-orbitals via the spin-orbit interaction will lead to positive g-shifts. His calculations give a reasonable explanation of the observed positive g-shifts in MgO and CaO - traditionally regarded as ionic crystals.

The above paragraph is by no means intended to present an exhaustive bibliography and further references may be found in the literature - see e.g. Low (1965) and Thyer (1967).

4.2. Perovskites.

The perovskite structure has the composition ABO_3 and derives its name from the naturally occuring mineral perovskite, $CaTiO_3$. The ideal structure is shown in fig. 4.1. The B ion, commonly Ti^{4+}, is surrounded by a perfect octahedron of oxygen ions whose axes are along the cubic axes. The A ion has twelve nearest oxygen neighbours and eight next-nearest titanium neighbours. The structure may be thought of as a framework of oxygen octahedra linked by their corners into a three-dimensional lattice enclosing large holes in which

the A ions reside. Goldschmidt has defined a tolerance factor, t, for stability of such a structure, such that $R_A + R_O = t\sqrt{2}\ (R_B + R_O)$ where the various R's are the ionic radii of the A, B and O ions. t may vary between 0.77 and 1 and permits a very large number of compounds. Elements of the iron group substitute mainly at the B-site.

Many of the perovskites have very interesting properties. Some such as $BaTiO_3$ and $PbTiO_3$ are ferroelectric at room temperature. The ferroelectric nature of many perovskites is usually regarded as ionic in origin i.e. it is supposed to correspond to a physical displacement of the positive (A^{2+} B^{4+} usually) lattice with respect to the negative (O_3^{2-}) lattice. Other perovskites such as $SrTiO_3$ are non-polar over nearly the whole temperature range. In reduced form this crystal is a semiconductor and becomes superconducting at very low temperatures. $LaMnO_3$ is antiferromagnetic whereas mixed $(La,Sr)MnO_3$ is ferromagnetic. The majority of perovskites undergo phase transitions at well-defined temperatures. $LaAlO_3$ however shows no phase transitions but exhibits a continuous deformation of the lattice as a function of temperature. In addition there are compounds such as $KMgF_3$ which preserve the ideal perovskite structure down to very low temperatures. As yet the extensive series of compounds having the perovskite

structure has received relatively little attention, due mainly to the difficulty of growing good single crystals. The most widely studied have probably been $BaTiO_3$ and $SrTiO_3$. Very few of the crystals have the ideal structure. For a more extensive survey and references to the literature see Low (1965).

Let us consider now individually, and in more detail, the three systems $BaTiO_3$, $PbTiO_3$ and $SrTiO_3$ with which the latter chapters will be concerned.

4.2. 1. $BaTiO_3$

$BaTiO_3$ undergoes three phase transitions. Above 390°K (the ferroelectric Curie point) it is cubic and the dielectric constant follows a Curie-Weiss law. Below the Curie point it becomes ferroelectric. From 390°K down to 278°K it is tetragonal with an axial ratio $c/a \simeq 1.011$. From 278°K down to 183°K it is orthorhombic and below 183°K, rhombohedral. At the 390°K phase transition the tetragonal E.P.R. spectrum collapses sharply into the cubic one indicating a first order transition. Such a transition is also indicated by the polarization and dielectric constant measurements. The lower temperature transitions have not been studied in detail but they are probably also first order (Megaw 1957). E.P.R. studies of the orthorhombic and rhombohedral phases have recently been reported by Takeda (1968).

When a single crystal undergoes transition from cubic to tetragonal the tetrad axis (c-axis) may be along any one of the three original cube edges. If the crystal is small and perfect it may transform to a single tetragonal crystal, otherwise it will twin in such a way as to reduce internal stresses to a minimum. Two kinds of twin are possible, 180° or 90°. 180° twins are magnetically equivalent and correspond to a reversal of the direction of the c-axis while the 90° twins, or more exactly $2 \tan^{-1} c/a = 90^\circ 38'$, correspond to a 90° rotation of the c-axis. In the tetragonal phase $BaTiO_3$ thus exhibits three more-or-less mutually perpendicular "domains" and in most crystals, which are in the form of thin plates, the majority of the crystal is "c-domain" i.e. has the c-axis perpendicular to the plane of the plate. The domain structure is also reflected in the optical properties of the crystal. Below the Curie point $BaTiO_3$ is doubly-refracting and extinguishes when examined under crossed nicols if either polarizer or analyzer is parallel to the tetrad axis. This provides a very convenient method of orientating crystals for E.P.R. work.

The Fe^{3+} spectrum in $BaTiO_3$ has been widely studied (Hornig et. al. 1959). Most of the results relate to the tetragonal spectrum, and in particular to c-domains. The tetragonal splitting is found to be temperature-dependent. In the cubic phase the cubic splitting is of

the same order of magnitude as that observed in MgO, $SrTiO_3$ and TiO_2 and this is taken as evidence that the Fe^{3+} ion substitutes at the Ti-site in $BaTiO_3$ where it will be surrounded, as in MgO, $SrTiO_3$ and TiO_2, by a regular octahedron of oxygen ions.

In addition to the above spectra Gainon (1965) has recently observed a spectrum at 77°K with $g_\perp \simeq 6$, $g_\parallel \simeq 2$ characteristic of Fe^{3+} in a strong axial field. This is thought to be produced by charge compensation at a nearest neighbour oxygen-ion vacancy.

4.2. 2. $PbTiO_3$

Most of the remarks of the previous section apply to $PbTiO_3$ as well as to $BaTiO_3$. At room temperature $PbTiO_3$ is tetragonal with an axial ratio c/a = 1.063 and is isomorphous with the tetragonal phase of $BaTiO_3$. The Curie point is 770°K. The only reported E.P.R. work is by Gainon (1964) who found an axial spectrum with $g_\perp \sim 5.97$, $g_\parallel \sim 2$ at X-band, again characteristic of Fe^{3+} in a strong tetragonal field. In this case this is the only spectrum observed and the large g -factor shows that the initial splitting must be larger than the normal tetragonal splitting in $BaTiO_3$, presumably because the axial ratio c/a is considerably greater. This spectrum could be produced by charge compensation but this would imply that all the Fe^{3+} centres are locally compensated

in an equivalent manner since no other spectrum due to Fe^{3+} is observed.

Gainon's measurements were not carried as far as the phase transition and he found no appreciable change in the spectrum between 150°K and 570°K. The initial splitting and $g_\perp$ would however be expected to be temperature dependent. Another phase transition has been reported at about 170°K (Kobayaski et. al. 1956) though Gainon's measurements do not indicate this. In the present work measurements have been made below the phase transition and the low temperature structure will be considered more fully in the final chapter. The low temperature phase is reportedly not ferroelectric.

4.2. 3. $SrTiO_3$

Unlike $PbTiO_3$ and $BaTiO_3$ this crystal has the ideal perovskite structure at room temperature. It undergoes phase transitions to tetragonal at 110°K, orthorhombic at 65°K, and possibly rhombohedral at 10°K (Lytle 1964). No definitive evidence has been produced to show that any of these phases are ferroelectric, although above 110°K the dielectric constant does follow a Curie-Weiss law. The E.P.R. spectra show a smooth transition from tetragonal to cubic structure probably indicative of a second-order transition. No

evidence from E.P.R. spectra has yet been found for the lower temperature transitions.

Below 110°K the spectra may again be interpreted as arising from three mutually perpendicular "domains". The iron group E.P.R. spectra in this phase are dominantly cubic with small tetragonal distortions along the cubic axes (Müller 1959) - the distortion of the cubic structure is very small indeed - much less than in $BaTiO_3$ where the spectrum is dominantly tetragonal. This is certainly true for the titanium-site (where the iron group elements substitute) although the results from the rare earths, which, it is believed, substitute predominantly at the strontium site, are not so consistent and the strontium site may undergo a somewhat larger displacement (Rimai and DeMars 1962). Both the cubic and axial terms in the Hamiltonian in the tetragonal phase are temperature dependent (Dobrov et. al. 1959).

In addition to the tetragonal splitting below 110°K Unoki and Sakudo (1967) have shown that there is a rotation, in the (100) plane, of the oxygen octahedra surrounding the Ti ions, the angle of rotation being small and temperature dependent. Evidence for this was provided by a careful study of the additional splittings observed in the Fe^{3+} spectrum which had previously been attributed to the formation of inequivalent domains. Confirmation that it is only the oxygen octahedra that rotate is provided

by the Gd^{3+} spectrum from the Sr-site in which no additional splittings are observed. The rotation goes some way towards explaining the anomalously large splittings of the rare-earth spectra at the Sr-site. The strong axial spectrum of Fe^{3+} (see below) is also found to undergo some additional splitting below 110°K corresponding to rotations of oxygen octahedra of about 30% less than for the normal site. In addition, in the low temperature phase still further splittings of the strong axial lines have been observed and it is thought that these may correspond to small cooperative movements of the Ti^{4+} cations (Unoki and Sakudo 1967). Such a movement, the "off-centre effect" (Megaw 1957) is well known, though not from E.P.R. work, and is thought to be directly related to the occurence of ferroelectricity. It is almost impossible to see how such a distortion could come about within a regular or nearly regular octahedron from purely ionic forces and suggests that the Ti - O bonds are to some extent directed, in which case they must have some covalent character. It is known that Pb^{2+} has a tendency to form unsymmetrical covalent bonds and it appears that in $PbTiO_3$ the covalent Pb-O system creates conditions which favour the development of unsymmetrical Ti-O bonds. It is not yet clear whether it is best to regard the permanent dipole moment giving rise to the ferroelectricity as arising directly from

distortions of the Pb-O cuboctahedron or whether the Pb plays an indirect role in producing a polarization in the oxygen octahedron surrounding the Ti atom. For a much fuller account see Megaw (1957).

Recently Kirkpatrick et. al. (1964) have found an axial spectrum with $g_{\parallel} \sim 2$, $g_{\perp} \sim 6$ in the cubic phase of $SrTiO_3$ and this they attribute to Fe^{3+} in the strong tetragonal field produced by local charge compensation at a nearest neighbour site (oxygen ion vacancy). From the frequency dependence of $g_{\perp}^{eff}$ at X- and K-bands Kirkpatrick et. al. concluded that $2D \sim 2.85$ cm^{-1}, though Low (1965) subsequently failed to observe the expected zero-field transitions and suggested that the zero-field splitting would have to be much greater than this. This spectrum has now been re-examined at millimetre wavelengths in the present work and the zero-field splitting accurately determined confirming the original predictions of Kirkpatrick et. al. The spectrum consists of three sets of lines with mutually perpendicular tetragonal axes: the axial field can occur along any one of three equivalent Ti^{4+} - oxygen ion vacancy directions which are along the original cube edges.

4.3. The Origin of the "g = 6" Signal.

Repeated reference has been made in the previous

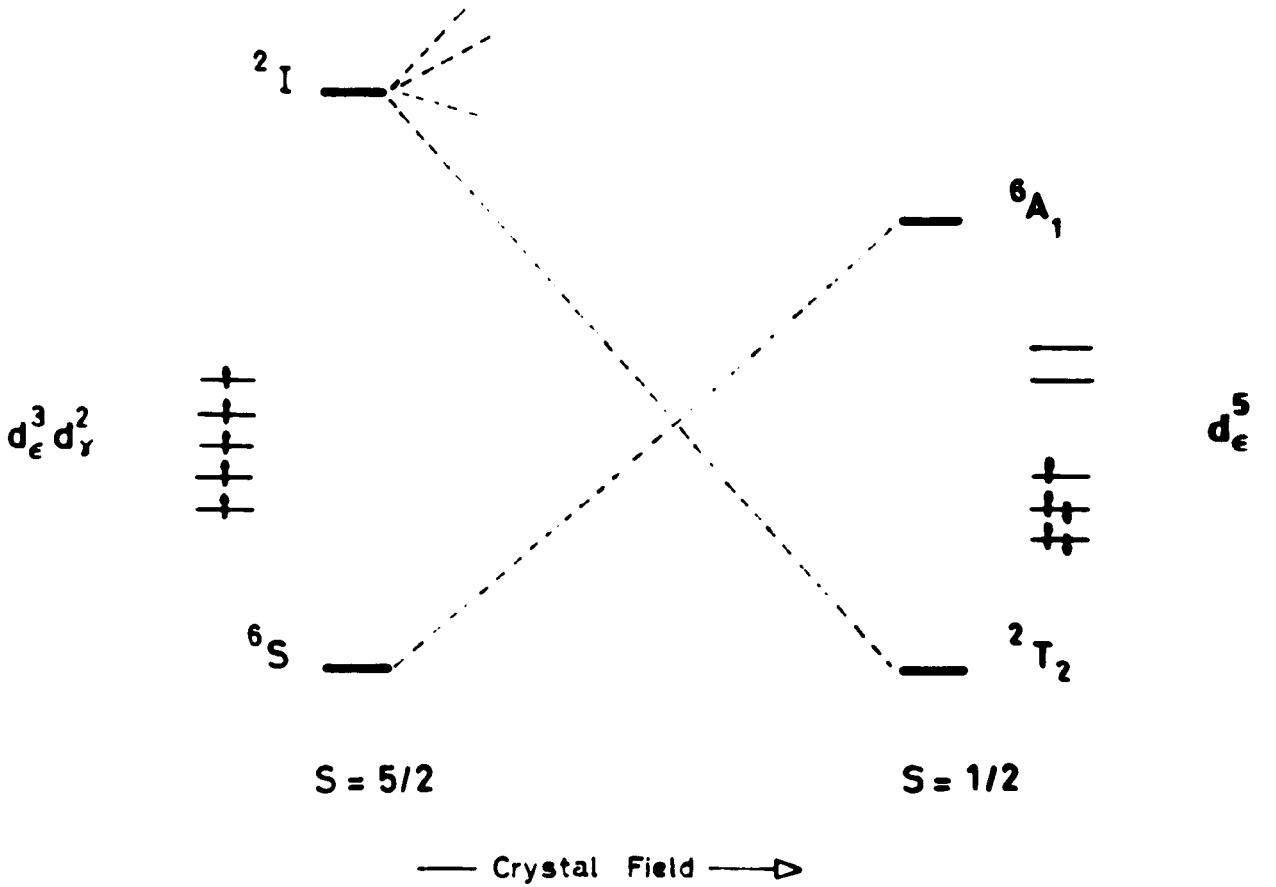

Fig. 4.2. Formation of high and low spin derivatives for d^5

sections to the g = 6 signal characteristic of ferric iron in a strong axial crystal field and it is instructive to consider why the resonance arises at this particular g-value. At this point, however, it is perhaps advisable to clear up a possible misunderstanding over the use of the adjective "strong". In text books on ligand field theory the adjective "strong" is usually used to describe crystal fields which dominate over the electrostatic repulsion term in the Hamiltonian and lead to "low-spin" rather than "high spin" derivatives. This is illustrated for the case of Fe^{3+} in fig. 4.2. If the interelectronic repulsion is stronger than the crystal field then Hund's rules apply and the five d-electrons will all go into different orbital levels leaving S = 5/2. If on the other hand the crystal field splits the d_γ levels off very much higher than the d_ϵ ones it will be energetically more favourable for the electrons to spin-pair rather than to go into the high lying d_γ orbital levels. Hund's rules will thus be violated and all the electrons will go into the d_ϵ levels leaving S = 1/2.

The above usage of the word "strong" has been assumed in chapter II of this Thesis when the relative magnitudes of the various terms in the paramagnetic ion Hamiltonian were under discussion. In all other parts of this Thesis, however, and in particular in the title

and in the present chapter a "strong" field is to be taken to mean one which while it is much stronger than those often encountered in E.P.R. work is nevertheless not sufficiently strong to force spin-pairing and is therefore "weak" in the above sense. This ambiguity in nomenclature is perhaps unfortunate but is well entrenched in the literature.

Returning to the original discussion the Hamiltonian for Fe^{3+} in a field of tetragonal symmetry is given by 2.23 as

$$\mathcal{H}_S = g_\perp \beta (H_x S_x + H_y S_y) + g_{\parallel} H_z S_z + D S_z^2 + \frac{F}{36}(7 S_z^4 - \frac{95}{2} S_z^2) + \frac{a}{6}(S_x^4 + S_y^4 + S_z^4) \qquad 4.1$$

if the symmetry is purely axial and the zero-field splitting so great that only transitions between the lowest $\pm 1/2$ levels can be observed then the secular determinant for H parallel to z becomes

	1/2	-1/2
1/2	$D/4 + \frac{1}{2} g_{\parallel} \beta H_z - E$	0
-1/2	0	$D/4 - \frac{1}{2} g_{\parallel} \beta H_z - E$

leading to $E = " g_{\parallel}^{eff} \beta H_z " = g_{\parallel} \beta H_z$

and $g_{\parallel}^{eff} = g_{\parallel} = 2$

And for H parallel to x

	1/2	-1/2
1/2	$D/4 - E$	$\frac{3}{2} g_\perp \beta H_x$
-1/2	$\frac{3}{2} g_\perp \beta H_x$	$D/4 - E$

leading to $\Delta E = "g_{\perp}^{eff} \beta H_x " = 3 g_{\perp} \beta H_x$

and $g_{\perp}^{eff} = 3 g_{\perp} = 6$

The spectrum can thus be described by a "fictitious spin" $S' = 1/2$ with $g_{\parallel} = 2$, $g_{\perp} = 6$. In a situation, however, where the Zeeman energy while still small is nevertheless not negligible, admixture between the various substates of $S = 5/2$ must be considered. Such a situation may be treated by perturbation theory and it will be convenient to summarize the results here for future reference.

In the full matrix of 4.1 for H parallel to Z the $\pm 1/2$ states still form a block i.e. they are not mixed with any of the other states in the $S = 5/2$ manifold by the zerofield or Zeeman terms and consequently we still have $g_{\parallel}^{eff} = g_{\parallel}$. For H parallel to x the matrix of 4.1 can be written as

	5/2	3/2	1/2	-1/2	-3/2	-5/2
5/2	A	$\sqrt{5}$ C	0	0	G	0
3/2	$\sqrt{5}$ C	B	$2\sqrt{2}$ C	0	0	G
1/2	0	$2\sqrt{2}$ C	0	3 C	0	0
-1/2	0	0	3 C	0	$2\sqrt{2}$ C	0
-3/2	G	0	0	$2\sqrt{2}$ C	B	$\sqrt{5}$ C
-5/2	0	G	0	0	$\sqrt{5}$ C	A

4.2

where $A = 6D - a/2 - F/3$

$B = 2D + 5a/a - 5F/3$

$C = \frac{1}{2} g \beta H$

$G = 5a/2$

and a constant factor has been subtracted from the leading diagonal so that the $\pm 1/2$ doublet in zero-field is the zero of energy. In order to be able to use perturbation theory to calculate the g-value of the $\pm 1/2$ doublet 4.2 must be transposed to a form in which the $\pm 1/2$ states are, to first order, diagonal. Doing this we obtain

	5/2	3/2	α	β	-3/2	-5/2
5/2	A	$\sqrt{5}$ C	0	0	G	0
3/2	$\sqrt{5}$ C	B	2 C	2 C	0	G
α	0	2 C	3 C	0	2 C	0
β	0	2 C	0	-3 C	-2 C	0
-3/2	G	0	2 C	-2 C	B	$\sqrt{5}$ C
-5/2	0	G	0	0	$\sqrt{5}$ C	A

4.3

where $\alpha = \frac{1}{\sqrt{2}} \left[|1/2\rangle + |-1/2\rangle \right]$ and $\beta = \frac{1}{\sqrt{2}} \left[|1/2\rangle - |-1/2\rangle \right]$, and applying perturbation theory to the $|\alpha\rangle, |\beta\rangle$ states leads, in third order, to

$$\Delta E = E_\alpha - E_\beta = "g_\perp^{\,eff} \beta H" = 6 C \left[1 - 2 \left(\frac{2 C}{\Delta^2} \right)^2 \right]$$

and hence

$$g_\perp^{\,eff} = 3 g_\perp = \left[1 - 2 \frac{(g_\perp \beta H)^2}{\Delta^2} \right] \qquad 4.4.$$

where $\Delta = 2 D - 5a/2 - 5F/3$.

It should be noticed that the additional terms "a" and "F" have no off-diagonal matrix elements connecting the $\pm$ 1/2 states with the rest of the manifold and hence that 4.4. is the same as given by Kirkpatrick et. al. (1964) except that 2D is replaced by an expression in a, D and F. It is also instructive to notice that the cubic term connects only the $\pm$ 3/2 and $\mp$ 5/2 states and has thus only an indirect effect (via admixture of the modified $\pm$ 3/2 states by the magnetic field) upon the $\pm$ 1/2 levels.

References

Barry T.I., Mcnamara P., and Moore W.J. 1965, J.Chem. Phys. 42, 2599

Bennett J.E., Ingram D.J.E., George P., and Griffith J.S. 1955, Nature 176, 394

Bogle G.S. and Symmons H.F., 1959, Proc. Phys. Soc. 73, 531

Carter D.L. and Okaya A., 1960, Phys. Rev. 118, 1485

Castner T., Newell G.S., Holton W.C. and Slichter C.P., 1960, J. Chem. Phys. 32, 668

Dobrov W.I., Vieth R.F., and Browne M.E., 1959, Phys. Rev. 115, 79

Ehrenberg A., 1966, Ed. "Second International Conference on Magnetic Resonance in Biological Systems" Wenner-Gren Symposium Series Vol. 9 (Pergamon, Oxford 1967)

Gainon D.J.A., 1964, Phys. Rev. 134A, 1300

Gainon D.J.A., 1965, J. Appl. Phys. 36, 2325

Holuj F., Thyer R.J. and Hedgecock N.E., 1966, Can. J. Phys. 44, 509

Hornig A.W., Rempel R.C., and Weaver H.E., 1959 J. Phys. Chem. Sol. 10, 1

Kedzie R.W., Lyons D.H. and Kiestigan M., 1965, Phys. Rev. 138A, 918

Kirkpatrick E.S., Müller K.A., and Rubins R.S., 1964, Phys. Rev. 135A, 86

Kobayashi J., Okamoto S., and Ueda R., 1956, Phys. Rev. 103, 830

Low W., 1965, Solid State Physics, 17, 135

Lytle F.W., 1964, J. Appl. Phys. 35, 2212

Megaw H., 1957, "Ferroelectricity in Crystals" (Methuen, London)

Müller K.A., 1959, Helv. Physica Acta 31, 173

Nilsen W.G. and Kurtz S.K., 1964, Phys. Rev. 136, A262

Peter M, 1959, Phys. Rev. 113, 801

Pryce M.H.L., 1950, Phys. Rev. 80, 1107

Rimai L. and deMars G.A., 1962, Phys. Rev. 127, 702

Sands R.H. 1955, Phys. Rev. 99, 1222

Takeda T., 1968, J. Phys. Soc. Jap. 24, 533

Thyer J.R., Quick S.M., and Holuj F., 1967, Can. J. Phys. 45, 3597

Troup G.J., and Hutton D.R., 1964, Brit. J. Appl. Phys. 15, 1493

Unoki H., and Sakudo T., 1967, J. Phys. Soc. Jap, 23, 546

Watanabe H., 1957, Prog. Theoret. Phys. (Kyoto) 18, 405

Watanabe H., 1964, J. Chem. Phys. Solids 25, 1471

Wemple S.H., 1963, Ph.D. Thesis M.I.T.

Wickman H.H., Klein M.P., and Shirley D.A., 1965, J. Chem. Phys. 42, 2113

CHAPTER V

EXPERIMENTAL TECHNIQUES

Introduction.

In this chapter the basic experimental techniques of Electron Paramagnetic Resonance Spectroscopy are outlined as a prelude to a discussion of millimetre wave spectrometers in general and a more detailed description of the 4mm. spectrometer used in the present work.

5.1. Basic Spectrometer Systems.

The basic E.P.R. experiment as was seen in Chapter II involves detecting the absorption from, or change in phase of, an r.f. field when it is swept through the resonance frequency of a paramagnetic sample placed in a static magnetic field. The basic E.P.R. spectrometer would thus consist of a microwave generator feeding power past a sample in a waveguide placed in a static magnetic field. The resonance would be detected as a drop in the power incident on a crystal rectifier placed at the far end of the waveguide when either the microwave frequency or magnetic field were swept through the resonance. In practise it would be usual to sweep the magnetic field since the characteristics of the microwave components are frequency dependent. While this simple direct transmission system could reasonably form

the basis of a gaseous absorption spectrometer it would be very insensitive for single crystal work when only a very small sample is available. In this case it is usual to employ some sort of resonant structure to concentrate the microwave energy in the region of the sample, and it is also customary to use an a.c. method of detection.

5.1. 1. Microwave Systems.

The first addition to the simple direct transmission spectrometer is usually a cavity in which a standing wave pattern is set up and in which the sample is placed. This has the effect of concentrating the oscillating magnetic field, h_1, at the sample and improving the sensitivity since the power absorbed is given by

$$P = \tfrac{1}{2}\omega h_1^2 \chi'' \qquad 5.1$$

where ω is the microwave frequency and χ'' the complex susceptibility as defined in Eq. 2.9. In general the signal ultimately observed is increased by the product of the quality or Q-factor of the cavity which is given by

$$Q = \omega \times \frac{\text{energy stored in cavity}}{\text{power dissipated per cycle}} \qquad 5.2$$

and is commonly of the order of several thousands, and the filling factor η defined by

$$\eta = \int_{\text{sample}} h_1^2 \, dV \Big/ \int_{\text{cavity}} h_1^2 \, dV \qquad 5.3$$

which makes allowance for the fact that the sample may not fill the cavity.

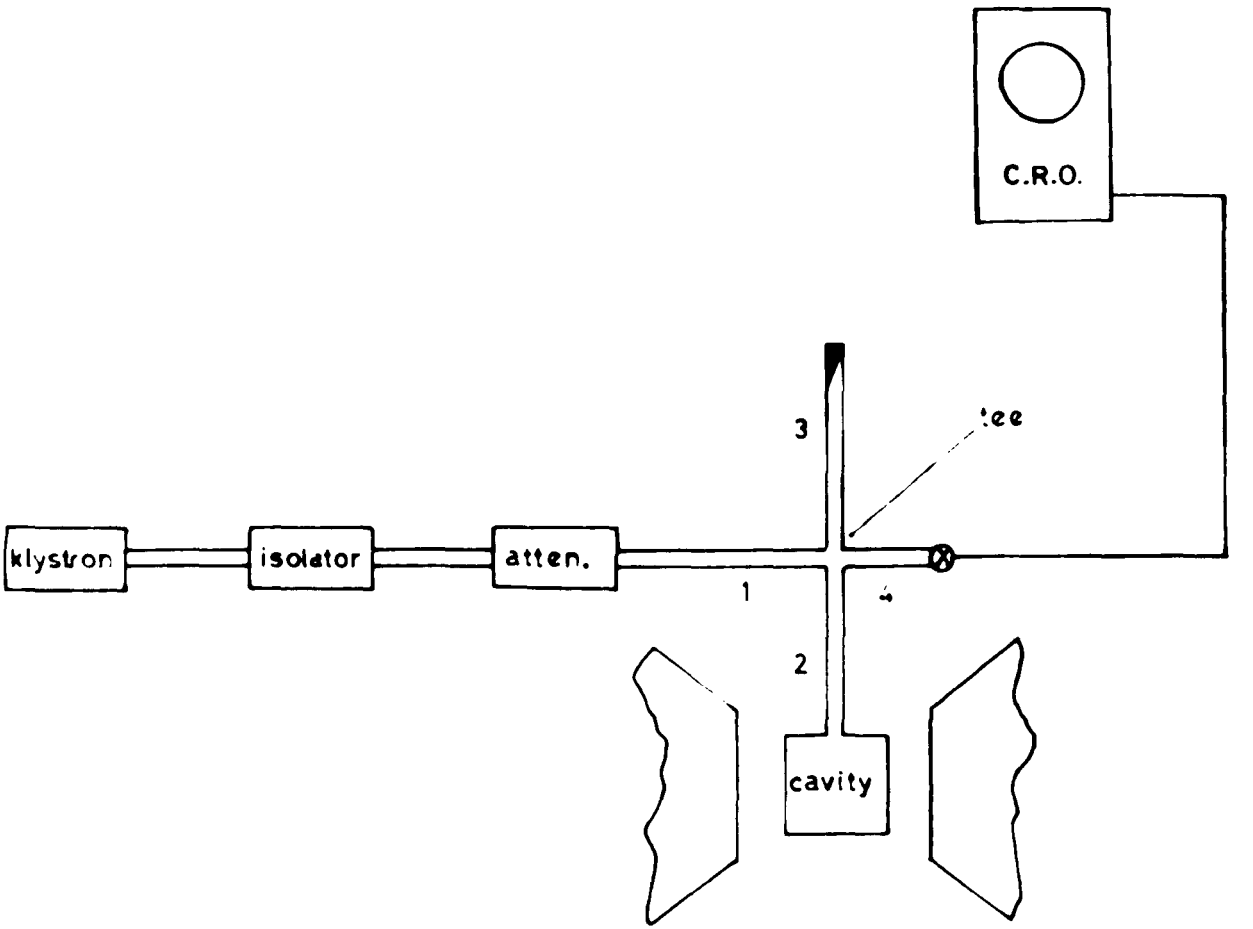

Fig. 5.1. Simple bridge reflection spectrometer

The direct transmission spectrometer suffers from the disadvantage that the power at the crystal cannot be adjusted independently of that at the cavity. It is desirable to be able to do this since the commonest microwave detector, the crystal rectifier, has an optimum working point governed by the amount of power on it: both conversion efficiency and noise power increase with incident power. In practise it is usual to bias the crystal detector either by a "bucking" arrangement - coupling a small amount of power off before the cavity and feeding it direct to the detector - or by using the type of microwave bridge arrangement shown in fig. 5.1. in conjunction with a reflection cavity. Here the power is fed to a "magic tee" which has the property that if arms 2 and 3 are matched and terminated by equal impedances then the power fed into arm 1 is equally divided between arms 2 and 3 and none goes to arm 4. The resonance is now best thought of as causing a change in the effective Q-factor of the cavity and hence a mismatch of the bridge. The signal at a detector placed in arm 4 of the bridge is proportional to the degree of mismatching. In practise it is usual to include a slide-screw tuner or attenuator and variable short circuit in arm 3 to reflect an amount of power variable in both phase and amplitude to slightly unbalance the bridge even in the absence of an E.P.R. signal. This serves to provide a constant bias on the

detector and ensures that the signal in arm 4 can be made a function of either χ' or χ''.

The behaviour of the cavity on resonance may be discussed in terms of an equivalent R, L, C circuit where R, L and C are the lumped equivalent resistance, inductance and capacitance of the cavity. The impedance on resonance can be shown to be given by

$$Z_R = R(1+4\pi\eta Q\chi'') + i\omega L.4\pi\eta\chi'/(1+4\pi\eta\chi) \qquad 5.4$$

Since the resistive term governs the energy dissipation eq. 5.4 shows that the resonant structure augments the effect of χ'' by a factor ηQ. Further the real part of the susceptibility χ' is seen to contribute a frequency dependent term which can lead to appreciable detuning of the cavity on sweeping through resonance if χ' is large (dispersion). This may be overcome either by tuning the microwave bridge to be sensitive to resistive unbalance but not to reactive unbalance, or better by locking the klystron frequency onto the sample cavity. In the latter case the klystron frequency follows the cavity shift through resonance, the reactive term is automatically compensated out, and pure absorption is observed.

Two methods of locking the klystron frequency are commonly in use. The original Pound system (see e.g. Ingram 1967) and the more direct klystron modulation

system. The latter system simply introduces a small modulation of the klystron reflector voltage at about 10 Kc/s. As the klystron drifts off the cavity resonance there is a reflected signal at the modulation frequency. Precisely on the cavity resonance there is no reflected signal at that frequency. If the reflected signal is phase-sensitive-detected a d.c. error signal is obtained which can be applied to the reflector to retune the klystron to the cavity resonance. This is the principle of "automatic frequency control" or a.f.c. Automatic frequency control also serves to reduce the noise arising from frequency instabilities in the microwave generator and random fluctuations of the resonant frequency of the sample cavity and is widely used. Many more sophisticated microwave systems have been described for improving spectrometer sensitivities, notably the techniques of balanced mixing and superhetrodyning. A comprehensive discussion is given by Poole (1967).

5.1. 2. Display and Detection Systems.

In most practical spectrometer systems the signal is detected by an a.c. method. In principle it is possible to amplitude modulate either the static magnetic field or the microwave power in order to achieve this. Both lead to a convenient form of signal display but the former method is almost always used. This is because the

signal intensity is directly proportional to the microwave power and if a power amplitude modulation were used the microwave carrier would have to be kept constant to within about 10^{-13} volts R.M.S. - a typical voltage change from a weak E.P.R. signal.

Two methods of magnetic field modulation and display are commonly in use, the so-called "crystal-video" and phase-sensitive-detection systems. In the former system a low frequency large amplitude modulation is used, sufficient to sweep over a range much larger than the E.P.R. linewidth. The detector output is amplified in a wide band amplifier and fed direct to a C.R.O., the horizontal plates of which are fed from the same source as the modulation via a phase-shifter to obtain a static display of the signal. This method is rather insensitive since all the noise generated at or before the detector is passed by the amplification system. The second method is a narrow-band approach and involves the use of a small magnetic field modulation - much less than the linewidth - superimposed on the static field which is varied slowly through the resonance. The detector output then contains a signal proportional to the first derivative of the E.P.R. line. This signal is then mixed with one obtained from the modulation source via a phase-shifter and the mixer (phase-sensitive-detector or p.s.d.) output can

be shown to contain a low frequency component whose amplitude is proportional to the amplitude of the detected signal multiplied by the cosine of the angle between it and the reference signal. The p.s.d. output is thus also proportional to the first derivative of the E.P.R. signal and is usually fed direct to a pen recorder for display purposes. Signals that have no fixed phase relative to the reference signal produce only transient effects in the output and these are generally further attenuated by an RC network on the p.s.d. output. The bandwidth of the detecting system can thus commonly be made as low as 1 c/s with a commensurate enhancement of the sensitivity. When employing phase sensitive detection it is essential that the modulation amplitude should be small in comparison with the linewidth and that the line should be swept through slowly in comparison with the time constant in order to obtain a true portrayal of the line.

5.2. Sensitivity Considerations.

The ultimate sensitivity of an E.P.R. spectrometer is usually specified as either the minimum detectable r.f. susceptibility or the minimum detectable number of free spins per gauss linewidth. (Feher 1957, Poole 1967). Two cases may be distinguished depending upon whether the sample is placed in a cavity or in short circuited waveguide.

In the case of an optimally coupled reflection cavity and a linear detector the maximum fractional voltage change obtainable on resonance is (Feher 1957)

$$\frac{\Delta V}{V} = \sqrt{2}\,\chi''\,\eta\,Q_0\,\pi \qquad 5.5.$$

The theoretical minimum detectable signal is obtained by assuming an ideal detector and equating ΔV to the R.M.S. Johnson noise voltage generated across an impedance R_0 at temperature T matched to the waveguide. Thus

$$V = \sqrt{2kTR_0\Delta f} \qquad 5.6$$

where k is the Boltzmann constant, R_0 the characteristic impedance of the waveguide and Δf the bandwidth, and

$$\chi''_{min} = \frac{1}{\pi\eta Q_0}\left(\frac{kT\Delta f}{2P_0}\right)^{1/2} \qquad 5.7$$

where $P_0 = V^2/2R_0$.

Equation 5.7 is idealized in that it neglects the noise which will be generated by random amplitude and frequency fluctuations at the microwave source, by the crystal itself - which will also contribute an insertion loss if it is not 100% efficient - and by the early stage amplifiers which generate their own noise in addition to amplifying an impressed signal. The expression for χ''_{min} must thus be multiplied by an appropriate factor, always greater than unity, to take account of these effects. For a paramagnetic system obeying the Bloch equations and the Curie law Eq. 5.7 can be further modified to yield the minimum detectable number of free spins (Poole 1967).

In shorted waveguide the power absorbed per unit volume by the sample is as given by Eq. 5.1 and hence the change in power on resonance is

$$\Delta P = \tfrac{1}{2}\omega\chi'' \int^{V} h_1^2 \, dV \qquad 5.8$$

and the corresponding voltage change is given by

$$\Delta V = \frac{R_o}{2V}\Delta P = \frac{R_o\omega\chi''}{2V}\int h_1^2 \, dV \qquad 5.9$$

This is again equated to the Johnson noise voltage across R_o to give

$$\chi''_{min} = \frac{2\sqrt{2}}{\zeta}\left(\frac{kT\Delta f}{2P_o}\right)^{1/2} \qquad 5.10$$

where $\zeta = \dfrac{\omega\int h_1^2 \, dV}{P_o}$ is analagous to the filling factor η.

The sensitivity in shorted waveguide is thus reduced by a factor $2\sqrt{2}\pi Q_o (\eta/\zeta)$ and the improvement gained from the Q of the resonant cavity may in certain circumstances be largely offset by the fact that ζ may be much greater than η.

5.3. Millimetre Wavelength Spectroscopy.

Since most of the results to be described in this thesis have been obtained on a 4mm. spectrometer and since such short wavelength spectrometers are, at the present time, rather unusual equipment a brief discussion of the particular problems involved will now be given.

5.3. 1. Generation of Millimetre Radiation.

Until recent years millimetre power has probably

been most commonly obtained be harmonic generation from longer wavelengths. The simplest method is to use the non-linear properties of an ordinary microwave crystal rectifier placed across the junction of a pair of crossed waveguides. The waveguide dimensions in one direction are such as to propagate the dominant mode at the fundamental frequency, and in the other direction such as to propagate the dominant mode at the desired harmonic frequency. The power generated in an ideal resistive element of this type can be shown to be proportional to n^{-2} where n is the order of the harmonic. This ideal can never be achieved in practise and a more common conversion loss for a 4mm. generator utilizing second harmonic power from a Q-band klystron is about 20-30dB (Johnson et. al. 1954). Unless a large amount of fundamental power is available the power obtainable at short millimetre wavelengths is thus rather limited.

An alternative approach to the production of millimetre radiation has been made by scaling down conventional klystrons. Such tubes require increasingly small and accurate dimensions and reduced tolerances in the electron beam focus. They are very expensive to manufacture and have relatively short lives, but nevertheless several klystrons are now available which will produce up to 100 mW of power at 4 and 2 mm. wavelengths.

There are several other sources of millimetre radiation which are either too noisy or give too little power to be useful as E.P.R. spectroscopy sources and the only other source in relatively common use is the backward wave oscillator. This employs a slow wave helix structure to extract energy from an electron beam and has the great advantage that it is non-resonant and can be tuned over a wide range by simply altering the beam voltage. Its disadvantages are again high cost and short life though it is an ideal instrument for the measurement of zero-field splittings (Peter 1959, Mock 1960).

5.3. 2. Waveguide Components.

These are usually simply scaled down versions of standard components. This approach is still feasible at 2mm. wavelengths though the manufacturing problems are considerable (Van Es 1960). Problems of attenuation are however encountered when long waveguide runs are required. The attenuation due to ohmic losses in the waveguide walls is frequency dependent and increases as the dimensions of the guide and the wavelength are lowered. The effect is accelerated by the fact that the surface resistance of the guide also increases as the wavelength is lowered. At short wavelengths it thus becomes a worthwhile proposition to launch the wave into oversized waveguide in order to alleviate some of these problems.

This is quite an acceptable procedure provided that the mode in the fundamental guide can be transferred to the oversized guide without generating any of the many degenerate modes which the latter will be able to support since these will constitute lost power when the wave is again recoupled to the standard guide. In practice satisfactory results can be obtained from carefully constructed tapers provided that the slope is less than about 10°. Many of the components normally required for E.P.R. work can be constructed in oversized waveguide though care must be taken to avoid the generation of high order modes and a combination of optical and conventional waveguide techniques must usually be used. (Taub 1963).

Microwave resonators, for use as wavemeters, reference cavities and sample cavities can still be used at 4mm. although due to difficulties in machining to the close tolerances required and to the decrease in electrical conductivity with increasing frequency Q-factors are not as good as those obtained at longer wavelengths. The former difficulty can be partially overcome by using higher order modes though in using this approach to construct a sample cavity care would have to be taken to suppress unwanted modes if the filling factor were not to be decreased.

Another approach is to use a dielectric cavity resonator. (Rosenbaum 1964). This consists of a

dielectric tube bounded by two metal endplates. Since the resonant modes of such a structure are a function of the dielectric constant and thickness of the tube as well as the overall dimensions of the resonator, it is in principle possible to construct a low order cavity which is physically larger, and therefore more accurately machinable, than the corresponding all-metal cavity. Below 4mm. it is at present more usual to make use of the greater filling factor obtainable in shorted waveguide as suggested by equations 5.7 and 5.10 especially since all other factors being equal the sensitivity is proportional to the three-halves power of the frequency anyway (Poole 1967).

5.3. 3. Detection.

Numerous detecting elements are available in the short millimetre wavelength region of the spectrum. Conventional point-contact crystal detectors and bolometers can be used although as the wavelength is reduced the performance of the crystal detector deteriorates due to the shunting effect of the contact capacitance. At 4mm. wavelengths crystal detectors are supplied as usual in sealed cartridges though at shorter wavelengths it is more practicable to make the point contact in situ since this removes the possibility of reflections from the detector window and enables many whiskers to be used with one crystal.

The Golay detector which is extensively used in the infrared region has also been used to detect millimetre radiation, its principal disadvantages being a slow response time and susceptibility to microphony. In addition there are various photodetectors which rely on an increase in conductivity following a band gap transition and the In Sb (Putley) detector in which the radiation is absorbed by the free carriers, raising them above the lattice temperature and thereby increasing their mobility and hence the conductivity. Some comparative tests of an InSb detector available for a short while indicated that its sensitivity was some 2 to 3 times better than that of a conventional IN53 crystal detector at 4mm. At 4mm, however, the conventional crystal detector is still widely used, its slightly inferior sensitivity being offset by its convenience in operation.

5.4. Description of 4mm. Spectrometer.

The 4mm. spectrometer used in this work has been described in detail by Slade (1968) and only a brief outline will be given here.

5.4. 1. The Microwave System.

The spectrometer is of the conventional bridge

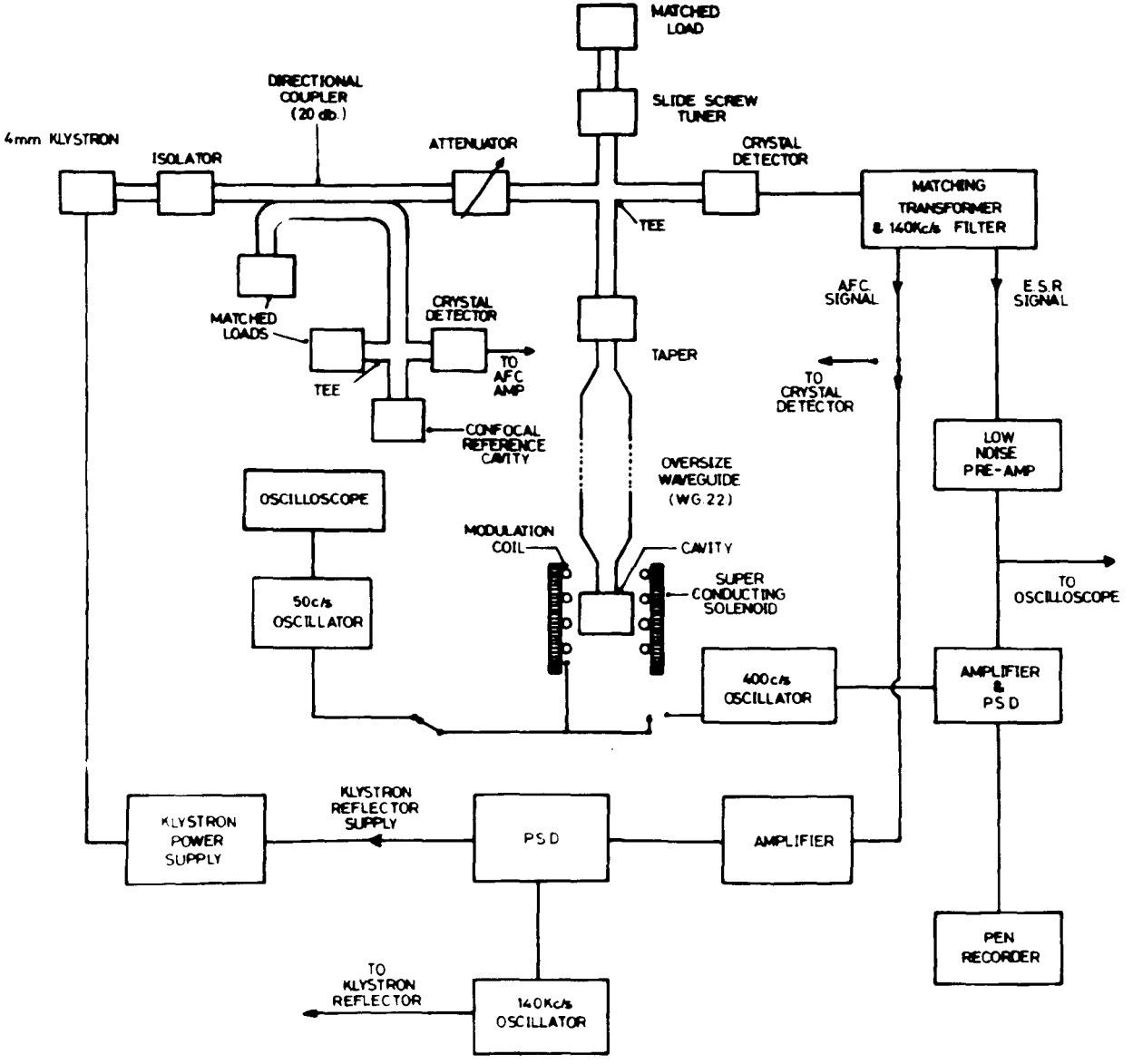

Fig. 5.2. 4mm. SPECTROMETER.

reflection type and constructed out of Phillips 4mm. waveguide components with the exception of the waveguide run between the bridge and the magnet which is in oversized waveguide, and the cavities which were manufactured in the University Workshop. The microwave source is a Phillips YK1010 reflex klystron capable of delivering up to 110mW of power in the frequency range 68 kMc/s - 72 kMc/s. The power falls off steadily as the klystron ages, the total guaranteed life being only about 400 hours. Klystrons of this type are still thermally and mechanically rather unstable and it was found necessary to fit water cooling jackets to the klystron in order to obtain a sufficiently noise-free output. In addition both klystron and isolator were found to be very sensitive to stray magnetic fields and both were screened with mu-metal since it was not practicable to move them far away from the magnet.

The waveguide system is shown in fig. 5.2. After passing through the isolator part of the power is coupled off in a 20dB coupler to a reference cavity to which the klystron may be locked when performing experiments with a shorted-waveguide sample holder. The rest of the power is fed via a calibrated attenuator to the microwave bridge at which it divides, one half being fed to the sample using tapers to W.G.22 (Q-band) and a suitable length of oversized guide. A slide screw tuner

may be placed in this arm to match out reflections from the tapers. The sample is contained in either a length of shorted waveguide or in a cavity. In the former case it is more convenient to use shorted oversize waveguide and to overcome the loss in sensitivity by using a larger sample while in the latter case the power is transferred back to standard waveguide to facilitate coupling to the 4mm. cavities. The balance arm of the magic tee, to which the other half of the power is fed, contains a slide screw tuner and matched load in order that a small amount of power may be reflected back to bias the detector if necessary and to enable the bridge to be tuned for absorption - or dispersion should this be required. The detector is an IN53 crystal rectifier mounted in a commercially manufactured holder of conventional design, but having the additional refinement that the crystal can be moved across the waveguide to obtain the most sensitive position.

5.4. 2. Cavities and Shorted Waveguide Sample Holders.

Two types of cavity are employed, one for use in a conventional electromagnet and one for use in a solenoidal superconducting magnet. It is most practicable to use cylindrical H_{012} cavities in both cases since the better Q obtainable from the relatively large H_{012}

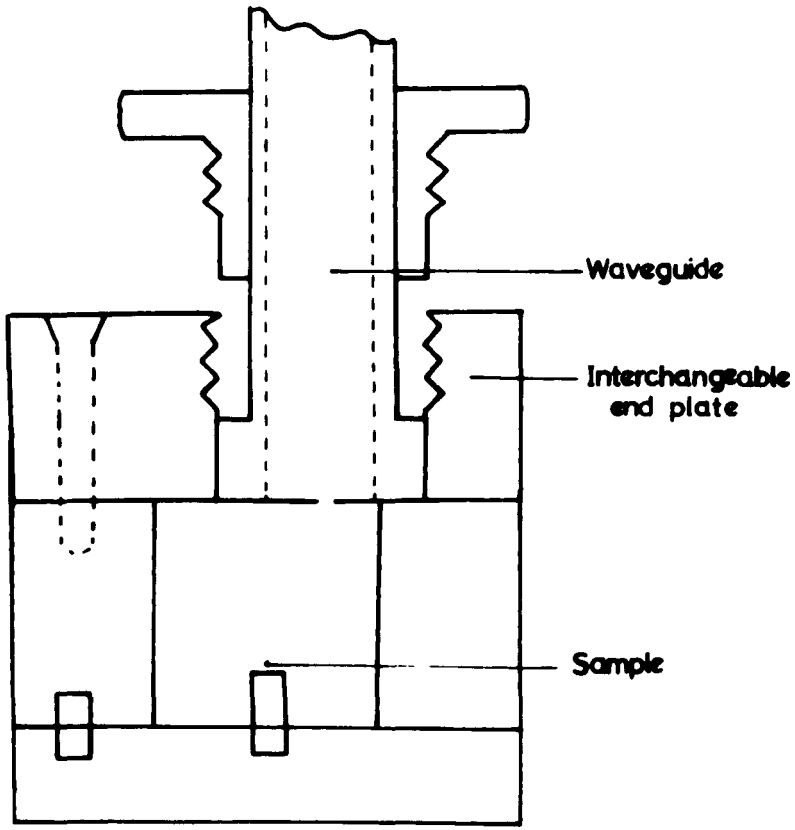

Fig 5.3 H_{012} Cylindrical cavity for use with electro-magnet

structure (in comparison with H_{011} and H_{111} cavities that is) more than offsets the decreased filling factor. The highest Q cavities are non-tuneable and are machined in brass, the internal surfaces being hand lapped with diamond paste to a mirror finish. Q-factors are in the region of 10,000 and do not increase appreciably on cooling to helium implying that they are limited by mechanical rather than electrical properties. The 4mm. cavity for use in the electromagnet is shown in fig. 5.3. from which the construction details should be apparent. The coupling hole is an integral part of the end plate of the cavity which must be changed if it is desired to vary the coupling. The 4mm. cavity for use in the superconducting magnet is very similar to this except that since its axis must be perpendicular to the waveguide to keep the r.f. and static magnetic fields at right angles the coupling hole is in the wall of the cylinder. A similar H_{011} cavity is available for use with the superconducting magnet at Q-band. A 4mm. dielectric cavity resonator was also built using "stycast Lo-K" resin, a commercially available microwave dielectric, for the barrel and brass for the end plates. The Q-factor of this resonator was extremely poor however, presumably due to the poor finish on the dielectric tube, and no E.P.R. signals were obtained using it.

For experiments in shorted waveguide it was

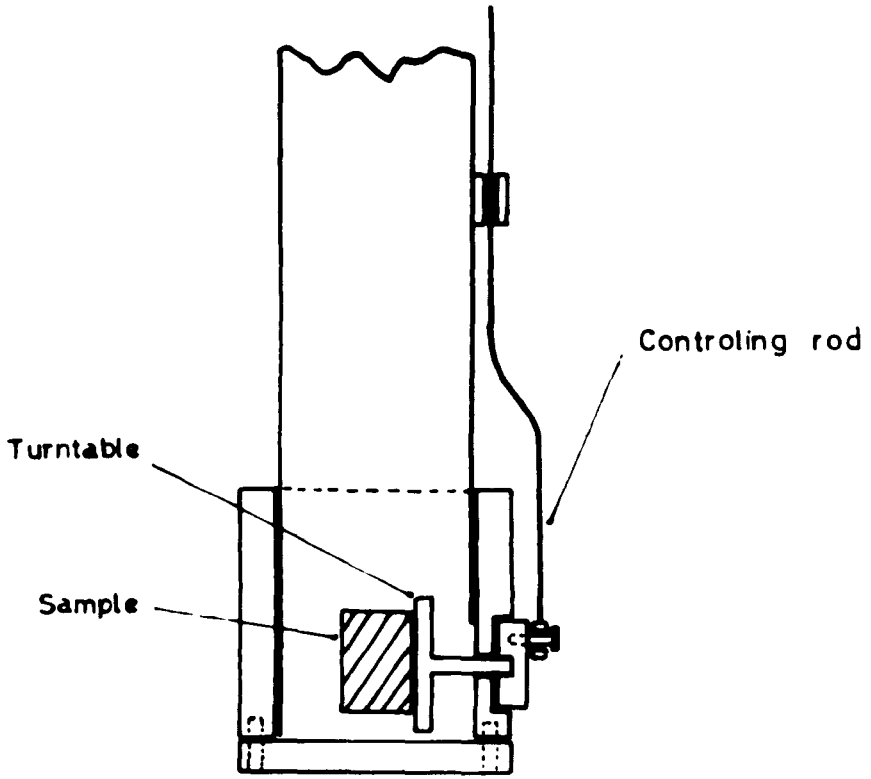

Fig. 5.4. Shorted waveguide turntable mechanism

found convenient to mount samples on stycast turntables as illustrated in fig. 5.4. This arrangement was used to most advantage in the superconducting magnet where it provided a simple method of performing angular rotation studies. Since the field in a solenoid is along the axis it is not possible to obtain an angular rotation spectrum by rotating the superconducting magnet in the usual way and instead the turntable was rotated by pushing and pulling a plate attached to it at right angles to a radius (see fig. 5.4). The controlling rod by which this movement was achieved was led up the side of the waveguide to a fine thread and nut outside the magnet cryostat so that the sample orientation could be altered remotely. When using the shorted waveguide holder in the electromagnet the rotating turntable provided a second degree of freedom in addition to the rotation of the magnet.

5.4. 3. Magnet and Detection Systems.

The 4mm. spectrometer can be used with one of two magnets, a conventional 8" Newport electromagnet capable of fields up to about 17kG or an Oxford Instrument Company superconducting magnet capable of a maximum field in excess of 50kG. The Newport magnet is used for low field work at temperatures down to 20^{o}K while the superconducting magnet can, at present, only be used at

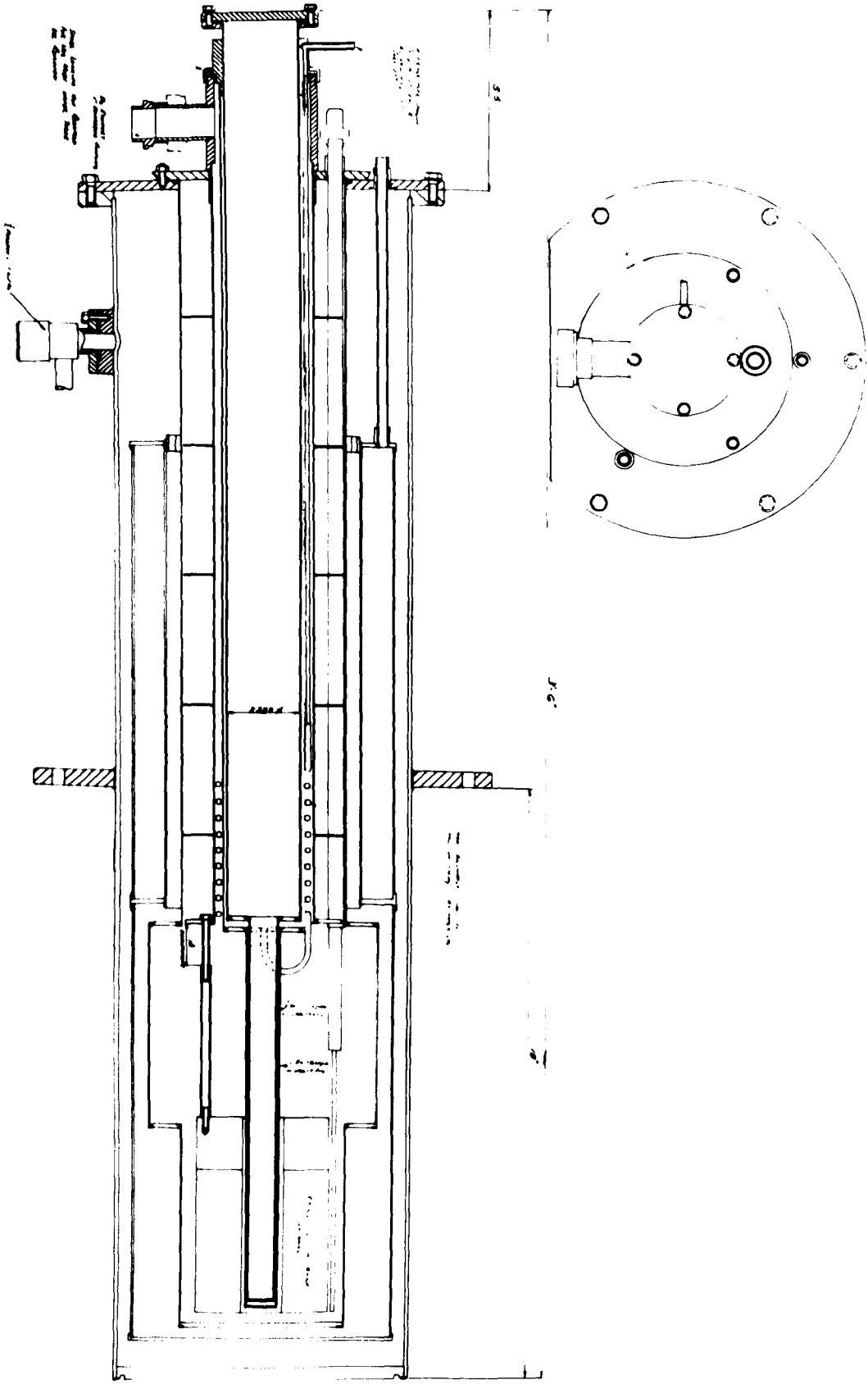

Fig. 5.5. Superconducting magnet and cryostat

helium temperatures although a room temperature insert is on order. The homogeneity of the superconducting magnet is specified as 3 parts in 10^5 over a 5mm. central region, that of the Newport magnet was found to be 1 part in 10^5 over a central cubic centimetre. Magnetic field modulation in the superconducting magnet is obtained from a single layer coil of superconducting wire wound beneath the main coil giving a maximum amplitude of 5 gauss peak-to-peak at 400c/s. The Newport magnet modulation is obtained from Helmholtz coils in the conventional manner 100 gauss peak-to-peak being available. The slow sweep for both magnets is obtained either by driving the respective control potentiometers with an electric motor and variable ratio gearbox or by feeding the output from a Newport Instruments ramp generator into the respective control circuits. In use the superconducting magnet is enclosed in a liquid helium cryostat an outer jacket of which is filled with liquid nitrogen while the central region in which the magnet is located is filled with liquid helium. The level of the liquid helium is monitored by three carbon resistors placed above the magnet. A diagram of the superconducting magnet and its cryostat is shown in fig. 5.5.

The electronic display system is quite conventional and the principles involved have been outlined earlier in

this chapter. Detected power is fed via a matching transformer to a Princetown Applied Research Corporation (P.A.R.) CR-4 low noise preamplifier. This may be used either in a wide band configuration for low frequency (50c/s) display or it may be peaked via a series of switched internal filters at any frequency between 30c/s and 300 kc/s. For phase-sensitive-detection a modulation frequency of 400c/s is used. This is rather low from the point of view of sensitivity considerations since 1/f noise from the crystal is still considerable: 100kc/s is more usual. However the use of relatively low frequency modulation enables the modulation coils to be placed outside the cavity. The advantages of this are twofold: the cavity Q is not impaired by an internal modulation loop and very large modulation amplitudes which compensate for the loss in sensitivity when observing broad lines may be used. Since the spectra reported in the present work were either very intense ($SrTiO_3$) or relatively broad ($PbTiO_3$) it was not found necessary to convert the spectrometer to 100kc/s modulation. The phase-sensitive-detector is a P.A.R. JB-4 which can be operated at any frequency between 15c/s and 15kc/s. The reference signal is derived internally and a variable output signal is also available and is fed through a power amplifier to provide the magnetic field modulation. Time constants ranging from 0.001 to 10 sec. are available and the low frequency

output is fed direct to a Varian G-10 pen recorder for signal display.

Automatic frequency control is provided by modulating the klystron reflector at 60kc/s. The error signal is taken from the crystal detector matching transformer and fed via a narrow band amplifier and isolating transformer to a transistorized p.s.d. floating at the reflector potential (-3kV). The reference signal is also applied via an isolating transformer and the p.s.d. output is applied directly to the reflector power supply in series with its own stabilizing voltage control, thus avoiding the need for further d.c. amplification. A block diagram of the electronic system is shown in fig. 5.2.

5.5. Spectrometer Operation.

In addition to the 4mm. spectrometer described in the previous section a simple Q-band bridge reflection spectrometer was assembled using the same electronic and display systems as the 4mm. spectrometer. This was generally used with the electromagnet but also occasionally with the super-conducting magnet when liquid helium temperatures were required. The sensitivity was measured to be approximately 5×10^{12} spins per gauss at 400c/s field modulation for a 1 sec. time constant and approximately 1 mwatt of power incident on the cavity.

5.5. 1. Magnetic Field and Frequency Measurement.

Fields in the electromagnet between 1 and 16kG were measured by observing the frequency of the nuclear resonance of protons in a sample of natural rubber. The r.f. power for this experiment is provided by a limited transistor oscillator which incorporates a variable capacitance diode in the tuning circuit so that its frequency can be controlled remotely by applying a variable d.c. bias to the varactor diode. The proton resonance signal can be observed on a C.R.O. with either 50c/s or 400c/s field modulation and thus pips can be put on a chart recording at frequent intervals as a magnetic field scan is in progress. The frequency of the proton resonance unit is measured with a digital readout Marconi Instruments frequency counter.

The field in the superconducting magnet is measured by making an accurate measurement of the current and assuming an exactly linear relationship between the two. The measurement is made by passing the magnet current through a standard 0.01 ohm resistance and measuring the voltage across it with a Cropico precision thermocouple potentiometer. The value of the standard resistance which is immersed in an oil bath to keep it at a constant temperature is specified to within $\pm$ 0.005%, and the voltage can be read to within about $\pm$ 0.05%. Pips are again put on the chart during a magnetic field scan by

setting the potentiometer at a fixed point, waiting for it to come into balance, marking the trace, moving the potentiometer on to the next fixed point, and so on. Magnetic fields can be determined in this way to within about $\pm$ 0.05%.

In order to obtain the field-current proportionality constant it is necessary to calibrate the superconducting magnet at a fixed point. This was done by employing a double spectrometer system to observe simultaneously the electron resonance signals from two samples of phosphorous-doped silicon, one in the electromagnet and one in the superconducting magnet. A previous check had been made to ensure that the g-value of the signal from phosphorous doped silicon did not change with temperature since the sample in the electromagnet was at room temperature while that in the superconducting magnet was at $4.2^{o}K$. The experiment was performed at Q-band using a 6dB directional coupler to split the microwave power from the Q-band klystron and feed each half of it to a separate microwave bridge. The klystron was locked to the cavity in the helium since this would obviously be the more stable. Using the two samples it was possible to adjust the field in both magnets to the same value and measure the field in the electromagnet using a proton resonance unit. The homogeneity of the superconducting magnet was checked in

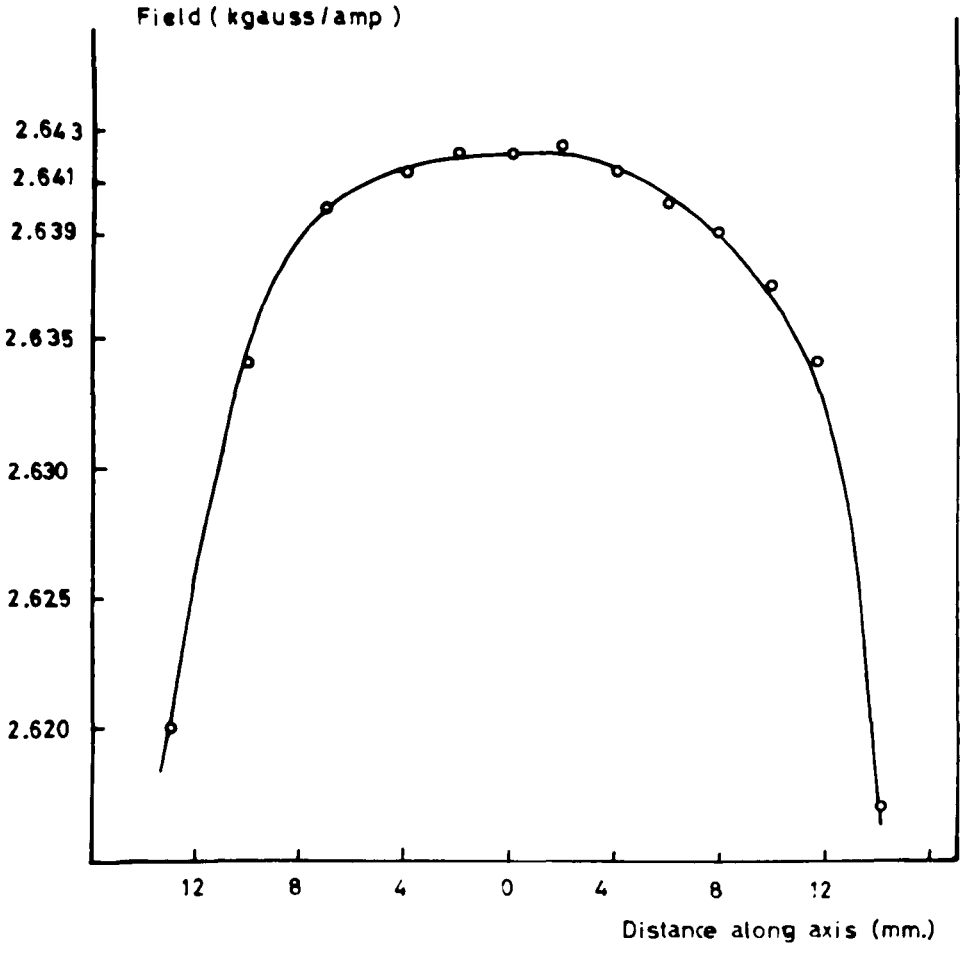

Fig. 5.6. Superconducting magnet calibration graph

this same experiment by moving the sample vertically along the axis of the solenoid. A plot of the magnet calibration as a function of the distance along the axis of the solenoid is shown in fig. 5.6 and the calibration at the centre of the solenoid was found to be 2.642 ± 0.001 kG/amp.

Frequency measurement at Q-band and at 4mm. when using the superconducting magnet presents no problems since frequency markers with accurately known g-values such as D.P.P.H. and phosphorous doped silicon can be employed. When using the electromagnet at 4mm. however $g = 2$ is not available and it is necessary to rely on the wavemeter. This was calibrated by the obvious method of observing the electron resonance signal from phosphorous doped silicon in the superconducting magnet; knowing g and measuring the magnetic field via the current as detailed above the frequency could be calculated. A check of this calibration at one spot frequency was carried out by placing the wavemeter in a formaldehyde maser system at present in operation in this Laboratory: the $0_{oo} - 1_{o1}$ rotational transition of formaldehyde occurs at 72.838Gc/s. The wavemeter was found to read consistently high over the whole frequency range by a factor of 0.11 ± 0.02Gc/s.

5.5. 2. Low Temperature Techniques.

For experiments at nitrogen and hydrogen temperatures with the electromagnet a glass single dewar is used and liquid is excluded from the cavity by enclosing it in a thin-walled metal tube closed at the lower end. To avoid condensation the cavity is either evacuated or flushed with helium before each run.

For experiments at helium temperatures the superconducting magnet is used. Before each run the vacuum jacket of the cryostat is evacuated to a pressure below 10^{-5} torr with an air-cooled oil diffusion pump and both inner and outer liquid jackets are filled with nitrogen. Filling the inner jacket with nitrogen serves to pre-cool the magnet before the helium is transferred to it. The magnet is generally pre-cooled overnight and the nitrogen then blown out of the inner jacket of the cryostat by pressurizing it with helium gas. The waveguide run from the bridge to the magnet and the cavity are then flushed with helium, covered with a metal tube and lowered into the cryostat. The microwave bridge and klystron are then connected to the sealed waveguide run and the cavity mode is displayed on the C.R.O. so that it can be followed down to 4.2^{o}K: it is rather difficult to find the mode among the reflections in the waveguide system if this is not done. When using shorted waveguide the klystron is not put on until the magnet is ready for

operation and neither is a can used to exclude helium from the waveguide run since liquid helium is not lossy at microwave frequencies and has a dielectric constant near one.

To operate the magnet helium is siphoned slowly into the cryostat until liquid begins to collect. This is evidenced by a sharp decrease in the boil-off rate (the gas is passed through a flow meter before being collected and compressed) and also happens to coincide with the point at which the magnet becomes superconducting. This generally takes about 800 c.c. of liquid and helium is then siphoned in rapidly until between 2 and 6 litres have been collected, depending upon the length of running time required. When the system has been allowed to settle the 50c/s klystron reflector modulation is removed and the 60kc/s a.f.c. modulation is applied to lock the klystron either to the sample cavity or to an external reference cavity. The bridge is then mismatched to bias the detector and the spectrometer operated in the usual manner. The sensitivity of the 4mm. spectrometer using a cavity at $4.2^{\circ}K$ is approximately 5×10^{10} spins per gauss.

5.5. 3. Measurements on Perovskites and Calcium Tungstate.

The measurements to be described in the next

chapter were carried out on single crystals of strontium titanate, lead titanate, barium titanate and calcium tungstate. The work on strontium titanate was carried out in shorted waveguide since only one large single crystal was available and this had an accurately machined (100) face which meant that it could be very conveniently orientated in shorted waveguide using a turntable as described in section 5.4. 2. The signals from this sample were furthermore quite intense and ample sensitivity was available using the shorted waveguide technique. In addition strontium titanate has a very large dielectric constant (about 250 at room temperature) and a fairly low loss angle ($\tan \delta = 0.001$) and can thus be used as its own resonator (Okaya and Barash 1962). This technique has been applied with considerable success to the study of rutile where effective Q-factors approaching 100,000 combined with the 100% filling factor have enabled excellent sensitivity to be obtained (Carter and Okaya 1960). Carter and Okaya showed the increase in sensitivity over a conventional metal-walled cavity (Eq. 5.10) to be $\epsilon^{3/2} Q_1/Q_2$ where ϵ is the dielectric constant, Q_1 the effective Q of the dielectric resonator and Q_2 the conventional cavity Q. In order to exploit this technique to full advantage the sample must be much thicker than the effective wavelength $\lambda/\sqrt{\epsilon}$ but not so great that the various microwave resonances overlap. No attempts were

made to satisfy these conditions in the present work.

The signals from lead titanate on the other hand were rather weak and since several samples of varying sizes were available it was found to be more convenient to use cavities for these measurements - except at helium temperatures, that is, where the increased sensitivity again prompted the use of shorted waveguide. The signals from barium titanate were weak and could only be seen using a cavity while a combination of cavity and shorted waveguide techniques was again found to be convenient for the measurements on calcium tungstate. The dielectric constants of the perovskites are strongly temperature dependent and stable conditions must be ensured if consistent results are to be obtained.

5.6. Crystallographic Description of Samples.

The strontium titanate crystal was grown by the Verneuil process with 0.03% Fe_2O_3 added to the feed and was pale green and translucent in appearance with dimensions approximately 2mm. x 3mm. x 4mm. The crystallographic axes were fairly easily determined from the cubic Fe^{3+} spectrum (Müller 1958) especially since one of the faces of the crystal was known to have been machined to within 0.3° of the (100) plane.

The lead titanate crystals were grown from a

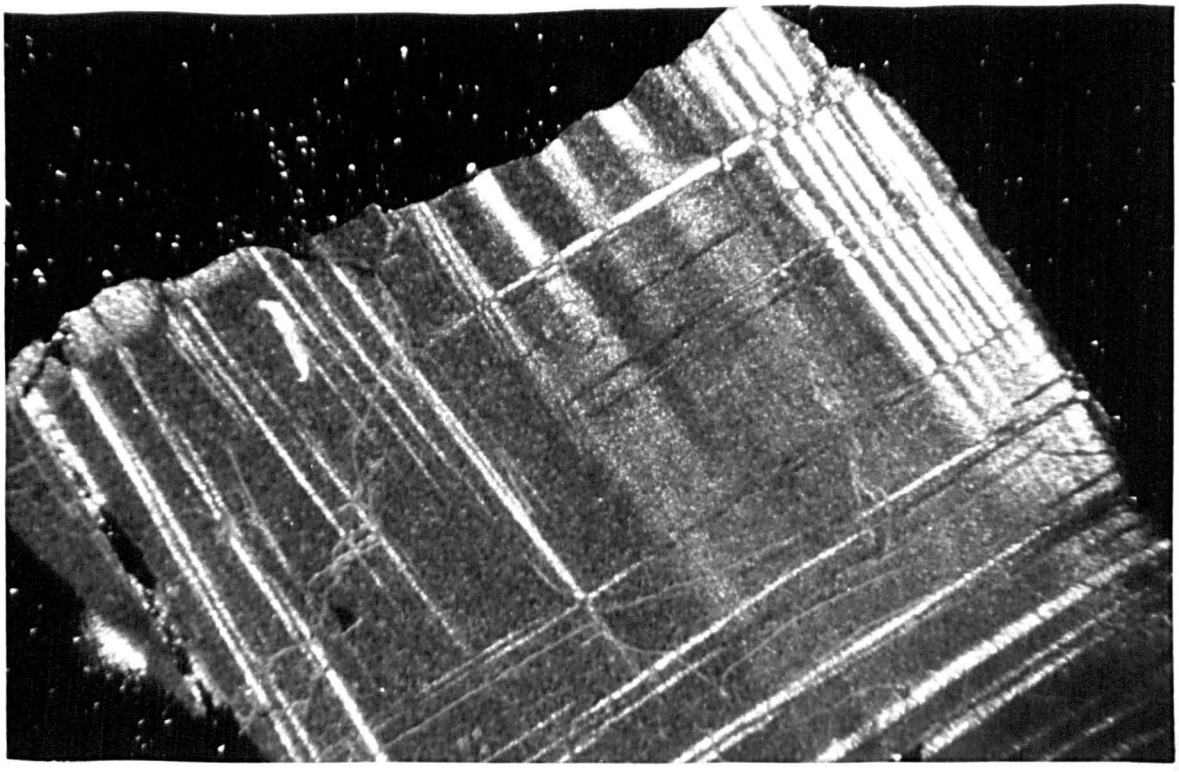

x 35

Fig.5.7. Thin section of $PbTiO_3$ under cross-polarized light

KF flux melt and were black and lustrous in appearance suggesting some non-stoichiometry or Ti^{3+} present. No dopant was added to the feed. Annealing the crystals in air at temperatures up to 1000°C for periods up to 6 hours produced no change in the spectrum suggesting that all the iron was in the trivalent state prior to the oxidation. The crystals were in the form of fairly well defined cubes with dimensions up to 4mm. x 4mm. x 4mm. In thin section they were pale green and exhibited well-defined domain structure when viewed under the polarizing microscope (fig. 5.7). Fig. 5.7 is a photograph of a section cut parallel to one of the well-defined faces and it will be seen that the tetrad axes lie roughly parallel and perpendicular to the faces of the cube.

The barium titanate crystals had a layered mica-like structure and under the polarizing microscope were found to be predominantly c-domain as expected (4.2. 1). Crystals ranged from pale yellow to pale brown depending upon the degree of iron doping. The crystals were rather lossy as were those of lead titanate and only small samples could be used in a cavity.

The calcium tungstate single crystals proved to be very lightly doped and it is believed that they were cut from a boule doped with 0.005% of Fe_3O_4. Measurements were made on one sample in the form of a colourless disc approximately 1mm. thick and 5mm. in diameter and on a

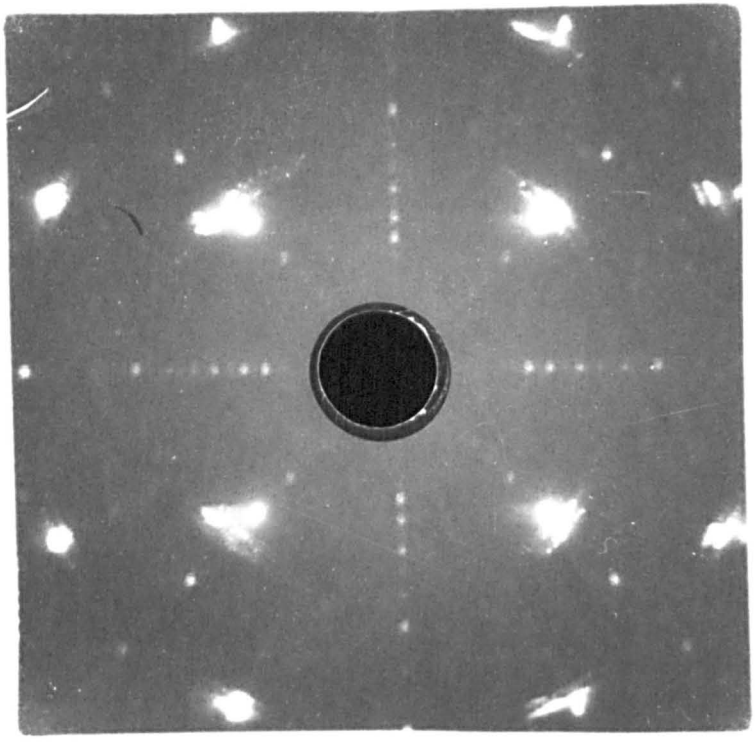

Fig. 5.8. c-axis back reflection photograph of $CaWO_4$

small chip broken from this disc. The axes of the small chip were determined by the Weissenberg X-ray technique and the approximate directions of the axes in the large disc were found by matching up the cleavage surfaces of the two samples under a high power binocular microscope. The axes of the large sample were then determined more directly from X-ray back reflection photographs (fig. 5.8), and it was found that one of the tetragonal "a"-axes was perpendicular to the plane of the disc. The approximate directions of the other two axes were scribed on the disc while it was on the X-ray machine. Because in both the large and small samples one of the "a"-axes was perpendicular to a well-defined face it proved a fairly simple matter to mount either of these samples so as to obtain spectra in the "a"-"c" plane. The positions of the second "a"-axis and the "c"-axis within this plane of rotation could not be so accurately determined however, and recourse was made to the symmetry of the E.P.R. spectra for more precise identification of these latter two directions.

References.

Carter D.L. and Okaya A., 1960, Phys. Rev. 118, 1485

Feher G., 1957, Bell. Syst. Tech. J. 36, 449

Ingram D.J.E. 1967, "Spectroscopy at Radio and Microwave Frequencies" 2nd Ed. (Butterworths, London)

Johnson C.M., Slager D.M. and King D.D., 1954, Rev. Sci. Inst. 25, 213.

Mock J.B., 1960, Rev. Sci. Inst. 31, 551

Müller K.A., 1958, Helv. Physica Acta 31, 173

Okaya A. and Barash L.F., 1962, Proc. I.R.E. 50, 2081

Peter M., 1959, Phys. Rev. 113, 801

Poole C.P. Jr., 1967, "Electron Spin Resonance" (Interscience, New York)

Rosenbaum F.J., 1964, Rev. Sci. Inst. 35, 1550

Slade E.F., 1968, Ph.D. Thesis University of Keele.

Taub J.J., Hinair H.J., Hinkelmann O.F. and Wright M.L., 1963, I.E.E.E. Trans. M.T.T. 11, 338

Van Es C.W. 1960, Phil. Tech. Rev. 22, 122

CHAPTER VI

RESULTS AND DISCUSSION

6.1. Strontium Titanate.

6.1. 1. Description of Q-band and 4mm Spectra.

The strong axial paramagnetic resonance spectrum of Fe^{3+} in $SrTiO_3$ first reported by Kirkpartick, Müller and Rubins, (1964) and described in 4.2. 3. has been re-examined at 4mm. where direct inter-Kramers' doublet transitions between the $\pm \frac{1}{2}$ and $\pm 3/2$ levels can be observed in relatively modest magnetic fields. In this way the zero-field splitting has been found to be

$$2.698 \pm 0.006 \text{ cm}^{-1}$$

in confirmation of the original estimate by Kirkpartrick et. al. and in opposition to the contention of Low (1965) that it must be much greater than this.

The original estimate of $2.85 \pm 0.15 \text{ cm}^{-1}$ for the zero-field splitting was based on measurements of the departure from 6 of $g_\perp^{eff}$ at two different frequencies, two measurements being necessary to obtain the two independent parameters $g_\perp$ and Δ in Eq. 4.4. From Eq. 4.4 the zero-field splitting can be seen to be given by

$$\Delta = \frac{g_\perp^{eff}(1)}{3\alpha}\left(\frac{\alpha-\delta}{1-\delta}\right)\beta\left(\frac{2\alpha H_2^2 - 2H_1^2}{\alpha - 1}\right)^{1/2} \qquad 6.1.$$

where $\alpha = g_\perp^{eff}(1) / g_\perp^{eff}(2)$ and $\delta = (H_1/H_2)^2$ and the indeces 1 and 2 refer to the two frequency bands. $g_\perp$ is given by

$$g_{\perp} = \frac{g_{\perp}^{\text{eff}\ (1)}}{3\alpha}\left(\frac{\alpha-\delta}{1-\delta}\right) \qquad 6.2.$$

From measurements at X- and K-bands Kirkpatrick et. al. obtained the values $\Delta = (2.85 \pm 0.15)\ cm^{-1}$, $g_{\perp} = 2.0106 \pm 0.0008$ and they also found $g_{\parallel} = g_{\parallel}^{\text{eff}} = 2.0054 \pm 0.0007$. The large error in Δ arises from the term $\alpha - 1$ since α is very close to 1. Kirkpatrick et. al. only considered a term in D in the Hamiltonian although as was discussed in 4.3 this does not affect the validity of their calculations provided that D is replaced by Δ. The use of perturbation theory to diagonalize the S = 5/2 matrix introduces errors in $g_{\perp}$ of 0.002% at X-band and 0.004% at K-band as compared with a direct computer diagonalization, and the value quoted by Kirkpatrick et. al. must thus be substantially correct and should be applicable to the present measurements at higher frequencies.

The axes of a $SrTiO_3$ single crystal were determined from a study of the cubic Fe^{3+} spectrum at X-band, this splitting pattern being well documented (Müller 1958). The alignment necessary for accurate studies at 4mm. was performed at Q-band. It was desired to align the crystal with a (100) axis vertical so that by rotating the electromagnet the variation of the axial spectrum with the Euler angles θ and ϕ could be simultaneously and independently monitored. This was achieved using the shorted waveguide technique and rotating the crystal in

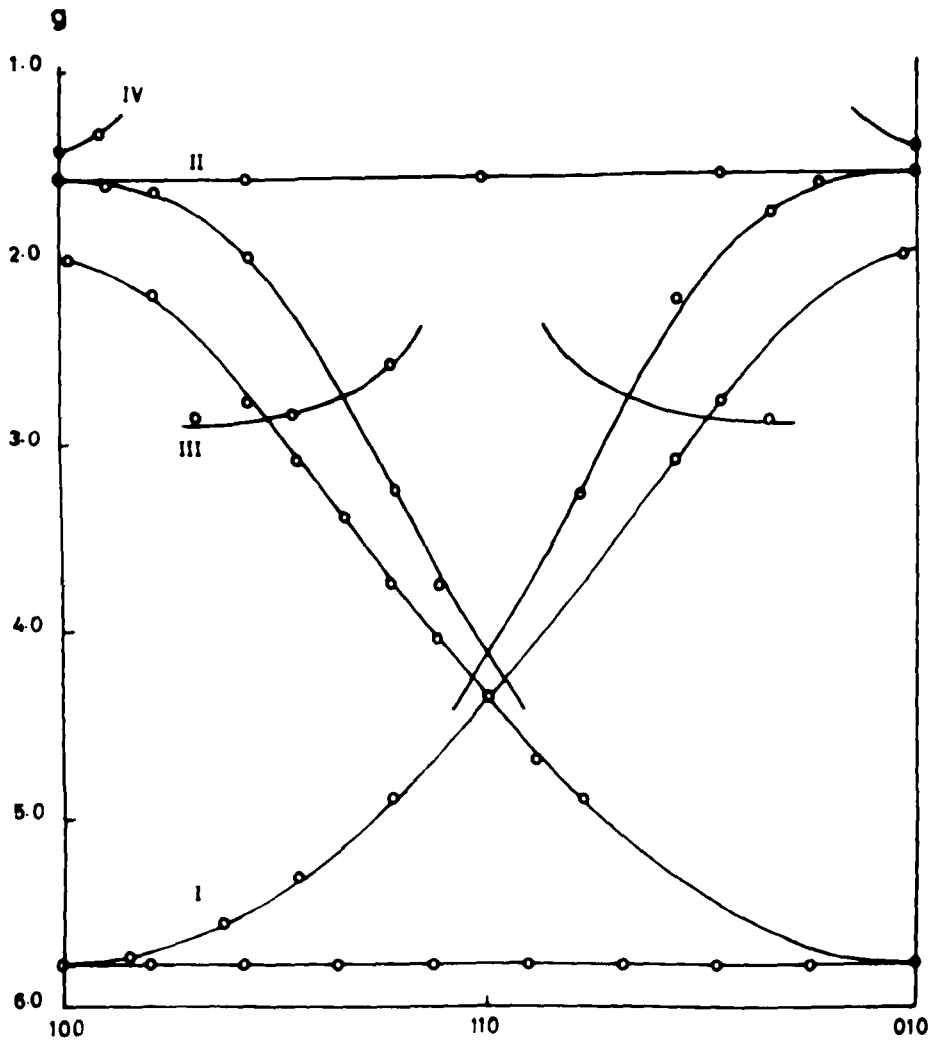

Fig. 6.1. Angular variation of the axial Fe^{3+}: $SrTiO_3$ spectrum at Q-band

the vertical plane until two of the three axial lines were observed to disappear into the main $g = 2$ cubic line at two points 90° apart in the rotation of the electromagnet. These two positions then necessarily corresponded to "parallel" (i.e. H parallel to z) orientations and the third tetragonal axis must have been vertical. An initial angular rotation study was made at Q-band and in addition to the expected three lines of the axial spectrum three other lines were seen which were later identified as the $+ 3/2$ to $- 3/2$, $+ 1/2$ to $- 3/2$ and $- 1/2$ to $- 3/2$ transitions (fig. 6.1). In fig. 6.1 these latter three transitions are denoted by II, III and IV respectively. Both II and III are seen to be forbidden in the "parallel" orientation as is expected. Leaving the sample undisturbed in the Q-band shorted waveguide holder the Q-band klystron and bridge were replaced by the 4mm. ones and the 4mm. angular rotation study of fig. 6.2 was carried out. The transitions here were identified from their behaviour with angular rotation and with frequency: for example if a line is isotropic it must correspond to the "perpendicular" orientation and it if goes to low field as the frequency is raised it must be between two converging levels in the magnetic field and therefore probably an inter-Kramers doublet or "zero-field" transition. It will be noted that due to the curvature of the levels in the magnetic field two

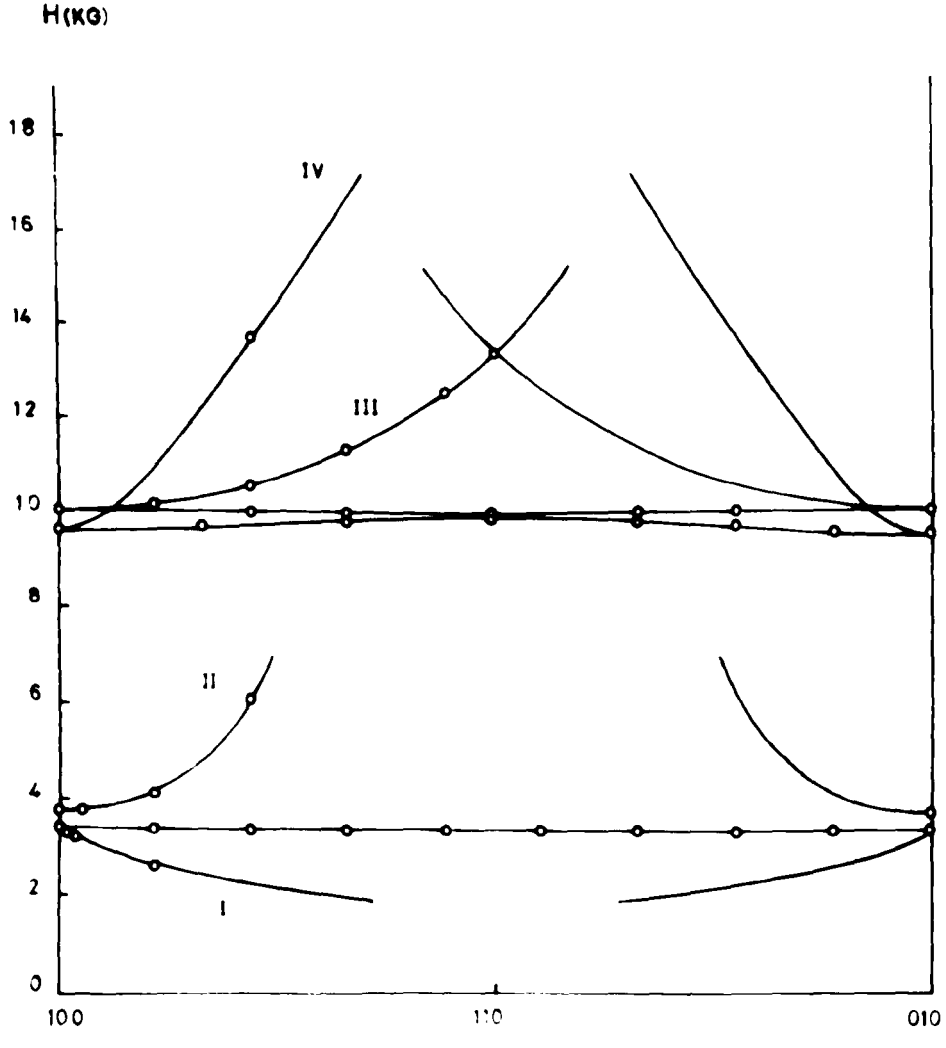

Fig. 6.2 Angular variation of the axial Fe^{3+}: $SrTiO_3$ spectrum at 4mm

transitions are observable at 4mm. between the + 1/2 and - 3/2 levels at different fields. It will also be noted that the high field + 1/2 to - 3/2 "isotropic" transition is not quite isotropic but has fourfold symmetry indicative of a small cubic variation of the spectrum: as was pointed out in 4.3 a cubic term is expected to have a greater effect on transitions involving the $\pm$ 3/2 levels than on those only involving the $\pm$ 1/2 levels. A small anisotropy of the + 1/2 to - 1/2 transition was also observed although it is too small to show up well in fig. 6.2. The observed transitions at Q-band and 4mm. are indicated in the energy level diagrams of figs. 6.3 and 6.4.

6.1. 2. Spin Hamiltonian Parameters.

As early attempts to fit the observed transitions to a spin Hamiltonian of the form 2.22 amply illustrated perturbation theory does not give an adequate description of E.P.R. spectra when the Zeeman energy is of the order of the zero-field splitting and a computer diagonalization of the S = 5/2 matrix was found to be necessary. A programme was therefore written for the University Elliott 4130 computer using a Jacobi diagonalization subroutine to obtain the eigenvalues of S = 5/2 and to plot them out as a function of field if required. After several cycles of trial and error values for the parameters a, D, F, $g_{\parallel}$ and $g_{\perp}$ were obtained which gave a 1% agreement between

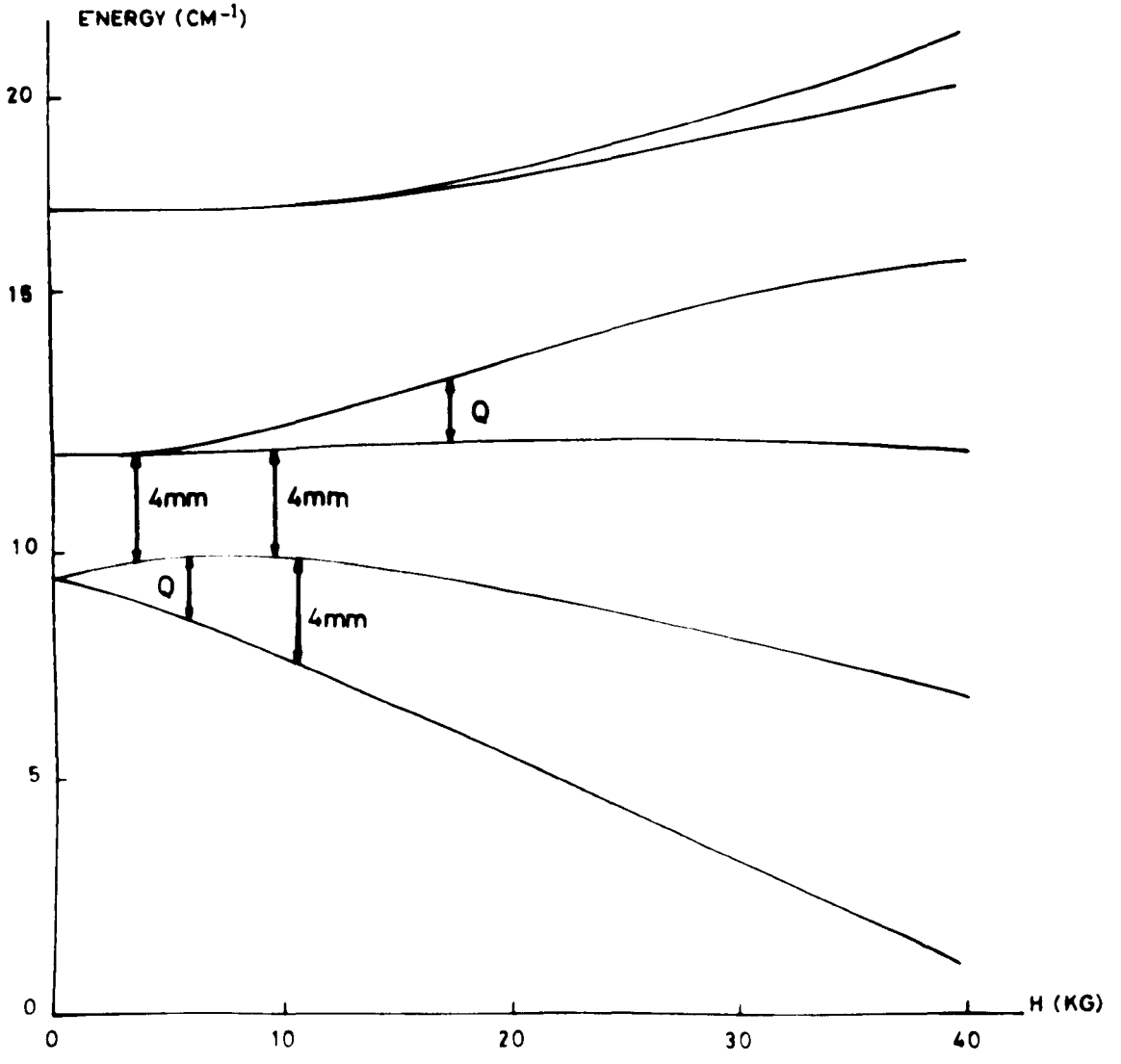

Fig. 6.3. Energy levels for Fe^{3+} in $SrTiO_3$: H perpendicular to z

theory and experiment and the solid curve in fig. 6.2 represents the theoretical expression while the open circles are experimental points.

A more careful study of the 4mm. spectrum along the principal axes revealed that the best fit was obtained with

$g_{\parallel} = 2.0054$

$g_{\perp} = 2.003$

$D = 1.373\ cm^{-1}$

$F = 0.009\ cm^{-1}$

$a = 133 \times 10^{-4}\ cm^{-1}$

All the transitions then fitted the theory within the estimated limit of experimental error of about $\pm$ 20 gauss arising mainly from orientation uncertainties. Since $g_{\parallel}$ could not be measured directly its value was taken to be that quoted by Kirkpatrick et. al. there being no reason why it should change with frequency; it was measured to be 2.006 $\pm$ 0.001 at Q-band. It will however be seen that the value of $g_{\perp}$ is not in agreement with the value of 2.0101 obtained by Kirkpatrick et. al. If an attempt is made to fit the results using the value of $g_{\perp}$ of 2.0101 then it is found that D can be chosen either to fit the zero-field transitions in which case the + 1/2 to - 1/2 transition occurs consistently some 35 gauss higher in field than it should, or it is found that D can be chosen to fit the + 1/2 to - 1/2 transition but that then the

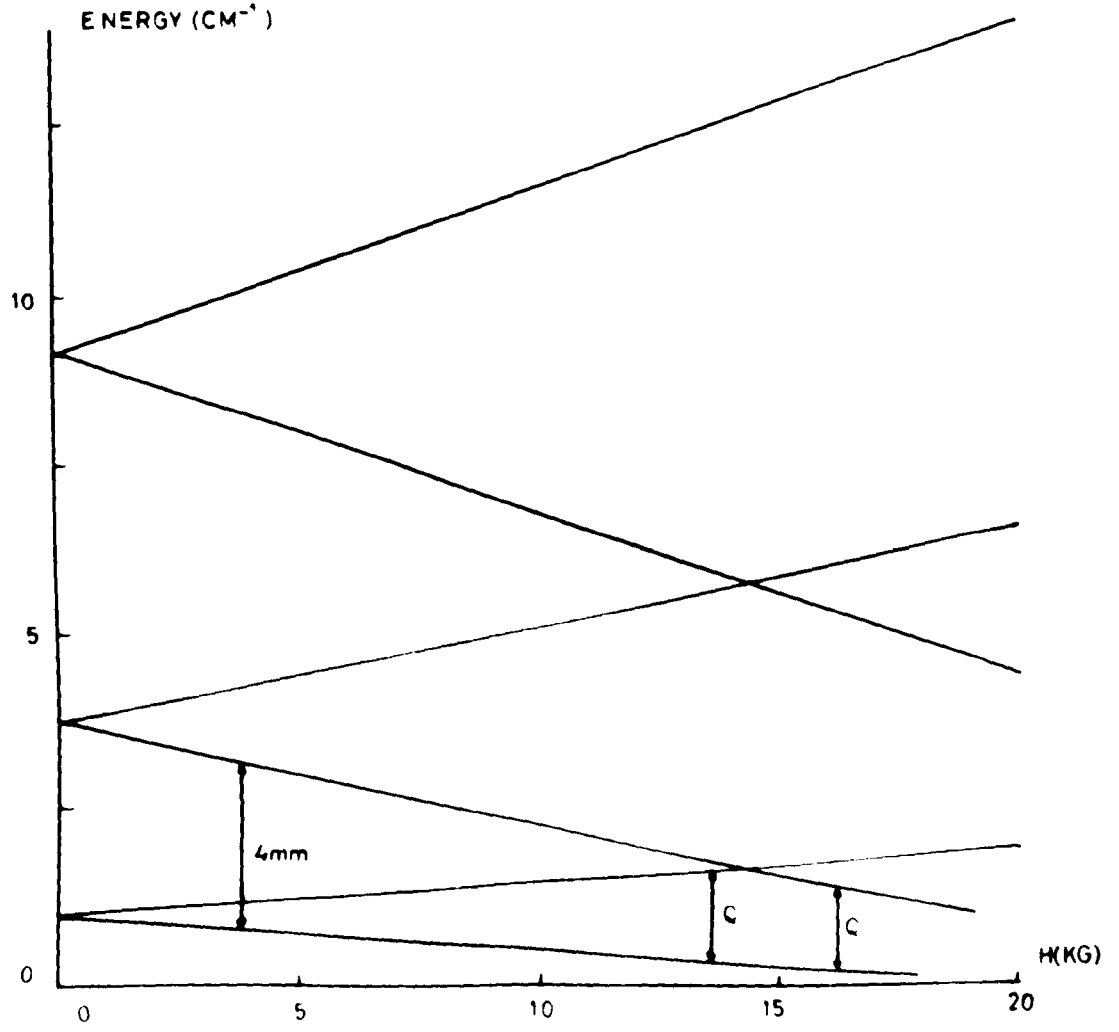

Fig 6.4 Energy levels for Fe^{3+} in $SrTiO_3$ H parallel to z

zero-field transitions become far removed from the predicted resonance fields. The large discrepancy in the latter case occurs because a change of D affects the + 1/2 to - 1/2 transition only in third order and a large change in D is therefore needed to bring about a small change in the position of the + 1/2 to - 1/2 transition. A discrepancy of this nature could be qualitatively understood in terms of the Hamiltonian of Koster and Statz. This in effect provides for the fact that the $\pm$ 3/2 and $\pm$ 1/2 levels may be modified differently in the field: the $\pm$ 3/2 and $\pm$ 1/2 levels could therefore have different g-values and in addition it would not necessarily be valid to extend a g-value measured at X-band to results at 4mm. In the former case it would presumably be possible to keep $g_\perp^{1/2}$ at 2.0101 and Δ at 2.670 cm^{-1}, the value needed to fit the + 1/2 to - 1/2 transition, and to fit the zero-field transitions by altering $g_\perp^{3/2}$. In the latter case the Hamiltonian parameters given above could be correct though this is unlikely since they have been fitted to a conventional Hamiltonian. In practise the situation which would occur would probably amount to a combination of both the above cases. The measured value of $g_\perp^{eff}$ of 5.772 at Q-band does not provide conclusive evidence for either Δ = 2.670 cm^{-1}, the value obtained from $g_\perp^{eff}$ at 4mm., or for Δ = 2.698 cm^{-1}, the value obtained from the best fit and zero-field transition fits at 4mm.

It may at once be remarked that a deviation of + 35 gauss in a fit otherwise within ± 20 gauss is hardly conclusive evidence for departure from a spin Hamiltonian especially since only three accurate 4mm. runs were performed. The experimental error arises mainly from orientation uncertainties which were estimated to be less than 1^{o} in θ and ϕ and this was confirmed by the smallness of the differences observed in the spectra at points 90^{o} apart in a rotation of the electromagnet. Further measurements would have been made had an insert on order for the superconducting magnet arrived in time for then g = 2 would have been accessible at 4mm. at room temperature: the frequency could have been measured accurately and direct alignment of the sample from the 4mm. E.P.R. spectrum would have been facilitated. As was discussed earlier the axial spectrum becomes quite complicated below the phase transition.

It should also be remarked that even in the absence of Koster and Statz type effects deviations from a spin Hamiltonian of up to 0.5% have previously been reported in $SrTiO_3$ (Müller 1958, Aisenberg et. al. 1959). These were originally attributed to covalent bonding but were later shown to be due to random distortions of the Fe^{3+} lattice site: a definite correlation was found between the individual linewidths and the departure of the position of the lines from a least squares fit with theory. In

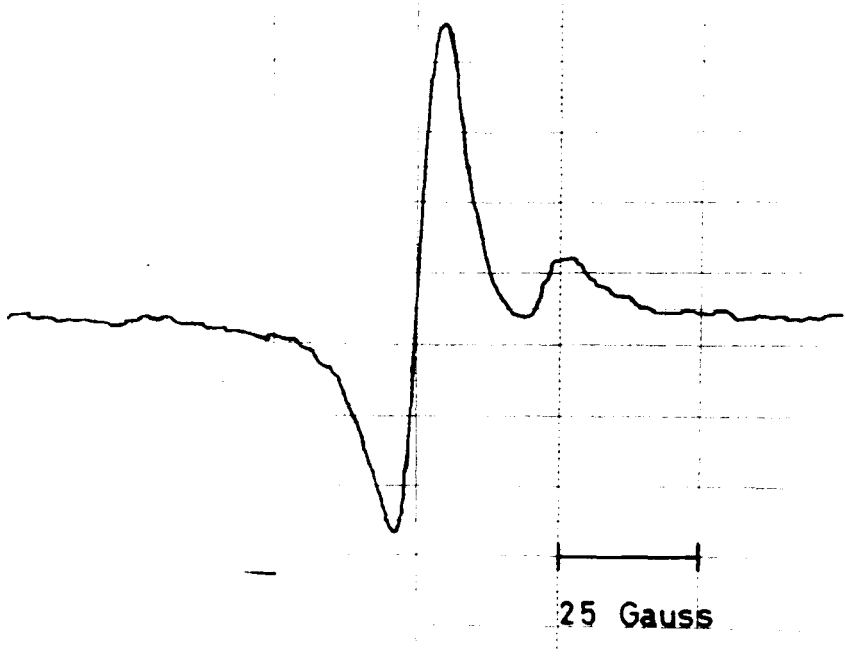

Fig. 6.5. Illustrating linewidths in $SrTiO_3$: the main $g = 2$ and weaker axial lines

addition the linewidths were found to vary with the level of doping being narrower in more heavily doped samples. Since the + 1/2 to - 1/2 transition of the axial Fe^{3+} spectrum is not affected in first order by the crystal field parameters it is the narrowest of the observed transitions (about 10 gauss at $\theta = 90^{\circ}$ at 4mm.) while the zero-field lines are broader - by a factor of about two. It is thus seen that an observed discrepancy between $\pm$ 1/2 and $\pm$ 3/2 transitions is explicable in terms of crystal imperfections as well as in terms of departure from a conventional spin Hamiltonian.

Even in the absence of covalency Koster and Statz expect deviations from a spin Hamiltonian of the order of

$$\frac{\text{(zero-field splitting) x (Zeeman energy)}}{\text{multiplet separation}}$$

For the axial Fe^{3+} spectrum in $SrTiO_3$ this amounts to a factor of about 10 gauss at 4mm. The relatively large g-values of the axial spectrum point towards some degree of covalency and deviations may thus be greater than this. The scatter between different lines due to lattice distortions is possibly of comparable magnitude, but may be smaller: at the relatively high doping level of 300 p.p.m. the present sample displays rather narrow linewidths and is presumably relatively free from distortion (Fig. 6.5). In the present work the effects of crystal symmetry and lattice distortions are thus seen to be of comparable

magnitude with the experimental error. In contrast in the experimental study of the cubic Fe^{3+} spectrum carried out by Aisenberg et al. the Koster and Statz terms were expected to be much smaller than the experimental error while the distortion terms were found to be greater. It thus seems that a more careful study of the axial spectrum, with particular regard to the variation with doping, might yield some very interesting results.

From the considerations outlined in the preceding paragraphs it will be seen that it is unwise to attribute too much significance to small departures of experimental results from theory, and in this connection the value quoted above for F should be treated with reserve. The cubic term, on the other hand is fairly unambiguously determinable from the angular variation of the spectrum in the "perpendicular" plane since variations in D and F affect the observed anisotropy only indirectly. The best values that can be quoted for the crystal field parameters are

$$D = 1.373 \pm 0.003 \text{ cm}^{-1} \quad (\text{For } F = 0.009 \text{ cm}^{-1})$$

$$a = (133 \pm 12)\ 10^{-4} \text{ cm}^{-1}$$

$$F = (90 \pm 50)\ 10^{-4} \text{ cm}^{-1}$$

$$\Delta = 2D - 5a/2 - 5F/3 = 2.698 \pm 0.006 \text{ cm}^{-1}$$

with the reservation that Δ may be slightly smaller than the quoted value. Since the cubic parameter "a" has

always been found to be positive in octahedral environments (Low 1960) and since the 4mm. E.P.R. spectrum indicates that "a" and "D" must have the same sign the values quoted above should be taken to be positive in the absence of any evidence to the contrary.

6.1. 3. Significance of Cubic Term.

It is interesting to compare the magnitude of "a" with the value of $(198 \times 10^{-4})cm^{-1}$ found for the cubic spectrum (Müller 1958). If the axial distortion in $SrTiO_3$ corresponded simply to the removal of one O^{-2} ion and no rearrangement of the remaining ligands took place then straightforward point-charge considerations (appendix II) show that the crystal field potential V_4^4 would be unchanged while the magnitude of the component V_4^0 would be decreased. Assuming that small changes in the crystal field parameters are reflected linearly in changes of the corresponding spin Hamiltonian parameters then the above situation would be represented in the spin Hamiltonian of $SrTiO_3$ by the same term in "a"$\sim(Y_4^0+\sqrt{5/14}[Y_4^4+Y_4^{-4}])$ and a small term in "F"$\sim(Y_4^{0'})$ of the opposite sign.

In order to account for a reduction in "a" it is necessary to postulate a distortion of the framework of O^{2-} ions surrounding the Fe^{3+} ion. For example moving the four coplanar O^{2-} ions out from their original positions by about 8% of the original Fe^{3+}-O^{2-} spacing (1.953 Å.U.)

would lead to a cubic crystal field potential 2/3 of the magnitude of the original one, and a term in $V_4^{o'}$ smaller than that in the undistorted case but still of opposite sign to the cubic term. A more likely consequence of the removal of an O^{2-} ion from the regular octahedral framework surrounding the Fe^{3+} ion would be a reduction in the spacing between the Fe^{3+} ion and the opposite O^{2-} ion (Fig. A2(2)). If this were the case then an angular displacement of the Fe^{3+} ion 15^{o} out of the plane containing the four undistorted O^{2-} ions would lead again to a cubic field reduced by a factor of 2/3 but this time to a term in $V_4^{o'}$ having the same sign as the cubic term - as is observed. In fact this precise distortion leads to a seemingly rather large value for $V_4^{o'}$, the unbalanced fourth-order component of the crystal field after the cubic term has been subtracted, and a small additional movement of the four coplanar O^{2-} ions - for example towards the O^{2-} ion vacancy - could be postulated to reduce this term. Since the exact relationship between the crystal field and spin Hamiltonian parameters is not known, however, it does not seem to be worthwhile to pursue such point charge considerations in any great detail. It would doubtless be possible to postulate alternative rearrangements of the ligands which would give rise to spin Hamiltonian terms of the correct magnitude and sign: while the above picture seems physically reasonable and gives a

semiquantitative explanation of the observed results it is not necessarily a unique description.

Since the completion of the work on $SrTiO_3$ detailed above essentially the same value for the zero-field splitting has been reported by Baer, Wessel and Rubins (1968) also from E.P.R. measurements at 4mm. These authors found no cubic variation of the spectrum and apparently experienced no difficulty in fitting their results to a conventional spin Hamiltonian using the X-band g-values. It is probably worth noting that their linewidths are up to five times those found in the present sample. On the one hand this would tend to make deviations from a conventional spin Hamiltonian due to crystal imperfections greater - though the magnitude of this effect for the axial spectrum is not really known, but on the other hand it would make accurate determination of line centres more difficult. It is still surprising that Baer et. al. fail to report the cubic variation of the spectrum. In addition to the magnitude of the zero-field splitting these authors also determined the sign of "D" directly by depopulation measurements at He temperatures and found it to be positive confirming the tentative conclusion reached above. From a series of linewidth measurements at room temperature as a function of frequency they also gave a plausible explanation of Low's earlier failure to observe the zero-field transitions in high magnetic fields at

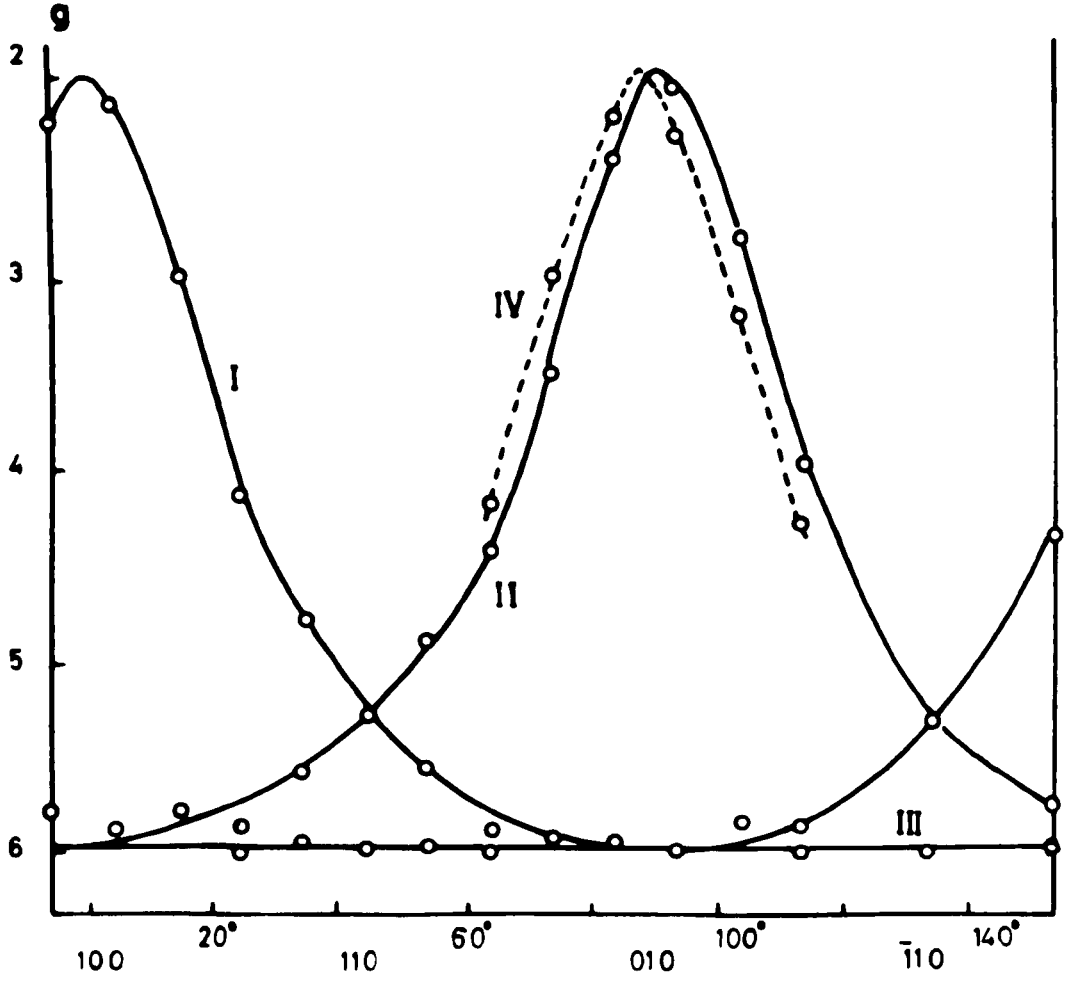

Fig. 6.6. Angular variation of the Fe^{3+}:$PbTiO_3$ spectrum at X-band

X-band by showing that the expected 1/2 to 3/2 transitions become excessively broadened only a few degrees off axis in this situation.

6.2. $PbTiO_3$

6.2. 1. Description of X- and Q-band Spectra.

A nominally undoped single crystal of $PbTiO_3$ yielded the spectrum of fig. 6.6 when examined at X-band and room temperature. This spectrum is identical with that reported by Gainon (1964) and is almost certainly due to a substantial Fe^{3+} impurity. The lines are relatively broad varying from about 40 gauss to 250 gauss depending upon orientation and the domain from which they arise: the three lines correspond to three mutually perpendicular twinning directions or "domains" within the crystal. The relative intensity and width of each line thus depends upon the fraction of the crystal with a given tetrad axis and upon the scatter of this axis within each domain. The relative intensities of lines I, II and III (fig. 6.6.), the + 1/2 to - 1/2 transitions, are approximately 0.6 : 0.3 : 0.06. The axis of the weak spectrum IV is approximately 3^o away from that of the main spectrum and it presumably corresponds to twinning at the angle of 2 $\tan^{-1}$ (c/a-1) = 3.5^o (see 4.2.2., c = 4.150Å, a = 3.904 Å). Additional weak resonances, not shown in fig. 6.6, were seen near

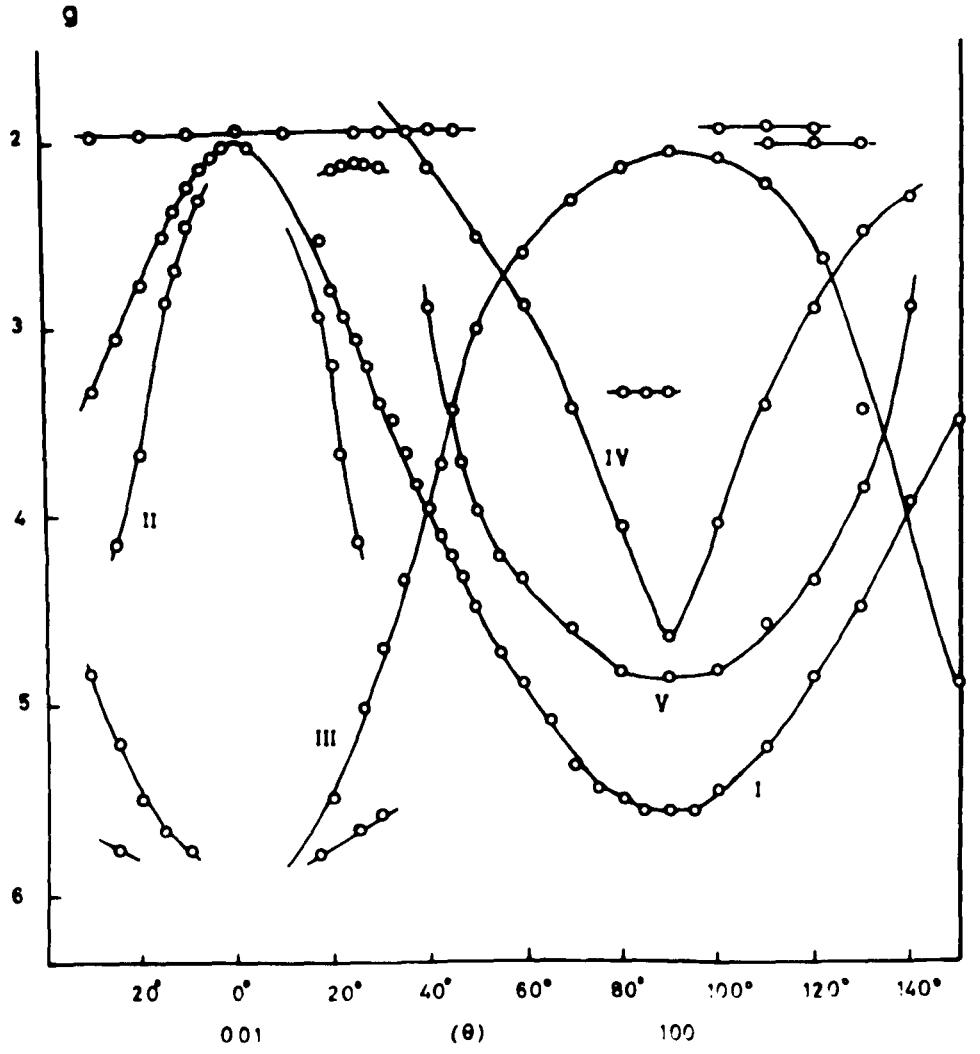

Fig. 6.7. Angular variation of the Fe^{3+}: $PbTiO_3$ spectrum in the a-c plane at Q-band

$g = 2$. The measured value of $g_{\perp}^{eff}$ for the strongly anisotropic main spectrum is

$$g_{\perp}^{eff} = 5.86 \pm 0.2$$

in agreement with the value quoted by Gainon.

The spectrum obtained from $PbTiO_3$ at Q-band and $77^{\circ}K$ is shown in fig. 6.7, and is qualitatively the same as that observed at room temperature and Q-band. Since considerably more sensitivity was available at X-band than at Q-band, even at $77^{\circ}K$, the additional resonances observed must presumably all arise from the same Fe^{3+} paramagnetic centre. This being the case transition I (fig. 6.7) is readily identified as + 1/2 to - 1/2 and several considerations lead to the supposition that all the other transitions observed come from the same domain as transition I. Consider, for example, transition III. It is conceivable that this might also be a + 1/2 to - 1/2 transition, its failure to reach $g = 2$ at 90° being due to misalignment of the sample. However if this were the case it would be difficult to imagine such a misorientation as would also cause transition I at 90° to be in a higher field than transition III at 0° - as is observed. In addition while the integrated intensity of transition I is approximately constant that of transition III is most definitely not; it is moderately intense and fairly broad at 90°, very weak and narrow at 0°. The facts that the relatively strong transitions IV and V are unobserved at 0° and that

there are no isotropic lines associated with transitions I - V also lend weight to the supposition that all the transitions shown in fig. 6.7 arise from a single domain, $\theta = 0^\circ$ corresponding to the magnetic field parallel to a tetrad axis and $\theta = 90^\circ$ to the perpendicular orientation. In view of the fact that the crystal used at Q-band was considerably smaller than that from which the thin section of fig. 5.7 was cut this seems quite a reasonable supposition.

Transition III (fig. 6.7) with $g = 6$ at $\theta = 0^\circ$ can only be + 3/2 to - 3/2, the fact that it is very weak at $\theta = 0^\circ$ being readily understandable since strictly it is forbidden in this orientation: the identification - 1/2 to - 3/2 is ruled out since this transition cannot be observed at both $\theta = 0^\circ$ and $\theta = 90^\circ$ with a fixed quantum. The origin of transition II (fig. 6.7) is obscure. It seems improbable that it should come from the $\pm$ 1/2 levels in a minority domain on account of its intensity and angular variation. It is most likely that it is derived from a pair of highly-admixed states, the upper one being mainly $(|+1/2\rangle + |-5/2\rangle)$ and the lower one mainly $(|-1/2\rangle + |-3/2\rangle)$. As will be seen from the energy level diagram of fig. 6.10 the four lowest levels in the parallel orientation cross one another very close to $g = 2$ at Q-band. The states thus become highly-admixed only a few degrees off axis and transitions which at first sight appear forbidden become strongly allowed: for example the "+ 1/2"

to "- 3/2" transition probability is already a half that of the main + 1/2 to - 1/2 transition only 1^{o} off axis. It is purely fortuitous that transition II occurs at $g = 2$ on axis and this considerably hampered early attempts to interpret the Q-band spectrum. Lines IV and V (fig. 6.7) are ascribed to the + 1/2 to - 3/2 and + 1/2 to + 3/2 transitions respectively. Line IV obeys the expected angular variation. However, it becomes rapidly narrower and stronger as Θ is rotated away from 90^{o} and between $\Theta = 30^{o}$ and $\Theta = 50^{o}$ it is the strongest line observed anywhere in the spectrum. This is very puzzling and there is no obvious explanation. An inspection of the energy level diagram of fig 6.9 shows that the remaining transition, line V of fig. 6.7 can only correspond to the + 1/2 to + 3/2 transition although its angular behaviour is critically dependent upon the magnitude of D and the size of the quantum and a direct correlation via the angular variation has not been attempted.

No detailed analysis of the linewidths, which vary from 100 gauss to 500 gauss, has been attempted though a few remarks may be in order. The linewidths increase with frequency, are temperature-independent, and vary markedly with orientation. These observations suggest that the major contribution is a g-value scatter proportional to $dg/d\Theta$. As will be seen from the thin-section photograph of fig. 5.7 there is a scatter of up to about 5^{o} in the

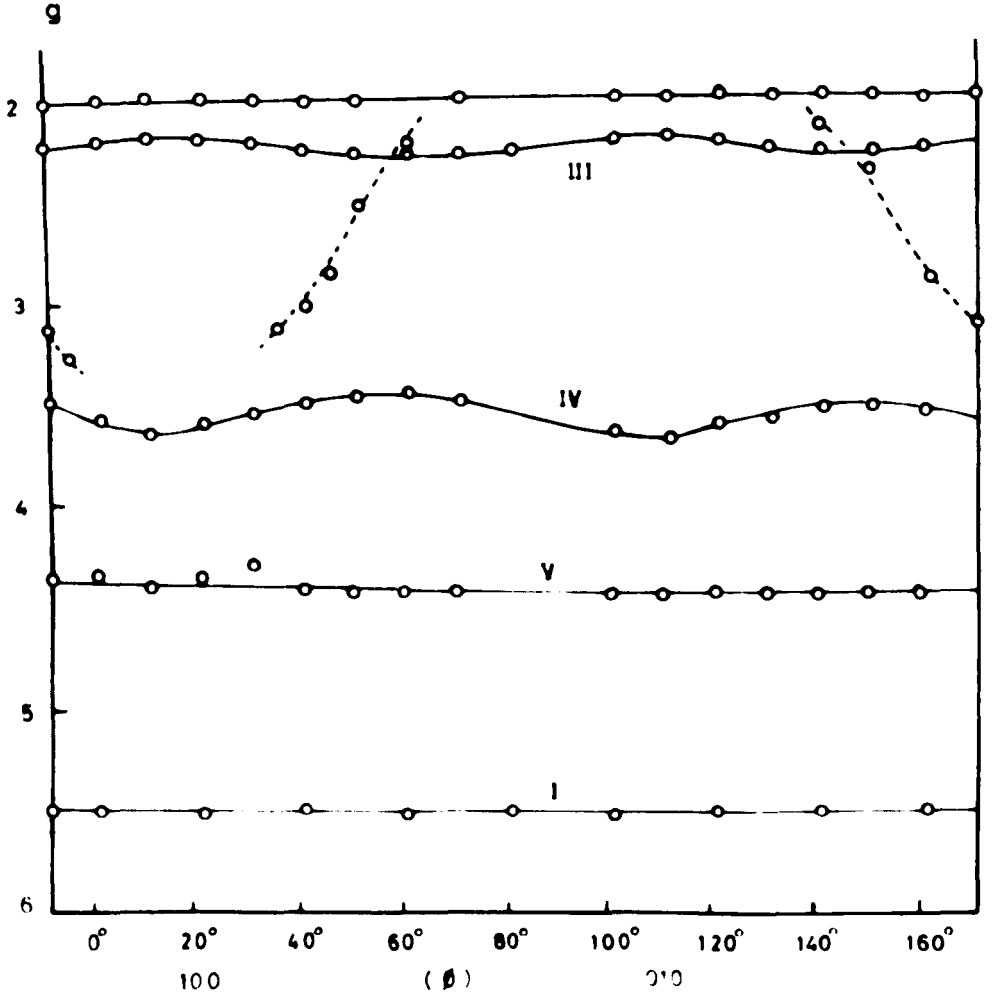

Fig. 6.8. Angular variation of the Fe^{3+}:$PbTiO_3$ spectrum in the a-a plane at Q-band

direction of the tetrad axis within each domain. This is of the order of magnitude of the twinning angle. Since it is not possible to write down an analytic expression for $g(\theta)$ when the Zeeman energy is of the order of the zero-field splitting it seems best to obtain an estimate of $dg/d\theta \simeq \delta g/\delta\theta$ from the experimental curves. Thus a value for $\delta\theta$ of about 3° is needed to account for the observed linewidth, of about 200 gauss, of the + 1/2 to - 1/2 transition at $\theta = 0^{\circ}$ at Q-band, and this seems to offer quite a reasonable explanation of the observed linewidth. Away from $\theta = 0^{\circ}$ the levels become strongly admixed and the lines considerably broader, particularly the + 1/2 to $\pm$ 3/2 transitions which have linewidths of up to about 500 gauss at $\theta = 90^{\circ}$.

A check on the identifications of the various transitions given above was provided by rotating the $PbTiO_3$ crystal through 90° in such a way that the supposed c-axis became perpendicular to the plane of rotation of the magnetic field. The spectrum of fig. 6.8 was then observed. It consists, as expected, of a series of broadly isotropic lines in positions corresponding to the $\theta = 90^{\circ}$ turning points of transitions I, III, IV and V of fig. 6.7. In addition there is a roughly isotropic line at g = 2 and a highly anisotropic one displaying the same angular variations as transition IV of fig. 6.7. This latter

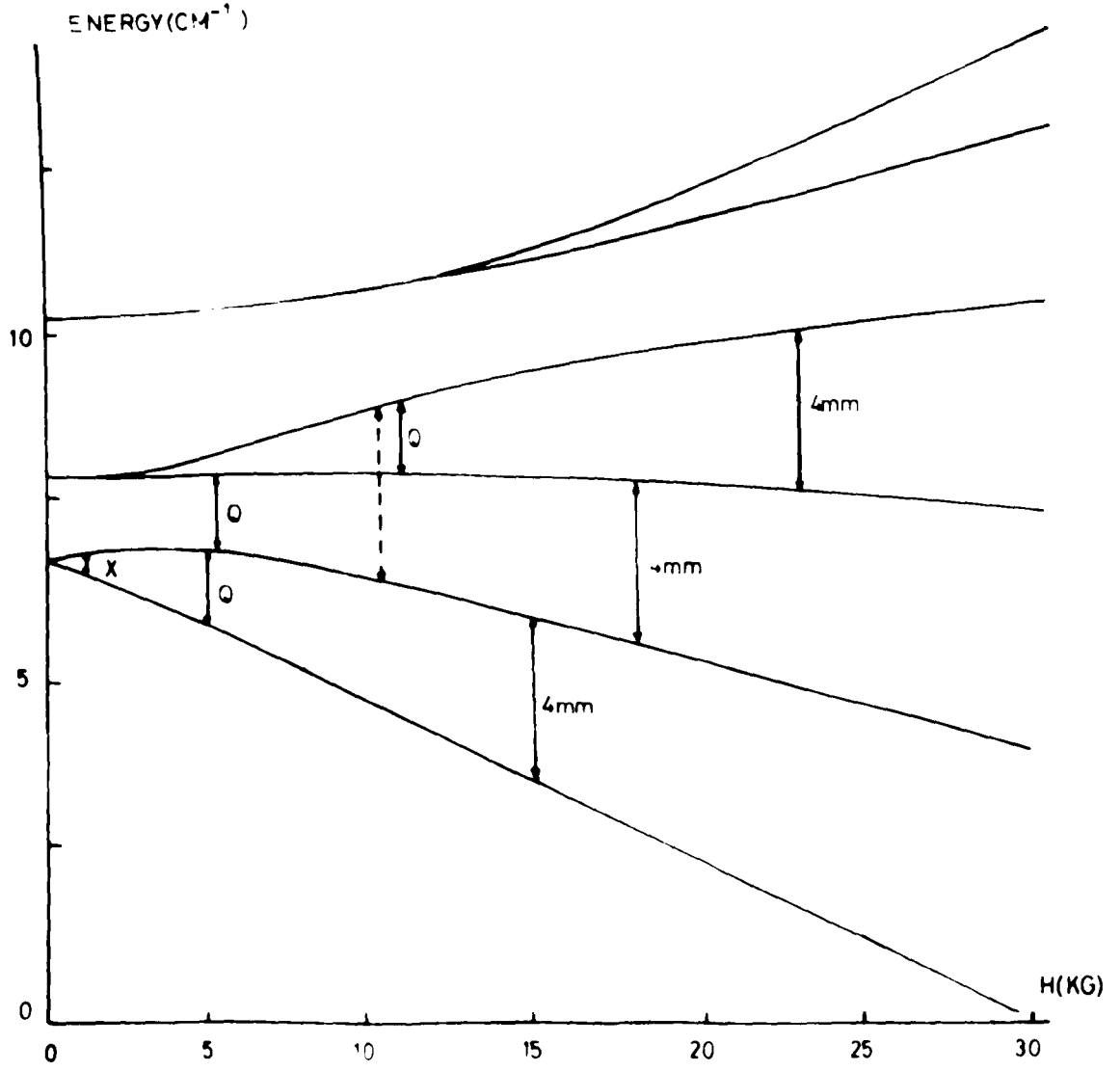

Fig. 6 9 Energy levels for Fe^{3+} in $PbTiO_3$ H perpendicular to z

transition most probably has the same origin as transition IV of fig. 6.7 but arises from a small domain perpendicular to the main one: since transition IV is by far the strongest, at least off axis, it is quite reasonable that this would be the only transition observed from a minority domain. The fact that it gets rapidly narrower and more intense as the magnetic field is rotated away from $\theta = 90^{\circ}$ explains why the signal from the minority domain is not seen on axis in either fig. 6.7 or fig. 6.8 - it should appear as an isotropic line in the former figure.

The slight degree of anisotropy of transitions IV and V in fig. 6.8 is presumably indicative of a cubic variation of the spectrum as in $SrTiO_3$: it will be seen that the maxima and minima of the anisotropy correspond to the crystal axes which is a priori unlikely if the anisotropy is due to sample misorientation.

One or two further points concerning the interpretation of the Q-band results are worth mentioning. Firstly there is the non-observation of the expected - 1/2 to - 3/2 transition near $\theta = 0^{\circ}$. Between $\theta = 0^{\circ}$ and $\theta = 25^{\circ}$ it would not have been seen since the magnetic field scan was not extended to sufficiently low fields. Near 25° it should have been seen moving rapidly to high field but was presumably broadened beyond observation by the g-value scatter. Several fragments of other transitions are

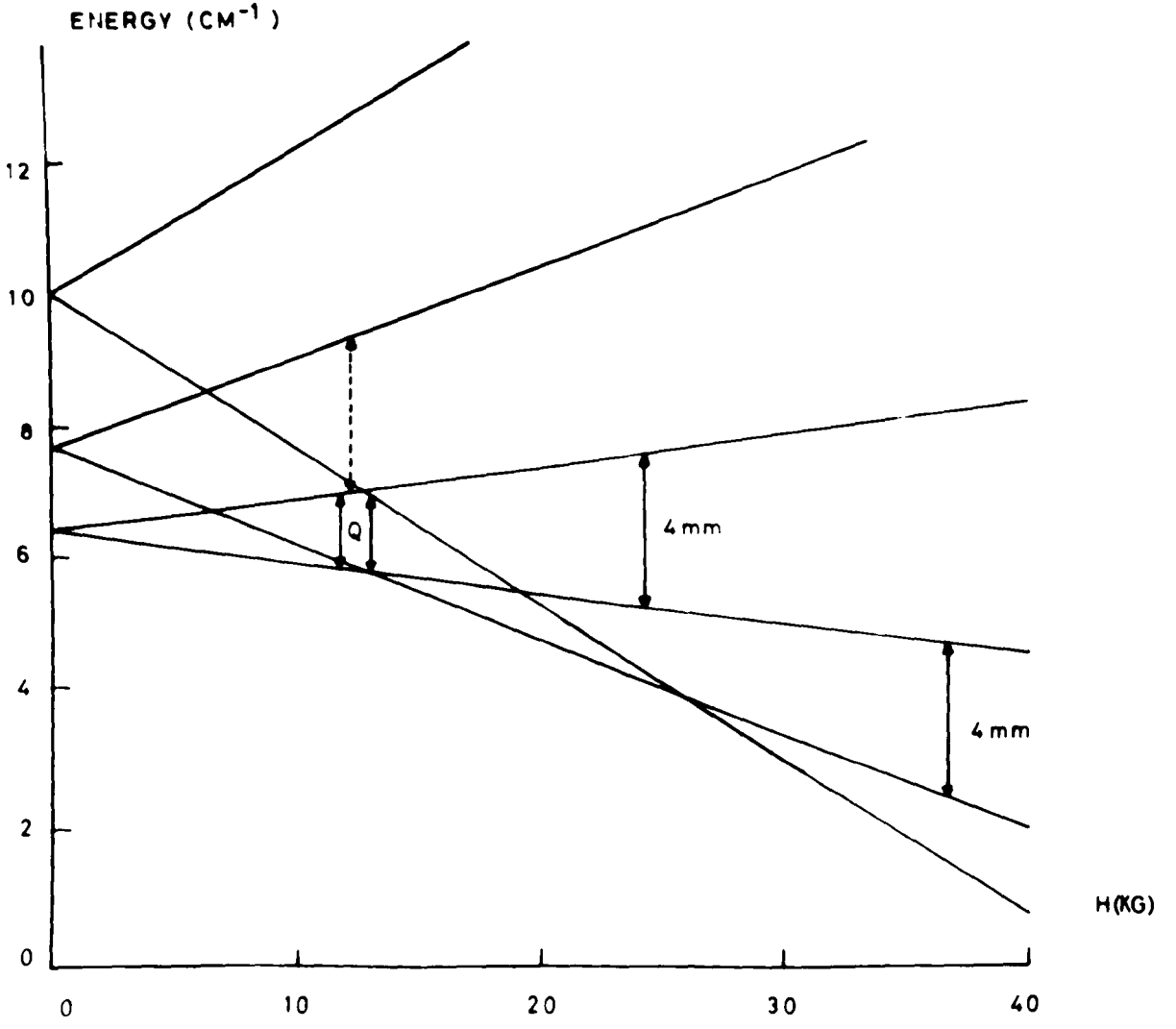

Fig 6.10 Energy levels for Fe^{3+} in $PbTiO_3$: H parallel to z

indicated but not identified in fig. 6.7 and it is not certain whether they arise from Fe^{3+} or not. As mentioned before the energy levels of the main spectrum become strongly admixed only a few degrees away from $\Theta = 0^{o}$ and the angular behaviour of the many allowed transitions becomes very complicated. No detailed analysis of the angular variation and intensities of the transitions off-axis has been attempted but the main features of the principal lines may be qualitatively understood in terms of the discussion of the origins of the various transitions given above.

6.2. 2. Spin Hamiltonian Parameters.

The Q-band results may be fitted to a spin Hamiltonian of the form

$$\mathcal{H} = g_{\parallel}\beta H_z S_z + g_{\perp}\beta (H_x S_x + H_y S_y) + DS_z^2 + \frac{a}{6}(S_x^4 + S_y^4 + S_z^4)$$

with, at room temperatures,

$$g_{\parallel} = g_{\perp} = 2.00$$

$$D = 0.65 \pm 0.15 \text{ cm}^{-1}$$

$$a = (270 \pm 40) \times 10^{-4} \text{ cm}^{-1}$$

$$\Delta = 2D - 5a/2 = 1.3 \pm 0.3 \text{ cm}^{-1}$$

The rather large error in D arises not so much from the experimental determination of resonance fields as from the different values of D indicated by the individual transitions. In view of the rather imperfect nature of the $PbTiO_3$ crystals

investigated and the surmized covalent nature of the Pb-O bond system such a lack of agreement with theory is perhaps not too surprising. Since from the nature of the E.P.R. spectra a and D must have the same sign it is again to be assumed as in $SrTiO_3$ that both are positive in the absence of any evidence to the contrary.

At 77°K the symmetry of the spectrum is the same as at room temperature but the + 1/2 to $\pm$ 3/2 transitions are seen to move to slightly lower fields at $\Theta = 90^{\circ}$ while the + 3/2 to - 3/2 transition moves to higher field. Both these observations indicate a slight increase in D, of approximately 0.1 cm^{-1}, thus

$$\Delta(77^{\circ}K) = 1.5 \pm 0.3 \text{ cm}^{-1}$$

The value of $g_{\perp}^{eff}$ (+ 1/2 to - 1/2) is little affected by a change in D of this magnitude and it is not surprising that Gainon failed to observe any change in the X-band spectrum between 300°K and 180°K.

The Fe^{3+}: $PbTiO_3$ spectrum was also studied at 4.2°K at 4mm., along the principal axes. The crystal used was the same as that at X-band: knowing the distribution of the crystal among the various domains from the relative intensities of the + 1/2 to - 1/2 transitions at X-band it was possible by running the 4mm. spectrum with the crystal in two mutually perpendicular orientations to determine from the changes in intensity which of the lines corresponded to the "perpendicular" orientation and which to the "parallel".

The results are summarized in the energy level diagrams of figs. 6.9 and 6.10. The observed transitions are seen to fit the energy levels extrapolated from Q-band rather well and this may be taken as an indication that there is no drastic change in the crystal structure between room temperature and $4.2^{\circ}K$. Some depopulation of the + 1/2 and - 3/2 levels is to be expected at $4.2^{\circ}K$ though not enough to render transitions from these levels unobservable.

6.2. 3. Structural Implications of Spin Hamiltonian Parameters.

The parameters a and D given above are best discussed in the context of the same parameters obtained for Fe^{3+} in similar perovskite lattices. These are summarized in table 6.1.

Table 6.1 : Comparative Data for Fe^{3+}

	$BaTiO_3$			$PbTiO_3$	$SrTiO_3$			$KTaO_3$	
	C	T	C.C	T	C	T	C.C.	C*	C.C
	$425^{\circ}K$	$300^{\circ}K$	$77^{\circ}K$	$300^{\circ}K$	$300^{\circ}K$	$77^{\circ}K$	$300^{\circ}K$	$4.2^{\circ}K$	$4.2^{\circ}K$
$2D(cm^{-1})$	0	0.186		1.3	0	0.0015	2.732	0	
$10^4 a(cm^{-1})$	34	102		270	198	220	132	350	
$c(\AA)$		4.036	$g_{\perp}=6.0$	4.150	3.902				$g_{\perp}=6.0$
$a(\AA)$		3.992		3.904				3.989($300^{\circ}K$)	
c/a		1.010		1.063	1				

C : Cubic T : Tetragonal C.C. Charge Compensated

* : The precise low-temperature structure of $KTaO_3$ (below

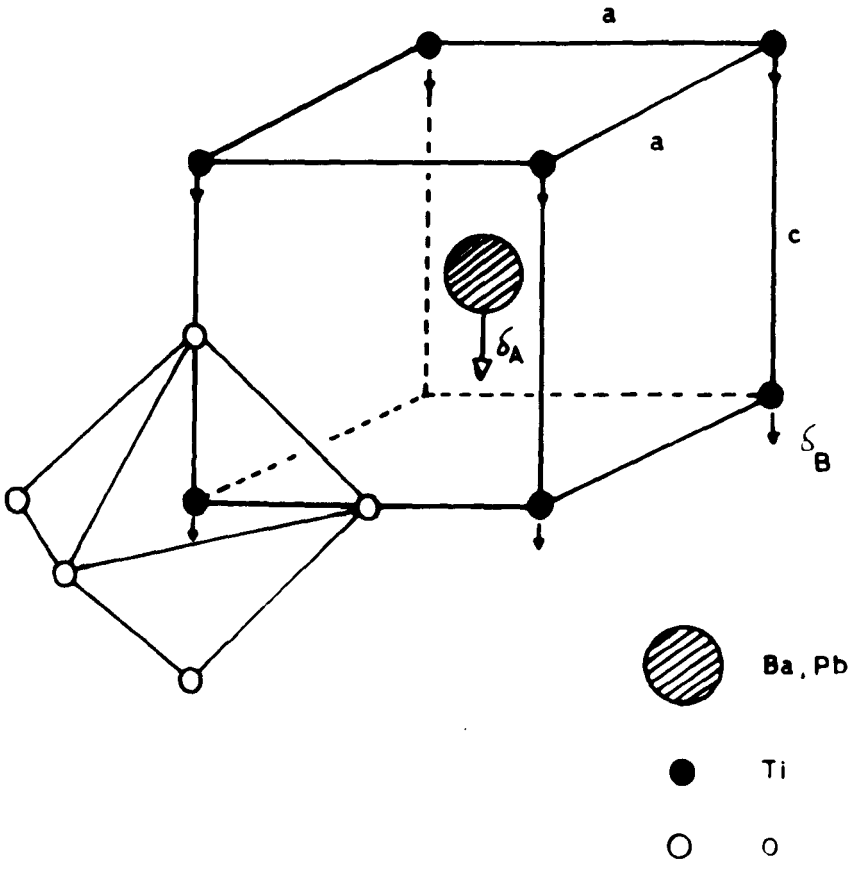

Fig.6.11. Illustrating the off-centre distortion in $PbTiO_3$ and $BaTiO_3$

$13^{o}K$, the ferroelectric Curie point) is not known.

The magnitude of the cubic parameter a in $PbTiO_3$ is seen to be comparable with that found in $SrTiO_3$ and $KTaO_3$ and this provides evidence, as discussed earlier, that the Fe^{3+} ion substitues at the Ti^{4+} site: point-charge considerations show that the magnitude of V_4^4 is about four times smaller for an ion substituting at the $A(Pb^{2+})$ site than for one substituting at the $B(Ti^{4+})$ site. The rather small value of a in $BaTiO_3$ is, as yet, unexplained - it is still believed, mainly from considerations of ionic radii, that Fe^{3+} substitutes at the Ti^{4+} site. Since the ferroelectric distortion in $PbTiO_3$ is considerably greater than in $BaTiO_3$ it does not appear that the explanation lies in this direction.

The value of D in $PbTiO_3$ is seen to be about seven times greater than that in $BaTiO_3$ and this is in reasonable agreement with what might be expected. The tetragonal phases of $BaTiO_3$ and $PbTiO_3$ are isomorphous and are illustrated in fig. 6.11. It is easiest to visualize this structure as derived from the cubic by stretching it slightly parallel to one cube edge and releasing all the atoms from their special positions so that they can have small displacements in this direction. It is found that the oxygen octahedra remain virtually undisturbed and it is most convenient to consider the framework of oxygen

octahedra as fixed and to express the distortion from a centro-symmetric tetragonal structure in terms of small displacements of the A and B ions. These displacements are in the same direction and represent the shift of the positive A^{2+} B^{4+} sublattice with respect to the O_3^{2-} framework which gives rise to the spontaneous ionic polarization and hence the ferroelectric behaviour of these substances. The displacements of the A and B ions are respectively 0.07 Å and 0.13 Å in $BaTiO_3$ and 0.46 Å and 0.29 Å in $PbTiO_3$.

Considering, as in appendix II, a nearest-neighbour approximation only, the crystal field parameter V_2^o in the distorted ABO_3 structure can be shown by a straightforward manipulation of Eq. A.2.1 to be given by

$$V_2^o \simeq \frac{C_2^o}{a^3}\left[\Delta - 2\delta_B^2\right] \qquad 6.3$$

where C_2^o is a constant, $\Delta = c/a - 1$, and δ_B is the fractional displacement of the B ion from the "normal" tetragonal position. The axial crystal field is thus seen to be approximately six-and-a-half times greater in $PbTiO_3$ than in $BaTiO_3$, about the same as the ratio of the axial spin Hamiltonian parameters. The uncompensated charge of Fe^{3+} may locally modify the crystal field and the simple point charge approach should be treated with circumspection. However it does seem quite reasonable that the origin of the large zero-field splitting of Fe^{3+} in $PbTiO_3$ should lie in

the large tetragonal distortion of the ferroelectric phase as suggested by Gainon.

The question now arises as to whether these results may be correlated with any of the theories of the zero-field splitting of S-state ions discussed in chapter III. The most reliable data for comparison seems to be that of Nicholson and Burns (1963) and this is summarized in fig. 3.1 of this Thesis. Nicholson and Burns found the sign of B_2^0 at the titanium site in $BaTiO_3$ to be negative as is also indicated by equation A.2.1 of this Thesis for the type of elongation of the oxygen octahedron encountered in $BaTiO_3$ and $PbTiO_3$. The values to be compared with the theory may thus be taken as

$$D(BaTiO_3) = 0.09 \text{ cm}^{-1}$$

$$D(PbTiO_3) = 0.65 \text{ cm}^{-1}$$

and $B_2^0(PbTiO_3) = 6.5\ B_2^0(BaTiO_3)$ (B_2^0 negative)

A tentative extrapolation of Nicholson and Burns' results (fig. 3.1) to D = 0.65 indicates that B_2^0 should be approximately twice as large in $PbTiO_3$ as in $BaTiO_3$. This is a somewhat smaller factor than the present point charge calculation of this ratio and suggests that the slope of the D vs. B_2^0 graph may be rather more gentle than indicated by Nicholson and Burns. Bearing in mind, however, the large discrepancies between the various different theories the present results are seen to be in substantial agreement with the semi-empirical relationship obtained by Nicholson

and Burns. It would be very interesting to try to fit the value of D of 1.35 cm^{-1} found in $SrTiO_3$ to this same theory. However both the sign and magnitude of B_2^0 in $SrTiO_3$ are critically dependent upon the rearrangement of the ligands following the removal of the O^{2-} ion at the sixth coordination point and without a much more sophisticated approach to the calculation of the new value of B_2^0 such a comparison would be meaningless.

The measured change in D in $PbTiO_3$ between 290°K and 77°K corresponds to an increase of approximately 15%. This may be understood in terms of the temperature-dependeent lattice deformation observed in $PbTiO_3$. A tentative extrapolation of the results of Shirane and Hoshino (1951) leads to an axial ratio c/a of approximately 1.085 at 77°K though this probably represents an upper limit. The value at room temperature is 1.063 and the increase in (V_2^0) on cooling to 77°K is thus seen from Eq. 6.3 to amount to approximately 19% which is in quite good agreement with the measured change in D. Since the quantity c/a - 1 is also directly related to the spontaneous polarization, P_s, a detailed study of the zero-field splitting parameter D in $PbTiO_3$ as a function of temperature would be very interesting from the point of view of ferroelectric theory, particularly in view of the similarity between $PbTiO_3$ and $BaTiO_3$ which has probably been the most extensively investigated of all ferroelectrics.

The phase change to a multiple cell tetragonal structure at 170°K reported by Kobayashi et. al. (1956) does not occur if the crystal is cooled rapidly through the transition temperature (Jona and Shirane 1960) as would have been the case in the present work. As was stated above the E.P.R. measurements at 4.2°K fit the room temperature Hamiltonian quite well and it seems that there can be no drastic change in the structure of $PbTiO_3$ between 300°K and 4.2°K when the cooling to 4.2°K is rapid.

6.3. $BaTiO_3$ and $CaWO_4$

6.3. 1. $BaTiO_3$

The $g_\perp^{eff} = 6$ signal characteristic of S = 5/2 in a strong axial field has also been reported in the iron-doped perovskites $BaTiO_3$ and $KTaO_3$ (Gainon 1965, Wemple 1963). Both these spectra occur in addition to the "normal" Fe^{3+} spectra and are presumably due to nearest neighbour charge compensation as in $SrTiO_3$. Charge compensation for Fe^{3+} is also to be expected in the many perovskites with the formulae $A^{1+}\ B^{5+}\ O_3^{2-}$ and $A^{2+}\ B^{4+}\ O_3^{2-}$

Samples of heavily iron-doped $BaTiO_3$ were investigated at Q-band in the present work in the hope of being able to measure the parameter D of the axial spectrum since this would have provided an interesting comparison for the $SrTiO_3$ results. Heavy iron doping is

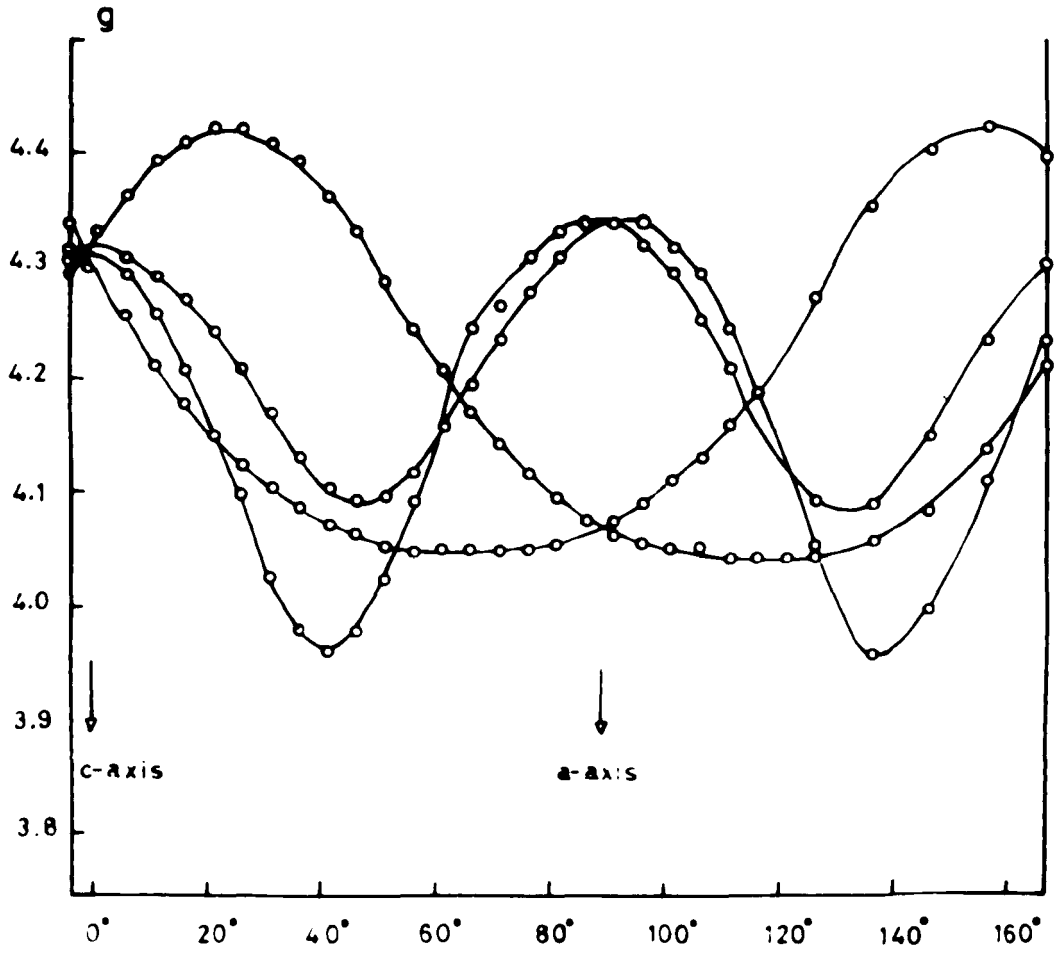

Fig 6.12. Angular variation of the Fe^{3+}:$CaWO_4$ spectrum in the a-c plane at Q-band

necessary in order to obtain a sufficient number of Fe^{3+} ions close to an oxygen ion vacancy to give an observable spectrum (Gainon 1965). Only the "normal" tetragonal spectrum could be observed from the samples available in the present work, the exact degree of iron-doping of these samples not being known. Investigations were carried out at room temperature using a Varian V4503 Q-band spectrometer and down to 20°K on the home-built spectrometer described earlier. From fig. 2 of Gainon's paper it appears that the spectrum is very weak even at 77°K and it will probably generally be necessary to use sensitive equipment at low temperatures in order to observe the axial spectrum. It was not convenient in the present case to use the Varian spectrometer at low temperatures.

6.3. 2. $CaWO_4$

In contrast to the $g = 6$ signal observed in the perovskites the paramagnetic resonance of Fe^{3+} in $CaWO_4$ is characterized by a nearly isotropic signal at $g = 4.3$. Such a resonance is normally characteristic of $S = 5/2$ in a completely rhombic field ($E/D = 1/3$) which is the interpretation put on the observed results by Kirton and Newman (1965). The $g = 4.3$ signal in a rhombic field arises from the middle pair of the three Kramers' doublets into which $S = 5/2$ splits in a crystal field of lower than cubic symmetry. Kedzie et. al. (Kedzie, Lyons and Kestigan 1965,

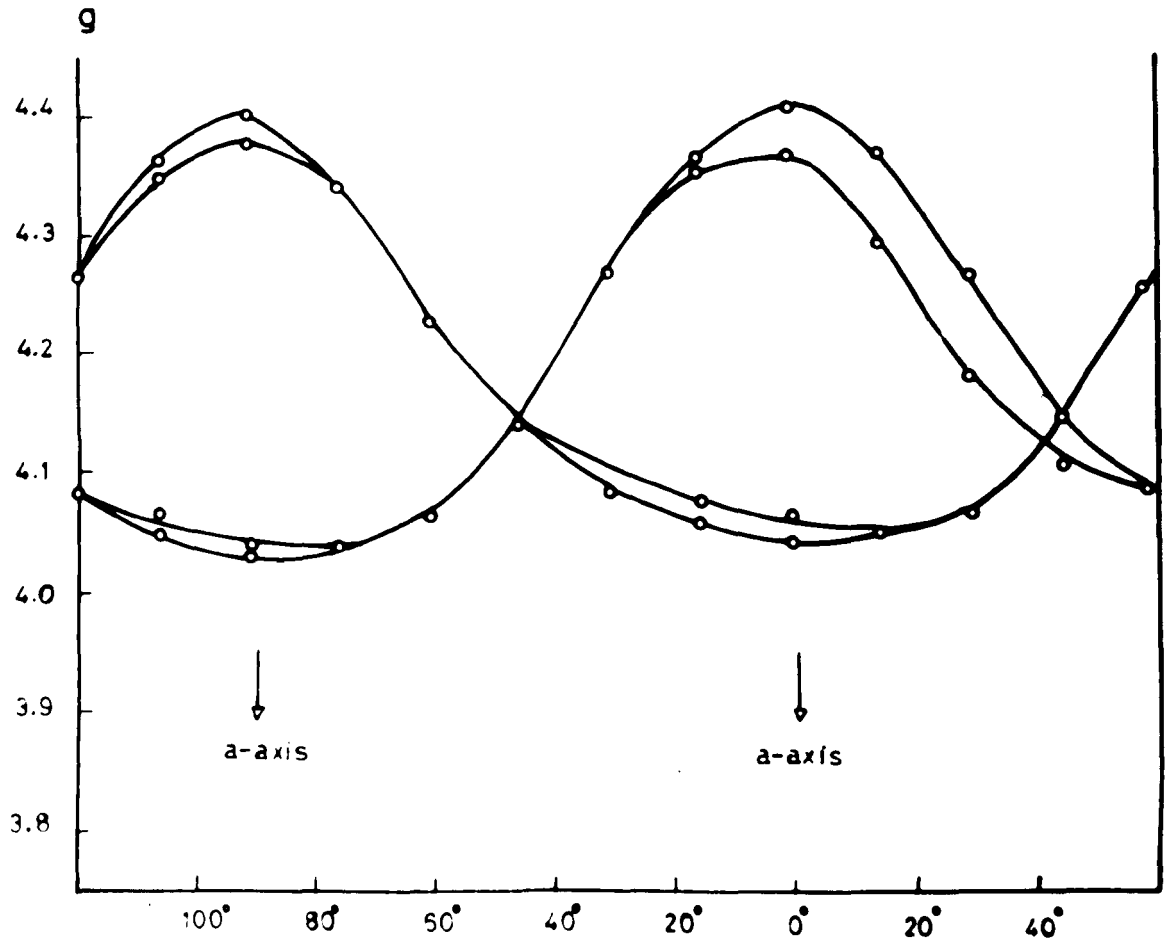

Fig. 6.13. Angular variation of the Fe^{3+}: $CaWO_4$ spectrum in the a-a plane at Q-band

Kedzie and Lyons 1965) have, however, shown that a $g = 4.3$ signal can be obtained from the ground doublet of $S = 5/2$ in a tetragonal field provided that a certain relationship holds between the second (D) and fourth (F)-order terms, and this situation they believe to hold in $CaWO_4$. One way of differentiating between these two models would be to make measurements at shorter wavelengths where inter- (as opposed to intra-) Kramers' doublet transitions should become observed, and this has been attempted in the present work (the initial experiments were carried out at X-band).

The room temperature variation of the Fe^{3+}:$CaWO_4$ spectrum at Q-band in the "a-a" and "a-c" planes is shown in figs. 6.12 and 6.13 which are similar to the X-band figures given by Kedzie, Lyons and Kestigan: the doubling of the lines in fig. 6.13 is due to a slight misorientation of the sample. These spectra were obtained using the Varian Q-band spectrometer: no $g = 4.3$ signals could be seen at room temperature or helium in either the home-built Q-band spectrometer, a Hilger and Watts Q-band Microspin, or the 4mm. spectrometer. It is not known whether this was due to lack of sensitivity - which is quite possible, or due to saturation - the lowest power it was convenient to use was about 2 mwatts, some 20 x more than was used by the above authors.

In place of the $g = 4.3$ resonance, however, the spectrum of fig. 6.14 was observed (at Q-band and $4.2^{o}K$).

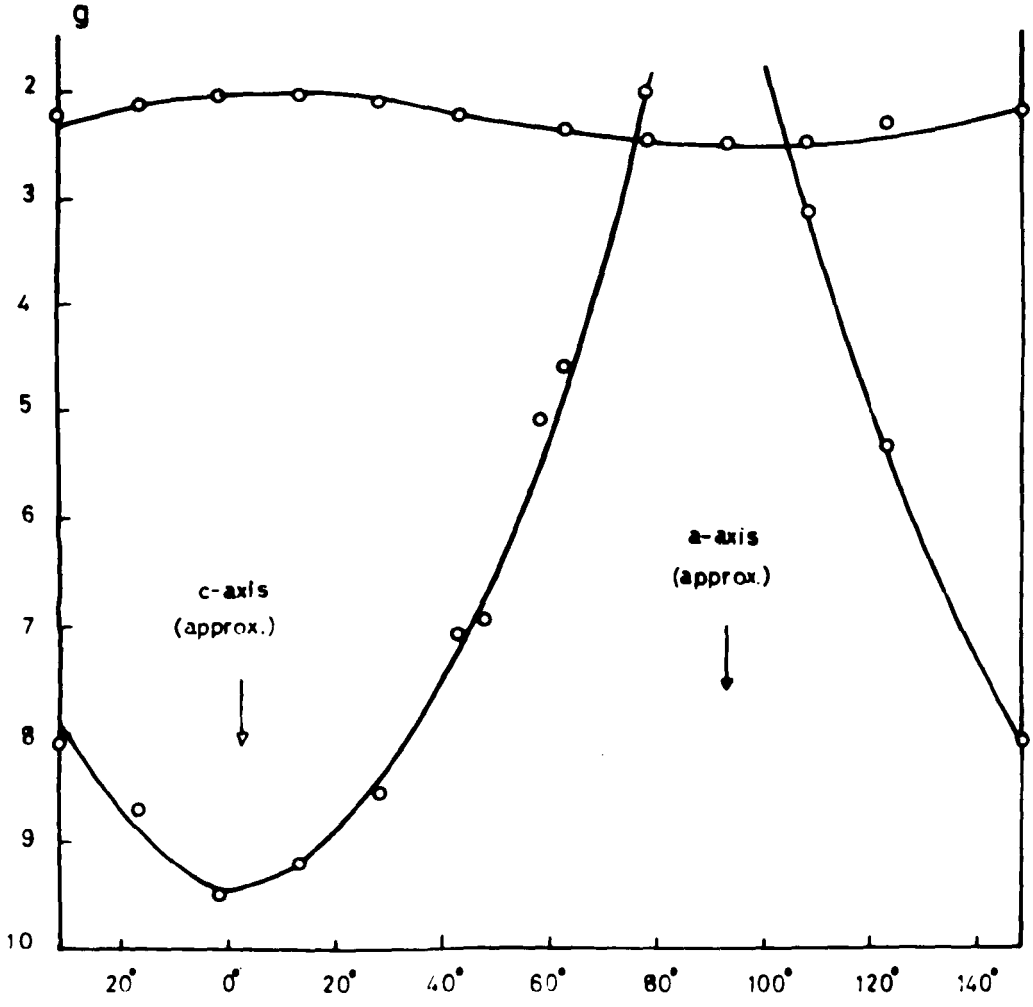

Fig. 6.14. The spectrum observed in $CaWO_4$ at 4.2°K

It consists of two fairly intense lines, one approximately 3 gauss wide and varying from g = 2 to g = 2.5, the other approximately 500 m.gauss wide (on the c-axis) and varying from g = 9.5 to g < 2. It seems unlikely, because of their intensities and the lack of a g = 4.3 signal, that these resonances should arise from Fe^{3+}. However the angular behaviour, particularly of the latter line is roughly what might be expected from the ground doublet of S = 5/2 in a rhombic field (see e.g. Wickman et. al. 1965) and it is conceivable that the observed resonances may arise from this doublet and that the middle doublet resonance is either much weaker, broadened by crystal strains (see Kedzie, Lyons and Kestigan), or saturated. The immediate objection to this theory is that essentially the same spectrum should be observed at X-band whereas in fact only the isotropic g = 4.3 signal is seen.

The short wavelength studies of $CaWO_4$ have only recently been initiated and the necessity for considerable further work is clearly indicated. It is possible that a detailed analysis of the room temperature measurements might shed some light on these problems, though as Blumberg (1967) has recently pointed out the analysis of Fe^{3+} spectra in rhombic fields in terms of a conventional g-tensor must be treated with care. It is hoped to pursue these studies on $CaWO_4$ further in the near future.

6.4. Summary and Suggestions for Further Work.

The E.P.R. spectra of $PbTiO_3$ and $SrTiO_3$ have been studied at 8mm. and 4mm. wavelengths where it has proved possible to induce transitions between the different Kramers' doublets. From measurements in fields of up to 15 Kgauss the zero-field splitting experienced by the Fe^{3+} ion substituting at the Ti site has thus been found in each of these lattices. The work on $SrTiO_3$ has indicated a possible departure from a conventional spin Hamiltonian though the results are not really conclusive and further work is needed. Since a cubic crystal field affects the $\pm$ 3/2 Kramers' doublet of the S = 5/2 spin system in first order it has proved possible to determine small cubic variations in the E.P.R. spectra in both $SrTiO_3$ and $PbTiO_3$ by studying the angular behaviour of transitions to these levels. The zero-field splitting in $PbTiO_3$ has been shown to be temperature dependent and the variation has been ascribed to the change in the axial ratio c/a which is also a function of temperature. Some simple nearest-neighbour point-charge calculations have been carried out to show that the observed zero-field splitting in $PbTiO_3$ is in general agreement with the theory of Nicholson and Burns for the zero-field splitting of S-state ions, and point-charge considerations have also been used to correlate the cubic field term in $SrTiO_3$ with a plausible rearrangement of the ligands following the removal of an O^{2-} ion from the

sixth co-ordination point of the Ti-site.

A more detailed study of the axial Fe^{3+} spectrum in $SrTiO_3$ would be of interest from two points of view. If the experiments could be extended to 2mm. it should be possible to obtain unequivocal proof of whether the Koster and Statz Hamiltonian does in fact provide a better description of high field, high frequency E.P.R. spectra than the conventional spin Hamiltonian. At 2mm. it should also be possible to observe transitions between the $\pm$ 3/2 and $\pm$ 5/2 doublets and so to obtain better values for the parameters a and F. These could then form the basis of a more sophisticated calculation to determine the sign and magnitude of B_2^0 at the modified Ti site in $SrTiO_3$, and hence a further experimental point could be added to the D vs. B_2^0 graph. This would be particularly useful since it would be at a larger value of D than previously attempted and would therefore provide a clearer indication of the functional dependence of D on B_2^0.

A more detailed study of the Fe^{3+}: $PbTiO_3$ spectrum at Q-band would also be particularly rewarding. The axial spin Hamiltonian parameter D could be determined as a function of temperature and the results related to the axial ratio c/a which has, as yet, not been determined fully as a function of temperature. As discussed earlier there is a correspondence between D and the spontaneous polarization P_s via the axial ratio c/a. The exact relationship between

the latter two quantities is by no means firmly established and the E.P.R. results might shed some light on this problem. More information on the nature of the large displacement of the A and B ions in the tetragonal phase of $PbTiO_3$ might also be gained, though better crystals than those used in the present work would probably be needed for this.

The many compounds possessing the perovskite structure have, as yet, received relatively little attention due mainly to the difficulty of growing good single crystals. As these become available, however, it is to be hoped that E.P.R. studies will provide useful supplementary information on the many interesting properties of these substances. $KTaO_3$ and $BaTiO_3$ suggest themselves for immediate further study at millimetre wavelengths.

References

Aisenberg S., Statz H., and Koster G.F., 1959, Phys. Rev. 116, 811

Baer R., Wessel G., and Rubins R.S., 1968, J. Appl. Phys. 39, 23

Blumberg W.E., 1967, "Magnetic Resonance in Biological Systems" (Pergamon, New York)

Gainon D.J.A., 1964, Phys. Rev. 134, A1300

Gainon D.J.A., 1965, J. Appl. Phys. 36, 235

Jona F., and Shirane G., 1960, "Ferroelectric Crystals" (Pergamon, New York) Chapter 5

Kedzie R.W., and Lyons D.H., 1965, Phys. Rev. Letters 15, 632

Kedzie R.W., Lyons D.H., and Kestigan M., 1965, Phys. Rev. 138, A918

Kirton J., and Newman R.C., 1965, Phys. Rev. Letters, 15, 244

Kirkpatrick E.S., Müller K.A., and Rubins R.S., 1964, Phys. Rev. 135, A86

Kobayashi J., Okamoto S., and Ueda R., 1956, Phys. Rev. 103, 830

Low W., 1960, Solid State Physics Suppl. 2 (Academic Press, New York) page 118

Low W., and Offenbacher E.L., 1965, Solid State Phys. 17, 172

Müller K.A. 1958, Helv. Physica Acta 31, 173

Nicholson W.J., and Burns G., 1963, Phys. Rev. 129, 2490

Shirane G., and Hoshino S., 1951, J.Phys.Soc. Japan 6, 265

Wemple S.H., 1965, Ph.D. Thesis M.I.T.

References

Wickman H.H., Klein M.P., and Shirley D.A., 1964, J.Chem. Phys. 42, 2113.

APPENDIX I

Application of Group Theory to the Determination of Crystal Field Splittings.

The application of group theory to the determination of crystal field splittings rests on the fact that the Hamiltonian must be invariant under a symmetry operation of the group of the crystal field. This is evident since by definition a symmetry operation brings the crystal into self-coincidence and hence obviously cannot affect the energy of the paramagnetic ion.

The symmetry operations are such rotations as C_2, C_3 etc. They may be "represented" by the effect which they have on a set of vectors, the "basis functions". Thus if we consider a triangular lamina under the rotation C_3 (120° about Oz) and choose e_1, e_2, e_3 as shown in fig. A1.1. to be basis functions, then

$$e_1' = C_3\, e_1 = e_2$$
$$e_2' = C_3\, e_2 = e_3$$
$$e_3' = C_3\, e_3 = e_1$$

or in a more condensed notation

$$(e_1'\ e_2'\ e_3') = (e_1\ e_2\ e_3) \begin{pmatrix} 0 & 0 & 1 \\ 1 & 0 & 0 \\ 0 & 1 & 0 \end{pmatrix} = (e_1\ e_2\ e_3)\ D(C_3)$$

The matrix $D(C_3)$ is a "three-dimensional representation" of the operator C_3. Similar representations can be found for all the other symmetry operations of the group of the

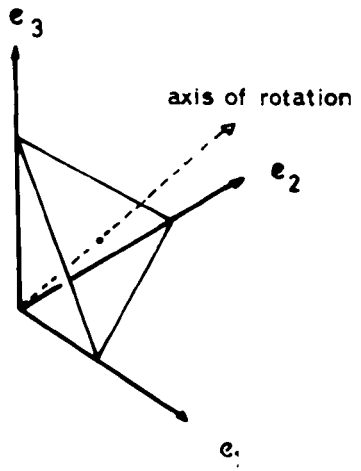

Fig. A.1.1. Basis vectors giving a 3-dimensional representation of C_{3V}

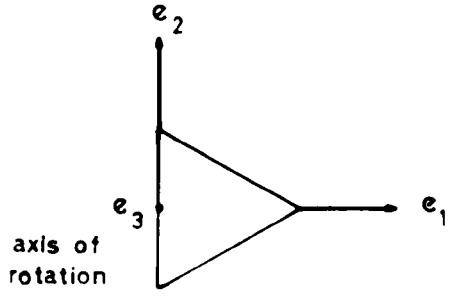

Fig. A.1.2. Basis vectors giving an irreducible representation of C_{3V}

equilateral triangular lamina, C_{3V}, and hence a three-dimensional representation of the whole group can be built up.

Now suppose we choose the basis functions to be as in fig. A.1.2. Then

$$(e_1' \; e_2' \; e_3') = (e_1 \; e_2 \; e_3) \begin{pmatrix} -\frac{1}{2}, & -\sqrt{3}/2 & 0 \\ \sqrt{3}/2, & -1/2 & 0 \\ 0 & 0 & 1 \end{pmatrix}$$

: using this basis e_3 transforms into itself and only e_1 and e_2 are mixed. The three-dimensional representation can thus be reduced to a two- and a one-dimensional representation. When it becomes impossible by changing the basis functions to reduce the block form of a representation any further it is said to be "irreducible".

Now atomic wavefunctions can be written analytically in the form $\underline{e} \cdot \underline{r} \, f(r)$ and they too can therefore provide bases for representations of a symmetry group. For example the three p-functions transform exactly like e_1, e_2, e_3 and they therefore provide just as good a basis for a representation of the symmetry group C_{3V} as do the Cartesian unit vectors e_1 e_2 and e_3. The effect of symmetry operations on the five d-functions can be considered formally in exactly the same way as above even though they cannot be visualized as vectors in 3-space. It is clear that the dimension of a reducible

representation is just equal to the number of basis functions one chooses and so the p-functions are said to "carry" a 3-dimensional representation, the d-functions a 5-dimensional representation, and so on. A reducible representation is said to "span" a number of irreducible ones.

We now return to our original statement that $\mathcal{H}$ is invariant under a symmetry operation. If a symmetry operation $\mathcal{C}_s$ leaves $\mathcal{H}$ invariant then clearly $\mathcal{H}$ and $\mathcal{C}_s$ commute and

$$\mathcal{C}_s \mathcal{H} \psi_i = \mathcal{C}_s E \psi_i = \mathcal{H} \mathcal{C}_s \psi_i = E \mathcal{C}_s \psi_i$$

i.e. $\mathcal{H}(\mathcal{C}_s \psi_i) = E(\mathcal{C}_s \psi_i)$

That is any function $\mathcal{C}_s \psi_i$ obtained by operating on one of the eigenstates ψ_i of $\mathcal{H}$ with a symmetry operator will also be an eigenfunction having the same energy as the original. So from any ψ_i we can get a whole series of other degenerate ones just be applying $\mathcal{C}_s$ to it, and thus any functionswhich transform among themselves are degenerate.

Returning to our example of the three p-functions in $\mathcal{C}_{3v}$ we see that the irreducible representations for which they provide a basis have just this property: p_x and p_y transform among themselves and carry a two-dimensional irreducible representation while p_z transforms into itself and carries a one-dimensional irreducible representation. We thus conclude that in a field of

symmetry C_{3v} the three p-functions split up into two levels one of which is two-fold degenerate and carries a two-dimensional irreducible representation and the other of which is non-degenerate and carries a one-dimensional representation.

This example illustrates a very important general theorem viz. that

"If $\mathcal{H}$ is invariant under a group of symmetry operations G and G has irreducible representations $\Gamma_1, \Gamma_2 \ldots$ then the eigenfunctions of $\mathcal{H}$ fall into groups which are degenerate and carry these representations".

Thus in group-theoretical terms the problem of finding how an initially degenerate level splits up in a field of any symmetry is that of finding the irreducible representations spanned by the reducible representation for which the initial functions provide a basis. It is not generally necessary to carry through the above sort of argument every time we want to do this, however. The matrix representation $D(\mathcal{C}_s)$ of any symmetry operator $\mathcal{C}_s$ can be specified by its character - the trace of $D(\mathcal{C}_s)$ - and a general theorem of group theory tells us just how to find the information we require. Suppose that we have set up a representation $D(\mathcal{C}_s)$ and we wish to find which irreducible representations it spans i.e. say it is of the form

$$D(\mathcal{C}_s) = n_1 D(\mathcal{C}_s) + n_2 D_2(\mathcal{C}_s) + \ldots\ldots$$

then it can be shown that

$$n_\beta = \frac{1}{g} \sum_{\mathcal{C}_s} \chi_\beta(\mathcal{C}_s)^* \chi(\mathcal{C}_s) \qquad \text{A.1. 1}$$

where g is the order of the irreducible representation, $\chi_\beta(\mathcal{C}_s)$ are the characters of the matrix representations for which the reducible functions form a basis, and $\chi(\mathcal{C}_s)$ those for which the irreducible representations of the symmetry group under consideration form a basis.

One of the commonest applications of these ideas is in calculating the degeneracies which arise when the symmetry of the free ion is lowered from purely spherical. In this case a convenient starting point is the fact that for a given angular momentum, j, the spherical harmonics in terms of which the wave-functions are usually written provide a basis for a $(2j + 1)$-dimensional representation, $D^{(j)}$, of the full rotation group.

The character (matrix trace) of a general rotation R is given by

$$\left.\begin{aligned} (R) &= \frac{\sin (j + 1/2)\, R}{\sin \frac{1}{2} R} && R \neq 0 \\ (R) &= 2j + 1 && R = 0 \end{aligned}\right\} \qquad \text{A.1. 2}$$

APPENDIX II

Point Charge Calculation for Strontium Titanate.

Consider the situation of Fig. A.2 in which a central metal ion is surrounded by an octahedral array of point charges, q_j, at positions (r_j, θ_j, ϕ_j) of $(a, \pi/2, 3\pi/2)$, $(a, \pi/2, 0)$, $(a, \pi/2, \pi/2)$, $(a, \pi/2, \pi)$, $(b, 0, 0)$, $(c, \pi, 0)$. Following Hutchings (1964) the potential at a point (r, θ, ϕ) near the central metal ion may be expanded in terms of spherical harmonics as

$$V(r, \theta, \phi) = \sum_j q_j \sum_n \frac{r^n}{R_j^{(n+1)}} \frac{4\pi}{2n+1} \sum_{m=-n}^{m} (-1)^m Y_n^m(\theta, \phi) Y_n^{-m} (\theta_j, \phi_j) \qquad \text{A.2. 1}$$

The crystal field potentials of interest in the present case, V_4^0 and V_4^4 are thus seen to be given by

$$V_4^0 = \frac{q\, r^4 \sqrt{\pi}}{12} \sum_j \frac{1}{R_j^5} (35 \cos^4\theta_j - 30 \cos^2\theta_j + 3) Y_4^0$$

$$V_4^4 = \frac{q\, r^4 \sqrt{35/2}}{12} \sum_j \frac{1}{R_j^5} (Y_4^{-4} e^{4i\phi_j} + Y_4^4 e^{-4i\phi_j}) \sin^4\theta_j \qquad \text{A.2. 2}$$

Or more explicitly

$$V_4^0 = A Y_4^0 \left[\frac{12}{a^5} + \frac{8}{b^5} + \frac{8}{c^5} \right]$$

$$V_4^4 = B (Y_4^4 + Y_4^{-4}) \cdot \frac{4}{a^5} \qquad \text{A.2. 3}$$

where $A = qr^4\sqrt{\pi}/12$ and $B = qr^4\sqrt{35\pi/2}/12$

If $a = b = c = 0$ we have the sixfold cubic coordination of the normal Fe^{3+} spectrum and

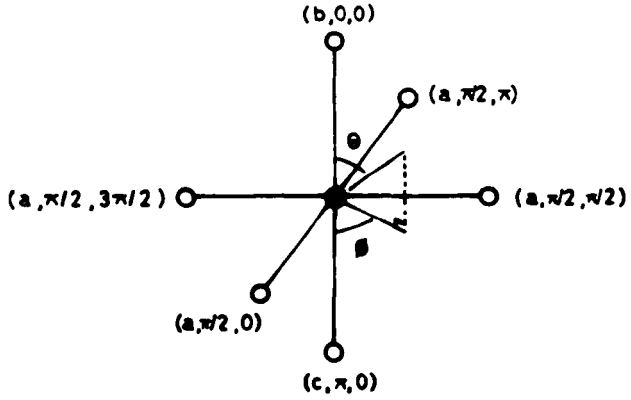

Fig. A.2.1. Co-ordinate system for point charge calculation

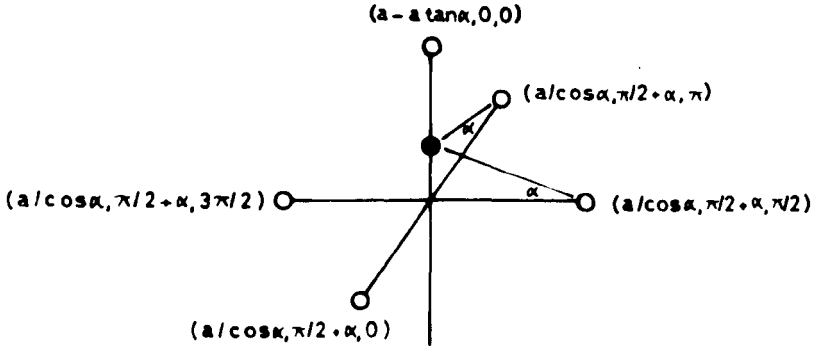

Fig. A.2.2. A possible atomic configuration in charge-compensated $SrTiO_3$

$$Vcub = V_4^0 + V_4^4 = \frac{28A}{a^5}\left[Y_4^0 + \sqrt{\frac{5}{14}}\ (Y_4^4 + Y_4^{-4})\right] \qquad A.2.\ 4$$

If b = a and c $\to \infty$ we have the case of the axial spectrum with no rearrangement of the remaining ligands and

$$\begin{aligned} V_{ax} &= V_4^0 + V_4^4 \\ &= \frac{20A}{a^5}\left[Y_4^0\right] + \frac{4B}{a^5}\ (Y_4^4 + Y_4^{-4}) \\ &= \frac{28A}{a^5}\left[Y_4^0 + \sqrt{\frac{5}{14}}\ (Y_4^4 + Y_4^{-4})\right] - \frac{8A}{a^5}\ Y_4^0 \\ &= Vcubic - \frac{8A}{a^5}\ Y_4^0 \qquad A.2.\ 5 \end{aligned}$$

The potential is thus seen to be the original cubic potential minus a term in Y_4^0. Y_4^0 has the same transformation properties as the term in "F" in the spin Hamiltonian 2.22.

If Vcubic is to decrease by a factor of 2/3 then V_4^4 must decrease by this amount. From A.2. 3 V_4^4 is seen to behave as $1/a^5$ and approximately an 8% increase in the ligand-central ion spacing would thus lead to the desired effect. V_4^0 may be recomputed from A.2. 3 assuming b = 1.08 a and c $\to \infty$ and one finds

$$V_4^0 = AY_4^0\left[\frac{2}{3}\cdot\frac{12}{a^5} + \frac{8}{a^5}\right] = \frac{16AY_4^0}{a^5}$$

Thus

$$\begin{aligned} V'_{ax} &= V_4^0 + V_4^4 \\ &= \frac{48}{3}\ AY_4^0 + \frac{2}{3}\ V_4^4\ (\text{cubic}) \\ &= \frac{2}{3}\ V_4^0\ (\text{cubic}) + \frac{2}{3}\ V_4^4\ (\text{cubic}) - \frac{8AY_4^0}{a^5} \qquad A.2.\ 6 \end{aligned}$$

- that is the cubic field is 2/3 of its original value and the remaining term in Y_4^0 while smaller than before still has the opposite sign to that of the cubic term.

If instead of postulating an outward movement of the four co-planar O^{2-} ions it is assumed that the Fe^{3+} ion moves closer to the remaining O^{2-} ion on the z-axis, as in fig. A.2. (2) then

$$V_4^4 = B\,(Y_4^4 + Y_4^{-4}).\ \frac{4\sin^4(\pi/2+\alpha)}{(a/\cos\alpha)^5}$$

and if this is again to be 2/3 of the cubic value

$$\sin^4(\pi/2+\alpha)\cos^5\alpha = 2/3$$

i.e. $\alpha \simeq 15^0$

In this situation V_4^0 is given from A.2. 2 as

$$V_4^0 = AY_4^0\left[\frac{4\,(35\cos^4(\pi/2+\alpha) - 30\cos^2(\pi/2+\alpha)+3)}{(a/\cos\ )^5} + \frac{8}{(a-a\tan\alpha)^5}\right]$$

$$\simeq \frac{42AY_4^0}{a^5}$$

and consequently

$$V''_{ax} = V_4^0 + V_4^4$$

$$= \frac{42AY_4^0}{a^5} + \frac{2}{3}V_4^4\ (\text{cubic})$$

$$= \frac{2}{3}V_4^0\ (\text{cubic}) + \frac{2}{3}V_4^4\ (\text{cubic}) + \frac{70\,AY_4^0}{3a^5}$$

The cubic field is thus again 2/3 of its original value but the sign of the remaining term in Y_4^0 has changed and is now the same as that of the cubic term.

Reference to Appendices.

Hutchings M.T. 1964, Solid State Physics 16, 227